Spring 2022

SYNTHESIS AND STABILIZATION OF GOLD NANOPARTICLES FROM CHLORIDE AND CYANIDE SYSTEMS

Kathryn Ariela Bozer

SYNTHESIS AND STABILIZATION OF GOLD NANOPARTICLES FROM CHLORIDE AND CYANIDE SYSTEMS

by

Kathryn Ariela Bozer

A thesis submitted in partial fulfillment of the
requirements for the degree of

Master of Science in Metallurgical and Mineral Processing Engineering

Montana Tech

2022

Abstract

Generating gold nanoparticles (AuNPs) from gold chloride solution by precipitating with compounds can be difficult due to the potentially required high temperatures. Tin chloride can be used to overcome this dilemma. The process that is known to make Purple of Cassius is a method where gold chloride and tin chloride solutions are mixed to form AuNPs and tin oxide precipitate. However, it is modified by adding hydrazine to resolubilize the tin oxide and provide a more stable solution for the AuNPs. A three-factor central composite experimentally designed model was created using Design Expert incorporating pH, temperature, and gold concentration as the variables. The response of AuNP size was obtained using a Malvern Zetasizer which measures the size of the AuNP agglomerates using dynamic light scattering. Field emission scanning electron microscopy (FESEM) confirmed the size and showed that the shape of the AuNPs tended to be spherical. Resulting statistical models yielded response surfaces with temperature and gold concentration having significant effects on the size of the AuNPs, whereas, pH did not have a significant effect.

From these initial results, a secondary gold chloride system was created. A three-factor central composite model was utilized with the factors being gold concentration, temperature, and thiol concentration. The thiol factor was added to test how a thiol stabilizer affected the size and shape of the produced AuNPs. The Malvern Zetasizer and the FESEM were used to determine the shape and size of the AuNPs. Two models were created for both the size and zeta potential of the data. A similar statistical designed model was created for the gold cyanide with oxalic acid system to determine its response to pH, temperature, gold concentration, and thiol concentration. The Malvern Zetasizer and SEM were the methods to determine the size and shape of the AuNPs. The experiments produced a size model and a zeta potential model. Testing using three different froth flotation chemicals was done on the gold cyanide system to determine if they are candidates for being stabilizers.

Keywords: gold nanoparticles, gold chloride, gold cyanide, stabilizer

Dedication

To my family who made it possible for me to find my love for metallurgical engineering, and to the teacher who made it possible for me to find my love for research.

Acknowledgements

I would like to firstly thank my advisor and committee chair, Dr. Courtney Young. He has been my mentor since I began my undergraduate degree here at Montana Technological University. This project began because of his initial interest in this project and its genesis with Ana Antunes Silva. I would also like to thank the rest of my committee, Dr. Avimanyu Das, Dr. Richard LaDouceur, and Dr. Ilaria Fratoddi. Their continued support and guidance made this project possible from start to finish. I would also like to thank Newmont Gold Corporation for their support and funding of my project over the past two years. With their funding, I have had the opportunity to follow my research findings to where they point me.

As a part of my senior design work during my last undergraduate year, Cameron Hughes began the initial proof of concept on the gold cyanide system and its overall feasibility which I deeply appreciate. Throughout my work during my undergraduate and graduate years on this project, I had the help of three hardworking undergraduate students: Lex McFarland, Steven Foster, and Garret Wanner. I would also like to thank everyone who was a part of the team to help me gain the honor of being named a Barry Goldwater Scholar in 2020. Although this honor was awarded to me during my time as an undergraduate student, receiving this award encouraged me to pursue my advanced degree. I would especially like to thank Dr. Marisa Pedulla, Dr. Courtney Young, Dr. Avimanyu Das, and Dr. Richard LaDouceur for all their guidance during the application process.

My family and friends were a main source of support while working on this project, and I would like to thank them all for their support and lending of an ear. I would like to especially recognize Jamison Ehlers, Cameron Hughes, and Ben Rathman for their thoughts during the editing process of this document.

Table of Contents

List of Tables

List of Figures

List of Equations

Equation

Glossary of Terms

Term	Definition
AuNP(s)	Gold nanoparticle(s)
MPS	Sodium 3-mercapto-1-propanesulfonate
PAX	Potassium amyl xanthate
KEX	Potassium ethyl xanthate
FESEM	Field emission scanning electron microscopy
DLS	Dynamic light scattering
mV	Millivolts
nm	Nanometers
BSE	Back scattered electrons
SE	Secondary electrons
AFM	Atomic force microscopy
TEM	Transmission electron microscopy
DLS	Dynamic light scattering
SEM	Scanning electron microscopy
TIMA	TESCAN integrated mineral analyzer
EDAX	Energy dispersive X-ray analysis spectroscopy

1. Introduction

1.1. General

Gold nanoparticles (AuNPs) have a lengthy history of uses. One of the first uses for AuNPs was to color glasses with a vibrant red color. The Lycurgus Cup is one such example of the coloration as it appears green in daylight, but when illuminated from the inside the color changes to red (Heiligtag & Niederberger, 2013). AuNPs have been of great interest in the past few years because of their numerous applications, e.g. electrical systems, coatings, drug delivery for medical applications, and catalysts (Amendola & Meneghetti, 2009; Habashi, 2016).

A common reducing agent for creating AuNPs is citrate ($C_6H_8O_7$). When citrate is used, elevated temperatures are required due to their weak reducing strengths (Panariello et al., 2020). Another disadvantage of these compounds is the time it takes for synthesis of these particles which can take upwards of thirty minutes to reach the terminal particle radius (Panariello et al., 2020). Most industrial methods for creating AuNPs include using $HAuCl_4$ as the starting material. The reducing agent can vary, but citrate still is one of the most common options. Other options for reducing agents include but are not limited to oxalate, hydrazine, and borohydride (Turkevich et al., 1951; Vaskelis et al., 2007). These nanoparticles are stabilized using capping agents that surround the particles to ensure the particles are isolated and do not coagulate. Two common kinds of capping agents for any AuNP is citrate and thiol (Suherman et al., 2018; Venditti et al., 2014). Thiol is defined as an organic chemical compound that has a sulfur atom in place of an oxygen atom in an alcohol or phenol like structure (The Editors of Encyclopaedia Britannica, n.d.). A thiol was utilized in this research as a stabilizer in two of the three experimental designs.

One typical method to measure the size of AuNPs is UV-vis spectroscopy. This methodology is a quick and convenient technique for most laboratories that have this sort of instrumentation (Panariello et al., 2020). UV-vis spectroscopy provides kinetic data during the nanoparticle formation which can then be used to determine a kinetic model further for the synthesis process (Panariello et al., 2020). It also has the capability to determine the AuNPs hydrodynamic size, concentration, and agglomeration level (Amendola & Meneghetti, 2009).

Transmission electron microscopy (TEM) is also a widely used method of measuring AuNPs. Some drawbacks of using TEM, in opposition to UV-vis spectroscopy, is the rigorous sample preparation required for the instrument. TEM sample preparation can cause sample error of the morphology or size distribution (Amendola & Meneghetti, 2009). The samples also contain the AuNPs within a solid matrix or in an environment that could cause adverse reactions with the AuNPs (Amendola & Meneghetti, 2009). Scanning electron microscopy (SEM) is another common technique that is similar to TEM. SEM cannot get as clear of resolution at the nanoscale as TEM, which is why TEM is the preferred method for imaging nanoparticles.

Dynamic light scattering (DLS) is another methodology that is applied to the hydrodynamic size of the particle similar to UV-vis. Unlike UV-vis, DLS cannot distinguish between isolated or agglomerated AuNPs (Amendola & Meneghetti, 2009). DLS is commonly used as a sizing method due to its quick response and ability to be used in conjunction with zeta potential measurements on instruments such as the Malvern Zetasizer (Acharya et al., 2018). This provides two valuable measurements at the same time. DLS measures the hydrodynamic diameter of nanoparticles based on the time-dependent changes of the scattering intensity. The scattering intensity depends on the interference resulting from the Brownian motion of nanoparticles (Acharya et al., 2018; Tscharnuter, 2000). A limitation of DLS is the case of

particle agglomeration or overlap, where the measurement becomes less accurate due to the blockage of the particles and agglomerates (Acharya et al., 2018; Tscharnuter, 2000).

1.2. Gold Chloride System

Purple of Cassius is a historic process that has been used since the 1650s when it was discovered by Andreas Cassius to color various materials (Habashi, 2016). It creates colloidal gold through a reaction with tin chloride and is said to be given its color by the gold and tin oxide particles in solution. These colloidal solutions have traditionally had particles between 40-900 nm in diameter and can range in color from red to purple based on the size of the nanoparticles (Habashi, 2016). The color of the solution can also be altered by adding other reagents such as iodine or various chemical solutions with hydrazine (Moir, 1910). Modern research on this system has been limited, and the goal is to expand on the knowledge of this system creating AuNPs (Vaskelis et al., 2007).

This research aims to determine if the difference between citrate and tin chloride reducing agents provides a notable change in AuNP size and shape. The other goal of looking at this historic system is to create predictive and statistically significant models for the size and zeta potential of AuNPs in Purple of Cassius using a design of experiments. Research has been completed on a similar colloid solutions which was found to begin coagulation 20-30 hours after synthesis and maintained colloidal stability for three to four days after coagulation takes place (Vaskelis et al., 2007). This will be a consideration when creating the AuNPs, as they will need to be analyzed directly after synthesis, to avoid coagulation effects.

Synthesized AuNPs can range in size and shape: cubes, hexapods, ribbons, cages, branches, polyhedral, and spheres (Kestell & DeLorey, 2010). The size range tends to be from 1-100 nm for most of these synthesized particles (Kestell & DeLorey, 2010). These particles can

be several micrometers in other axial directions. The size of the individual gold nanoparticles found in the colloid structures range 5 to 100 nm in diameter (Ji et al., 2007; Kestell & DeLorey, 2010). SEM and UV-vis spectroscopy have been used to determine the size of these AuNPs.

Half-cell reactions for the system are shown in Equations (1), (2), and (3). Within the system, gold chloride goes to solid gold, creating AuNPs that may agglomerate, while the tin is converted from tin (II) ions to tin (IV) oxide above a pH of approximately 1.2. The combination of the tin (IV) oxide and the gold particles forms Purple of Cassius.

$$Au^{3+} + 3e^{-} = Au^{o} \quad (1)$$

$$Sn^{2+} + 2H_2O = SnO_2 + 4H^{+} + 2e^{-} \quad (2)$$

$$(SnO_2)_3(Au)_2 \rightarrow Purple\ of\ Cassius \quad (3)$$

Figure 1 shows the E_H-pH diagram for the gold chloride and tin chloride system. Below a pH of 1.2, the tin (II) ions are stable and do not form tin oxide (SnO_2); therefore, the system only has gold precipitating into the solution. The blue region on Figure 1 shows where the gold reduction occurs while the orange region shows where the tin oxidation occurs (Young & Huang, 2019).

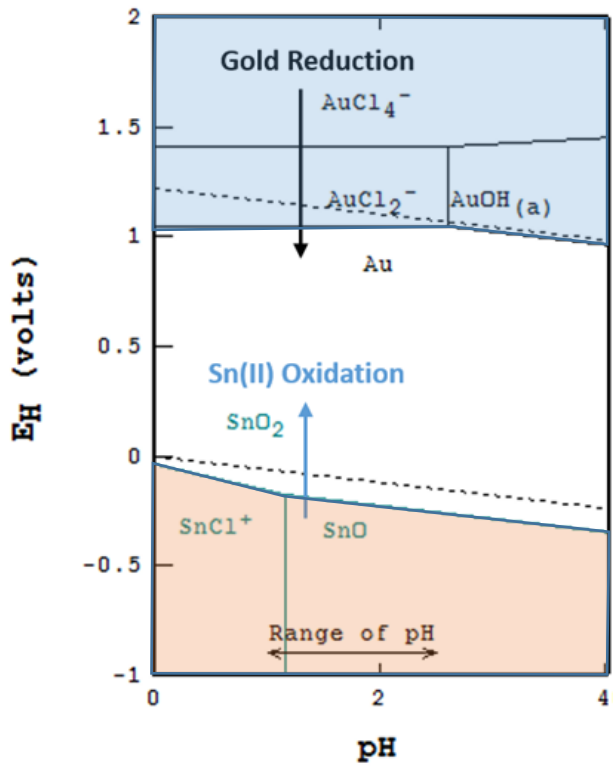

Figure 1: E_H-pH diagram for the gold chloride-tin chloride system that shows were the gold reduction and tin oxidation occurs (Young & Huang, 2019).

1.3. Gold Cyanide System

Gold cyanide systems to produce gold nanoparticles have not been explored in the literature. In particular, potassium gold cyanide and oxalic acid have not been explored as a system. One book from 1906 has cited that a previous researcher deemed the system of potassium gold cyanide and oxalic acid together producing metallic precipitates is feasible, but no paper was found during the literature review that has discussed the system further (Rose, 1906). Another paper researched using AuNPs in a solution containing potassium cyanide and sodium hydroxide to understand the electrochemical dissolution behavior of the AuNPs (Suherman et al., 2018). The gold cyanide and oxalic acid system is of interest as another feasible way to produce AuNPs. It is simple, only requiring potassium gold cyanide and oxalic

acid with a stabilizer and a pH modifier such as sodium hydroxide. The reaction that is possible within the system is limited to creating the AuNPs with no other precipitates.

Half-cell reactions for the gold cyanide and oxalic acid system can be seen in Equations (4), (5), and (6). The reaction produces gold nanoparticles and various forms of carbon dioxide:

$$Au(CN)_2^- + e^- = Au^o + 2CN^- \quad (4)$$
$$C_2O_4^{2-} = 2CO_2 + 2e^- \quad (5)$$
$$CO_2 + H_2O = H_2CO_3\ (HCO_3^-,\ CO_3^{2-}) \quad (6)$$

Figure 2 shows the E_H-pH diagram for the gold cyanide and oxalic acid system created using StabCal software by Dr. Hsin-Hsiung Huang. The blue region outlines where the gold cyanide species reduces to gold. The orange region shows where the oxalate oxidizes to carbon dioxide. Because these experiments must stay in the basic pH range to ensure the cyanide ions stay in solution, the basic portion of the graph is the of interest for this set of designs.

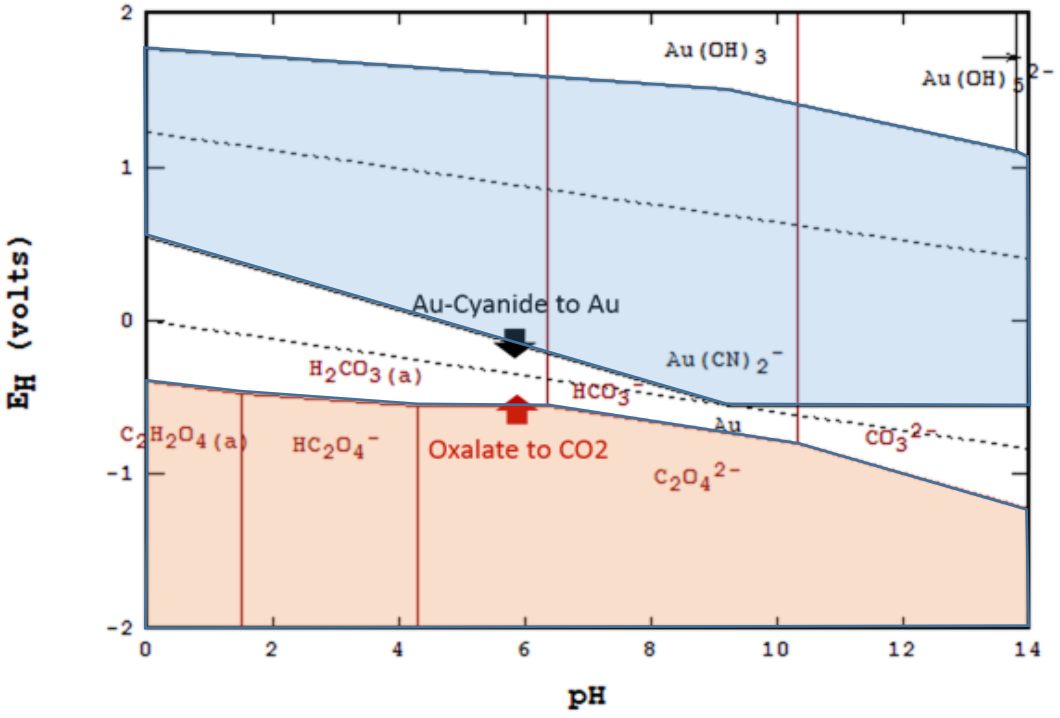

Figure 2: E_H-pH diagram for the potassium gold cyanide-oxalic acid system.

1.4. Nucleation

Classic nucleation is defined as the initial location where crystal growth occurs. Many chemical systems can be described by classical nucleation. Growth after nucleation is typically described by two mechanisms: surface reactions and solid diffusion to the surface (Thanh et al., 2014). Noble metals have been of interest due to their difference in nucleation and growth of their particles in comparison to the standard understanding of those processes (Thanh et al., 2014). The overall understanding of nanoparticle synthesis is incomplete and is still being investigated on some of the oldest synthesis processes, such as the role of citrate in the work of Turkevich *et al*. (Heiligtag & Niederberger, 2013; Turkevich et al., 1951).

Nucleation of gold particles have been shown to depend on the pH of the solution, and thus can take one of two paths (Thanh et al., 2014). The formation of AuNPs using citrate as the reducing agent has shown that, in lower pH ranges, fast attachment and intra-particle ripening occurs. In higher pH ranges, nucleation and slow growth predominate (Ji et al., 2007; Polte et al., 2010). These nucleation processes have been researched on other systems, such as the gold chloride with citrate and the gold chloride with sodium borohydride systems (Thanh et al., 2014). Coalescence typically occurs in these systems, which is indicated by bimodal size distributions (Thanh et al., 2014). Coalescence has also been shown to occur in solution when a thiol stabilizer is present. The coalescence causes some of the particles to become globular or aggregated. When the samples are dried, they can appear on an atomic force microscope (AFM) as gold clusters and complexes (Mikhlin et al., 2011).

1.5. Stabilization of Nanoparticles

Stabilizers are utilized due to their ability to cap and inhibit the growth of AuNPs. One such stabilizer that is utilized for AuNP synthesis is sodium 3-mercapto-1-propanesulfonate

(MPS) which is also classified as a thiol stabilizer. MPS is an ideal candidate for stabilizing AuNPs since it has the potential to enhance the water solubility of the system, and has proven to provide a changeable size and low size variation within the hydrogen tetrachloroaurate and sodium borohydride system (Venditti et al., 2014). MPS is an appropriate stabilizer for the solution because it has shown to impede the growth and agglomeration of AuNPs in systems such as hydrogen tetrachloroaurate with sodium borohydride (Porcaro et al., 2016). The structure of the MPS molecule can be seen in Figure 3.

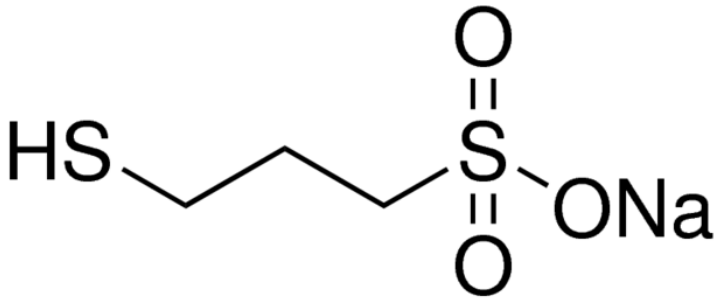

Figure 3: Structure of sodium 3-mercapto-1-propanosulfonate.

MPS is stable in both acidic and basic conditions. Typically MPS is used within the pH range of 3-10 (Park et al., 2004). These pH ranges have typically been chosen because of other reagents within the system. Testing for both the secondary gold chloride and gold cyanide systems are outside of these typical ranges but was desired to be evaluated anyway.

Additional stabilizer possibilities were desired for these systems. For this reason, some other surfactants were looked at, including xanthates. Traditionally, xanthates are used as a collecting agent in froth flotation practices. Xanthates are similar in structure to MPS as they both contain a thiol group. There are many xanthates to choose from with varying lengths of chain. The chain length is important because it provides different options for functionalization of the AuNPs. Thiols traditionally provide this avenue for the possibility of functionalization of the AuNPs for biomedical applications (Venditti et al., 2014; Zhou et al., 2009). The corresponding

salt attached to the xanthate is another variable which depend on what extraneous element in solution would not interfere with the other reactions occurring. Two xanthates that are commonly used in froth flotation were chosen for this project: potassium amyl xanthate (PAX) and potassium ethyl xanthate (KEX). Potassium is to be a spectator ion in the gold cyanide system. Xanthates can only be used in basic conditions as their structure breaks down in lower pH ranges (Young, 1987). Another froth flotation chemical known as Orfom D8 (disodium carboxymethyl-tri-thiocarbonate) was chosen to be tested in the basic system because of its similar structure to MPS. Orfom D8 is suitable in the high pH ranges that the cyanide system was completed within (pH 11-13).

2. Methods

2.1. Design of Experiments

The Design Expert program was used to create all of the statistical design of experiments used in this project. Depending on the desired knowledge on the interactions within the system, either three or four factors were used for creating the resulting model which had to be statistically significant. Design factors were chosen based on the E_H-pH diagrams for gold chloride and gold cyanide systems. Since temperature and gold concentration are the main driving factors in most AuNP synthesis systems, all three designs used these factors.

2.1.1. Initial Gold Chloride System

For this system, the factors chosen included the pH of the solution, the temperature of the solution, and the concentration of gold to be used. The amount of tin chloride used was held constant between experiments at 20% excess of the stoichiometric amount required for the 500 ppm gold trial. A 20% excess value was chosen to ensure that there was sufficient excess of the reducing material in the solution. In this system, the gold concentration ranged from 5-500 ppm. Values of 5-500 ppm for the gold concentration were chosen due to previous proof of concept experiments which determined concentrations above 500 ppm created large agglomerates. The pH was chosen to be between 0 and 4, based on the E_H-pH diagram for the system (see Figure 1). Also, the temperature was between 20 and 60°C. The temperature limit was set so that the solution would not boil. This initial gold chloride system design consisted of 20 experiments in a central composite model with multiple midpoint duplicates. A summary of the factors for each experiment in the system can be seen in Table I.

Table I: Initial gold chloride system design of experiments.

Run	Temp. [°C]	pH	Au Conc. [ppm]
1	60	0	500.0
2	20	2	252.5
3	40	2	500.0
4	40	2	252.5
5	60	2	252.5
6	40	2	252.5
7	20	0	500.0
8	20	0	5.0
9	40	0	252.5
10	60	0	5.0
11	40	2	252.5
12	60	4	500.0
13	40	4	252.5
14	60	4	5.0
15	40	2	252.5
16	20	4	500.0
17	40	2	5.0
18	40	2	252.5
19	40	2	252.5
20	20	4	5.0

2.1.2. Secondary Gold Chloride System

The secondary gold chloride design of experiments decreased the gold concentration to between 1 and 20 ppm since the results in the initial design of experiments produced large agglomerates, with no individual nanosized particles. This range was chosen based on a looking at other documentation that agreed that lower gold concentrations would be more ideal for creating solely AuNPs (Venditti et al., 2014).

Because of a fluctuation in room temperature, the range was changed to between 25 and 60°C. The pH parameter was taken out for multiple reasons. The first reason was because the results from the first system showed that pH did not influence the size of the AuNPs. Secondly, tin oxide was precipitating in the solution and proved to have a negative influence on both the

Malvern Zetasizer and the FESEM. Removing the pH factor also eliminated the need for hydrazine in the system, taking out another variable to the design.

A thiol concentration parameter was added to the system to determine the effect of the MPS on the system. MPS was added using zero, five, or ten times the stoichiometric requirement of the gold in solution for the 20-ppm solution. Typically, four or five times the stoichiometric amount of thiol is standard in AuNP producing systems (Venditti et al., 2014). Ten times the stoichiometric amount of thiol was chosen to give a range out of the typical amount used for stabilizers in AuNP systems. A summary of the factors for each experiment in the system can be seen in Table II.

Table II: Secondary gold chloride system design of experiments.

Std	Run	Au Conc [ppm]	Temp [°C]	Thiol Conc.
20	1	10.5	42.5	5
11	2	10.5	25.0	5
7	3	1.0	60.0	10
16	4	10.5	42.5	5
5	5	1.0	25.0	10
18	6	10.5	42.5	5
14	7	10.5	42.5	10
17	8	10.5	42.5	5
4	9	20.0	60.0	0
2	10	20.0	25.0	0
3	11	1.0	60.0	0
6	12	20.0	25.0	10
12	13	10.5	60.0	5
1	14	1.0	25.0	0
15	15	10.5	42.5	5
8	16	20.0	60.0	10
10	17	20.0	42.5	5
13	18	10.5	42.5	0
19	19	10.5	42.5	5
9	20	1.0	42.5	5

2.1.3. Gold Cyanide System

The gold cyanide and oxalic acid system was statistically designed with four parameters. The included factors were pH, gold concentration, thiol concentration, and temperature. Each factor's range were as follows, respectively: pH 11-13, 1-20 ppm gold concentration, 0-10 times the stoichiometric thiol requirement, and 25-60°C. The amount of oxalic acid added to the solution during testing was 20 times the stoichiometric amount required to react with all of the gold within the 20-ppm gold concentration solution. Oxalic acid was added in excess to ensure that complete conversion of the gold would occur in the solution. Similarly, to the secondary gold chloride system, the thiol was based on five times and ten times the stoichiometric amount required to react with all the gold at a concentration of 20 ppm. These thiol amounts were chosen as standard because these amounts were the smallest that could be accurately measured on the available scale. The gold concentrations were chosen to match the secondary gold chloride system since the range was determined to be more adequate. Because the direct comparison of these the secondary gold chloride and gold cyanide systems was desired, these ranges were chosen to be the same. Consequently, the parameters between the two systems were kept the same in all possible cases. These lower gold concentrations were also chosen based on previous research completed at Montana Technological University, where it was determined that even lower than 1 ppm gold concentrations gave independent AuNPs (Hughes, 2021). In total, this design included thirty experiments with midpoints. The design was made so the design points would not be exceeded in the experiments. A summary of the factors for each experiment in the system can be seen in Table III.

Table III: Gold cyanide system design of experiments.

Std	Run	Au Conc. [ppm]	Temp [°C]	pH	Thiol conc.
1	12	1.0	25.0	11	0
2	30	20.0	25.0	11	0
3	7	1.0	60.0	11	0
4	21	20.0	60.0	11	0
5	19	1.0	25.0	13	0
6	26	20.0	25.0	13	0
7	13	1.0	60.0	13	0
8	3	20.0	60.0	13	0
9	24	1.0	25.0	11	10
10	25	20.0	25.0	11	10
11	4	1.0	60.0	11	10
12	27	20.0	60.0	11	10
13	9	1.0	25.0	13	10
14	28	20.0	25.0	13	10
15	11	1.0	60.0	13	10
16	23	20.0	60.0	13	10
17	2	1.0	42.5	12	5
18	16	20.0	42.5	12	5
19	20	10.5	25.0	12	5
20	8	10.5	60.0	12	5
21	17	10.5	42.5	11	5
22	29	10.5	42.5	13	5
23	15	10.5	42.5	12	0
24	10	10.5	42.5	12	10
25	6	10.5	42.5	12	5
26	5	10.5	42.5	12	5
27	14	10.5	42.5	12	5
28	22	10.5	42.5	12	5
29	18	10.5	42.5	12	5
30	1	10.5	42.5	12	5

Furthermore, the midpoint of all the factors, except for thiol concentration, was used for the testing Orfom D8 after completion of the original design. Although a separate statistical design was not used for Orfom D8 as it was a proof-of-concept stabilizer, testing Orfom D8 was of interest because of its structural similarity to the MPS. The structure of Orfom D8 can be seen in Figure 4 (Young et al., 2022).

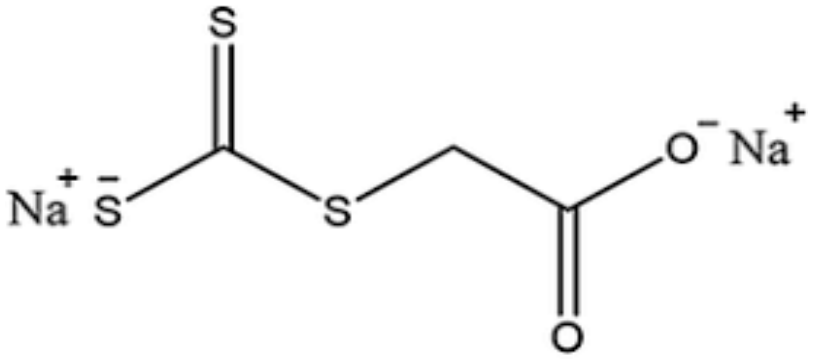

Figure 4: Structure of Orfom D8 (Young et al., 2022).

Two xanthates, potassium ethyl xanthate (KEX) and potassium amyl xanthate (PAX), were also used on the 20 ppm gold concentration solutions to determine the general size and shape of the AuNPs and gold agglomerates using structurally similar structures chemicals. The structures of KEX and PAX can be seen in Figure 5 and Figure 6, respectively.

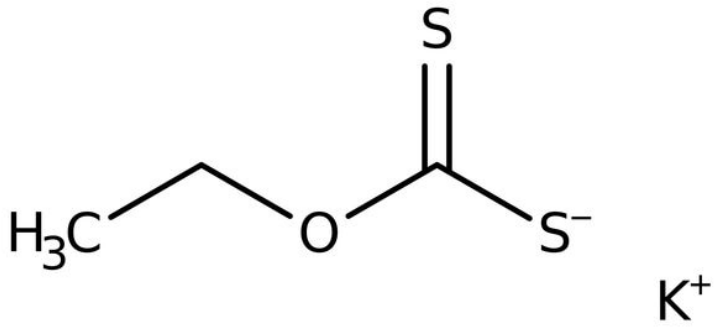

Figure 5: Structure of potassium ethyl xanthate (Fisher Scientific, n.d.-b).

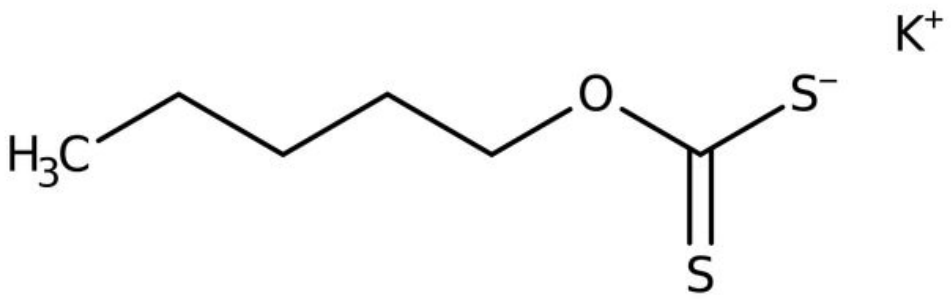

Figure 6: Structure of potassium amyl xanthate (Fisher Scientific, n.d.-a).

All three of the tested chemicals are traditionally used as froth flotation chemicals in the mining industry. Because of their similar structures, these three chemicals were chosen as proof-of-concept stabilizers for the gold cyanide system since all three of them are used in basic systems.

2.2. Synthesis of Gold Nanoparticles

2.2.1. Gold Chloride System

2.2.1.1. Initial Gold Chloride System

Gold chloride ($HAuCl_4$) and tin chloride ($SnCl_2$) were the reactants. Hydrochloric acid (HCl) was used as needed to meet the pH requirements of the system. The two solid products from the Purple of Cassius reaction are gold nanoparticles and tin (IV) oxide. Each solution was separately brought to the required pH and temperature for the specific experiment. The solutions were put into 25 mL beakers that were separately brought up to the required temperature. The specified temperature was then held constant for five minutes and measured using a glass thermometer. Afterwards, the solutions were then mixed and held at the desired temperature for an additional 5 minutes. Immediately, the reacted solution was then used for Malvern Zetasizer analysis and prepared for the FESEM on an aluminum stub mount with carbon tape. Similar

experiments on this system were reacted for a total of 0.5-1 minutes (Vaskelis et al., 2007). The increase is to ensure that proper homogeneity of the solution occurs (Pacławski et al., 2012).

2.2.1.1.1. Addition of Hydrazine

Hydrazine was added to reduce the tin (IV) oxide to tin (II) ions in the aqueous solution. Using hydrazine allowed the only precipitate in the solution to be the AuNPs. Hydrazine was not added in excess in stoichiometric relation to the tin oxide present in solution in order to prevent any adverse reaction between the acidic environment and the hydrazine. The following Equations (7) and (8) show the half-cell reactions between the precipitated tin (IV) oxide in the solution and the added hydrazine:

$$SnO_2 + 4H^+ + 2e^- = Sn^{2+} + 2H_2O \quad (7)$$

$$2N_2H_4 = 2NH_4^+ + N_2 + 2e^- \quad (8)$$

Both the natural solution and the hydrazine reacted solutions were analyzed on the Malvern Zetasizer and FESEM.

2.2.1.2. Secondary Gold Chloride System

Gold chloride ($HAuCl_4$) and tin chloride ($SnCl_2$) were the reactants. Hydrochloric acid (HCl) was used as needed to meet the pH requirements of the system. MPS was used as the stabilizer within this system as it is a thiol group that can be used in acid conditions (Venditti et al., 2014). Stock gold chloride solutions were made at the specified concentrations of 1, 10.5, and 20 ppm at a pH of 0. A stock solution of 20 times the necessary concentration of oxalic acid was also made at a pH of 0. Each experiment consisted of 5 mL of both the gold chloride and oxalic acid solutions being put into separate beakers and covered with parafilm. In this secondary design of experiments, the samples were 10 mL in total solution. The samples were stirred at 600 rpm separately until they reached the temperature required for the designated experiment. At that

point, a five-minute timer was started to let the tin and gold solutions mix separately. The two solutions were then mixed, and another five-minute timer was started. Finally, the solution was collected immediately and used for the Malvern Zetasizer and an aluminum stub for the FESEM. The Malvern cell was then loaded into the Malvern to be tested first for size data, and then for surface zeta potential data. The remainder of the solution was kept in a test tube for further observation and record keeping.

2.2.2. Gold Cyanide System

Potassium gold cyanide ($K[Au(CN)_2]$) and oxalic acid were the reactants. Sodium hydroxide (NaOH) was used as needed to meet the pH requirements of the system. MPS was used as the stabilizer for this experimentation because of its ability to be used in basic systems (Park et al., 2004). Stock potassium gold cyanide solutions were made at the specified concentrations of 1, 10.5, and 20 ppm at each required pH of 11, 12, or 13. A stock solution of 20 times the necessary concentration of oxalic acid was also made at each required pH of 11, 12, and 13. 5 mL of each solution were put into separate beakers and covered with parafilm. The beaker with the gold cyanide in it was stirred at 600 rpm and both were set on the hot plate at the required temperature. A five-minute timer was set once the solution was within 1 degree of the required temperature. After the 5-minute timer, the oxalic acid solution was added into the gold cyanide solution and allowed to mix and react for another five-minutes with parafilm still over the top.

Afterwards, the solutions were immediately prepared in both the Malvern cell and on the FESEM aluminum stub mount with carbon tape. The cell was then loaded into the Malvern Zetasizer to first measure size and then zeta potential. The remainder of the solution was kept in a test tube for further observation and record keeping.

2.3. Zeta Potential

Zeta potential is a measure of the solution potential at the shear plane. From the zeta potential value, a surface charge can then be inferred. A negative zeta potential implies a negative surface charge. Similarly, a positive zeta potential implies a positive surface charge. The surface charge gives information on the overall stability of the solution and whether the precipitates within the solution will coagulate or flocculate (C. Young, personal communication [Surface Charge and Zeta Potential lecture notes], September 10, 2020).

A zeta potential of above 25 mV is desired to give the solution moderate stability as can be derived from Table IV (C. Young, personal communication [Surface Charge and Zeta Potential lecture notes], September 10, 2020; Kumar & Dixit, 2017). Other documents cite that zeta potentials with a magnitude greater than 30 mV normally considered stable (Lata et al., 2015). The slight discrepancy between the two sources could be due to a difference in the density of the particle being examine. For particles of the same size, the denser particle requires a higher zeta potential to be stable in solution. This table shows the magnitude of zeta potential that is desired. The zeta potential can be either negative or positive at these magnitudes and still maintain the described colloid stability. Coagulation is to be avoided when characterizing the size of particles using a suspended particle analysis system like a Malvern Zetasizer. It is useful to use for the AuNPs because knowing what charge is needed for a particular stability can be used to analyze the system.

Table IV: Zeta potential indication parameters of solution stability (C. Young, personal communication [Surface Charge and Zeta Potential lecture notes], September 10, 2020).

Zeta Potential (mV)	Colloid Stability	Flocculation or Coagulation
0-5	None	Excellent/Rapid
5-25	Incipient	Strong
25-40	Moderate	Moderate
40-60	Strong	Weak
>60	Excellent	None

Zeta potential is a metric that is commonly used in froth flotation. The reason for this is it describes how mineral particles are interacting with the collectors, frothers, and other added chemicals. In a similar manner, this applies to stabilizing chemical for precipitating AuNPs.

For the gold cyanide system and the secondary gold chloride system, the Malvern Zetasizer Nano ZS was used to determine the zeta potential, while the ZetaPal was used on the initial gold chloride system. The zeta potential data was determined for every experiment. Not all data was within the desired boundaries of the instrument.

2.4. Dynamic Light Scatter Size Analysis

The Malvern Zetasizer Nano ZS was utilized for measuring the size of the particles. Dynamic light scattering (DLS) is the method the instrument uses to measure the size of the particles within the range of 1-999 nm. A refractive index of 0.2 was used for the gold particles in both the gold chloride and gold cyanide systems (Nobbmann, 2014). The instrument used can be seen Figure 7.

Figure 7: Malvern Zetasizer Nano ZS series that was used for experimentation.

2.5. Field Emission Scanning Electron Microscopy

For these experiments, a field emission scanning electron microscope (FESEM) with a TESCAN MIRA 3 Integrated Mineral Analyzer (TIMA) FESEM model with energy dispersive analysis X-ray spectroscopy (EDAX) attachments was utilized. This instrument was used for analysis of the shape and size of the AuNPs and associated gold particles. AuNP samples were prepared on aluminum stub mounts with carbon tape attached. Each experiment had an aluminum stub mount associated to the experiment that was dropped onto the carbon tape and left to dry with the lid of the sample box closed to ensure that no dust in the air would interfere with the samples. A beam intensity index of 17.00 using a field emission gun tungsten tip and a

working distance of 15 mm were the typical operating parameters, though variations occurred depending on the sample.

FESEM samples were difficult to image due to the drying of the solution which precipitated either the sodium hydroxide or the hydrochloric acid. Samples that were difficult to image were washed using 18 megaohm water to try to mitigate this issue. The number of times the samples were washed depended on the success of imaging on the individual sample. Some samples still could not be imaged even after the washing procedure. Acetone was also tried to clean these samples. A purification method of centrifuging and washing the AuNPs with water was also attempted, but the total amount of gold in the solution was too low to collect the AuNPs after centrifuging.

Two beam responses were used in the analysis of the AuNPs: the secondary electron beam (SE) and the backscattered electron beam (BSE). BSE was primarily used because of its strength in showing the difference in elemental composition as a function of grayscale, which made it easier to image the AuNPs and see the general size and shape of the AuNPs. SE was used to further understand the shape of the particles once they were visualized using the BSE. SE shows the topographical aspect of the AuNPs better. The EDAX was used to confirm that the imaged particles were gold. See Figure 8 for the TESCAN FESEM and EDAX assembly equipped with TIMA software used in this research for characterizing the size and shape of the AuNPs.

Figure 8: FESEM with EDAX attachment instrument used for analysis.

3. Results and Discussions

3.1. Initial Gold Chloride System

3.1.1. Synthesis

The data for the initial gold chloride system included solutions with and without hydrazine added. Malvern size data for the solutions containing hydrazine was used as the primary data since no tin oxide precipitate was present in the solution. Some experiments had coagulation of the tin oxide and gold nanoparticles that occurred before the solution could be properly tested. In the case of particle coagulation, the experiment was performed again. Coagulation occurred when pH was either 2 or 4. The solutions that were at a pH of 0 had a yellow color while solutions at a pH of 2 or 4 exhibit the classic purple color that Purple of Cassius is known for (see Figure 9).

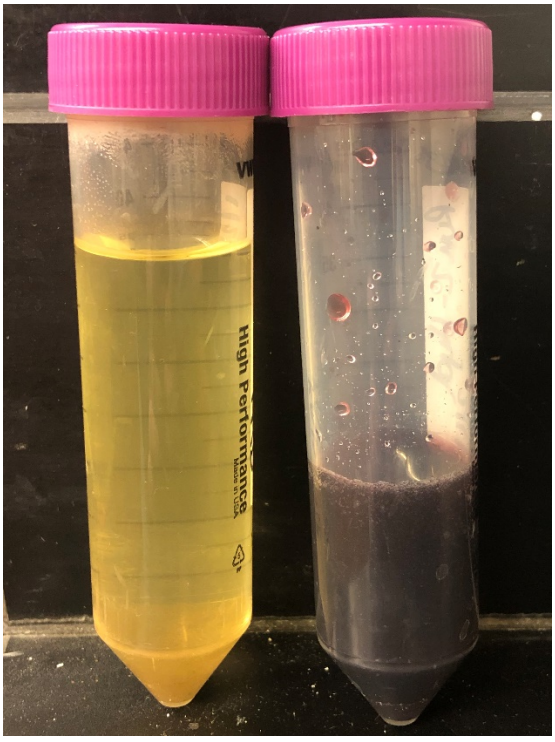

Figure 9: Example showing a solution at pH 0 (left) and at pH 2 (right) in the gold chloride system.

The reasoning for the coloration is thought to be the tin oxide creating the purple color around the gold nanoparticles. If hydrazine was added in excess to the tin in solution, all the purple color should disappear from the solution and the solution to return to the yellow color that the pH 0 solutions exhibit. This was attempted using a new experiment, but a color change was not observed. In this regard, the gold nanoparticles were seemingly encapsulating some of the tin oxide precipitate within its structure.

It was observed that the yellow-colored solutions maintain their color even when the gold particles have coagulated in the solution and settles to the bottom of the solution after a 24-hour stabilization period. The AuNPs were visibly darker in color than the solution when they collect at the bottom of the test tube following these 24 hours. This is seemingly due to the concentration of the particles at the bottom causing the color to be more apparent. Even after settling occurred, some particles were still in suspension in solutions at all pH points. Consequently, this was proven by use of a laser directed through the solution, which showed suspended particles interrupting the beam of light.

With a few samples, coagulation was observed because settling was apparent. Consequently, the tests were rerun. None of these repeat tests exhibited coagulation. Thus, only non-coagulated data was used for data analysis for both the sizing data and the FESEM data.

3.1.1.1. Addition of Hydrazine

The solutions that did not have hydrazine added to them tended to drop all particles out of solution within 24 hours. Solutions that had hydrazine added to them generally did not coagulate the solution, most of the solutions still maintained the purple color and had some of the gold particles suspended as indicated by the maintained purple color of the solution, even a year later. Solutions with hydrazine added could also be shaken to resuspend the AuNPs fully. Figure 10

shows an example of the effect hydrazine has on the solution. The left solution has no hydrazine added, and therefore most of the tin oxide precipitate and the AuNPs have coagulated in the solution after 24 hours. The right solution has hydrazine added and almost none of the AuNPs or leftover tin oxide precipitate coagulated to the bottom of the solution. Also, as described previously, occasionally a solution immediately had all the nanoparticles and tin oxide precipitates drop out of solution. It has not yet been determined why this occurred, as it did not repeat for the same test when a rerun was performed under the same conditions.

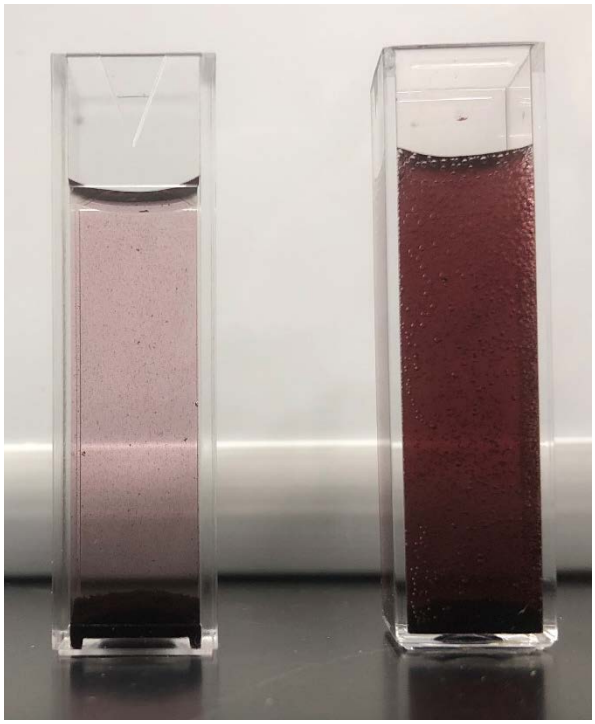

Figure 10: Experimental results showing gold nanoparticles in suspension after 24 hours. The left solution has no hydrazine added. The right solution has hydrazine added.

3.1.2. Design of Experiments

The design of experiments for the initial tests showed the gold concentration and the temperature were the two factors that influenced the system. pH was shown to not be significant in this model, as can be seen in Table V. Overall, the model was significant with a p-value of

0.0031. The remaining factors and interactions of the factors that are shown in Table V are significant in the model.

Table V: ANOVA table showing initial gold chloride system size response model statistics.

Source	Sum of Squares	df	Mean Square	F-Value	p-Value
Model	1.42E+05	4	35466.36	6.49	0.0031
A-Temperature [°C]	52056.23	1	52056.23	9.53	0.0075
C-Au Conc. [ppm]	29278.92	1	29278.92	5.36	0.0352
AC	24090.13	1	24090.13	4.41	0.0530
A^2	36440.18	1	36440.18	6.67	0.0208
Residual	81922.04	15	5461.47		
Lack of Fit	64499.57	10	6449.96	1.85	0.2576
Pure Error	17422.47	5	3484.49		
Cor Total	2.24E+05	19			

The gold concentration, which can be seen in Figure 11 at high (red lines) and low (black lines) concentrations, had an interaction with the temperature of the system. At low temperatures, the low gold concentrations produced large agglomerates whereas at the same low temperature the high gold concentrations produced considerably smaller agglomerates. At the high temperatures the concentration had slight variation on agglomerate size between the high and low gold concentrations. The reason this occurs is competing nucleation sites. The nucleation sites at the low concentrations are not competing for space as much as they are at the high concentrations.

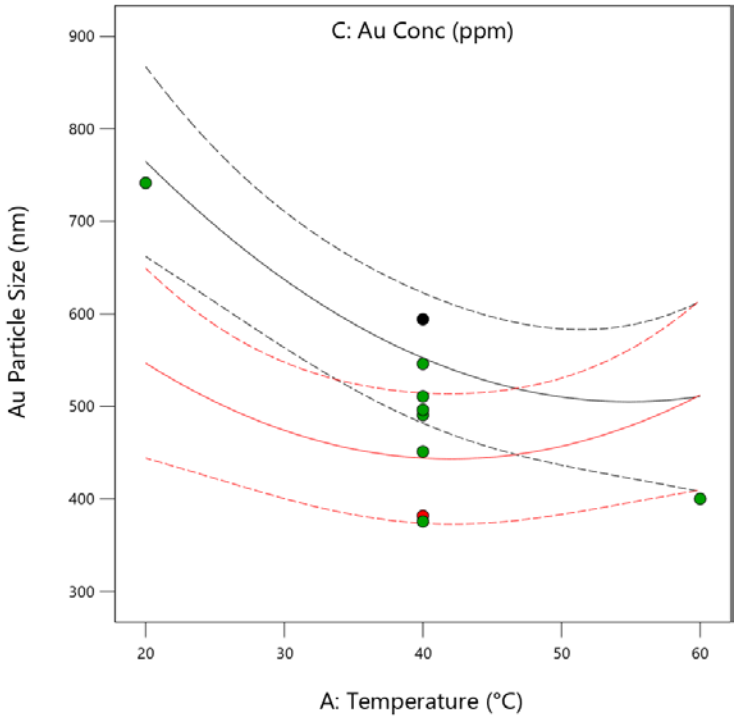

Figure 11: Design expert multi factor results showing the effect that temperature has at high (red lines) and low (black lines) gold concentrations.

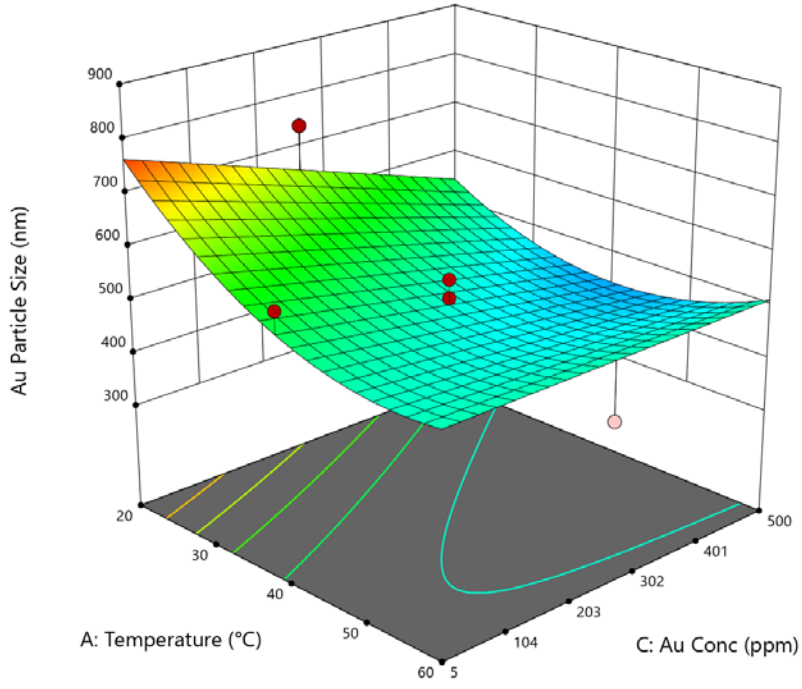

Figure 12: Design Expert response surface results showing the effect that temperature and gold concentration have on gold nanoparticle size.

Experimentation was run in a central composite model with a total of 20 experiments. After rerunning a few experiments, the developed model fit the data well. The model showed that the gold concentration and the temperature were contributing factors in the size of the gold nanoparticles. At low temperatures and low concentrations, the size of the gold nanoparticles was the largest due to gold crystal nucleation sites had fewer competing sites, thus the crystals were able to grow to a larger size. The experiments run at a high temperature with a high concentration of gold or at a low concentration at any temperature have a smaller particle size because there are more competing nucleation sites, which inhibits the growth of the crystal to a large particle size.

The fit statistics for the model can be seen in Table VI. From this, it can be said that the model does not have strong predictive power but has sufficient fit.

Table VI: Design Expert initial gold chloride system size model fit statistics.

R^2	0.6339
Adjusted R^2	0.5363
Predictive R^2	0.3115
Adequate Precision	8.6768

The pH of the solution was not a contributing factor in the size of the gold nanoparticles, as was seen in Table V. This is due to it only changing what precipitates in the reaction. Tin oxide only precipitates above roughly a pH of 1.1. This means that the experiments at a pH of 2 and 4 are the only experiments that form tin (IV) oxide precipitate. The reaction chemistry only affects what precipitates, but not the kinetics of the formation of the gold nanoparticles, therefore it is not a significant variable in the statistical design.

3.1.3. Dynamic Light Scattering Size Analysis

Results from the Malvern Zetasizer were obtained for all the experiments, including the portions of the experiments that had hydrazine added to the solution. The Malvern Zetasizer uses DLS to determine the size of the agglomerated nanoparticles. Three size distribution records were taken for each solution. The average of the three records was taken as the size of the gold nanoparticle agglomerates for each experiment.

The Malvern results that were used for the Design Expert model were the hydrazine results for the pH 2 and pH 4 experiments. The reasoning for this is twofold. Firstly, the solutions in this pH range that did not have hydrazine added coagulated faster than the machine could collect results. Secondly, the solutions had another precipitate which accounted for another size peak on the data. For these reasons, the solutions with hydrazine which had a very low amount of the tin oxide precipitate in the solution were used for the Malvern sizing data.

3.1.4. Field Emission Scanning Electron Microscopy

The FESEM was used to see the size and shape of individual AuNPs. Generally, the shape of the AuNPs seemed spherical, except for in a few photos where the shapes were on the microscale. As Figure 13 demonstrates, the agglomerates are visible and shown to contain AuNPs within. It can be difficult to ascertain where one agglomerate ends and the next one begins due to the nature of drying these agglomerates on an aluminum stub mount.

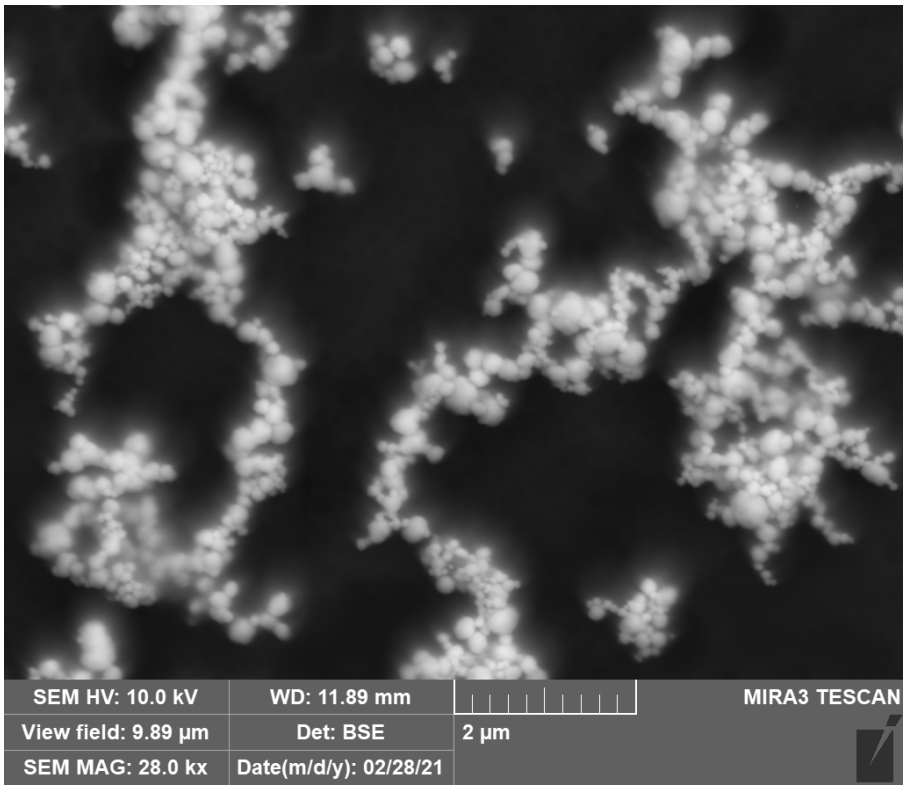

Figure 13: Gold nanoparticle agglomerates shown via SEM imaging at 28.0 kx magnification.

FESEM data from this system first presented the issue of the tin oxide precipitate being present. This was a driving factor in using the solutions with hydrazine. The data showed the same spherically shaped particles throughout all samples that were able to be analyzed. Size data from the Malvern matched up with data from the FESEM results regarding the size of the agglomerates. Malvern size data could be compared to the FESEM data because the AuNPs were mostly part of agglomerates. The size of the AuNPs within the agglomerates was consistent throughout the imaged samples on the FESEM. Additional images of this system can be found in Appendix B.

Typically, transmission electron microscopy (TEM) is recommended for nanosized particles due to its imaging range, but, due to equipment limitations at the time of experimentation, the TEM was not utilized.

3.1.5. Zeta Potential Analysis

The zeta potential was found using a ZetaPal machine. A stable solution has a bare minimum zeta potential of -20 to 20 mV. Experiment 4 with hydrazine added was used, since the head solution still maintained its color after weeks without color change. The average zeta potential after three runs was found to be -19.18 mV, as can be seen in Figure 14. This means that the solution is just outside of the range for being classified as a stable condition, and instead was classified as a semi-stable solution. Since the solution is only semi-stable, the gold nanoparticles have a high chance of dropping out of solution and forming a sediment layer at the bottom of the test tube.

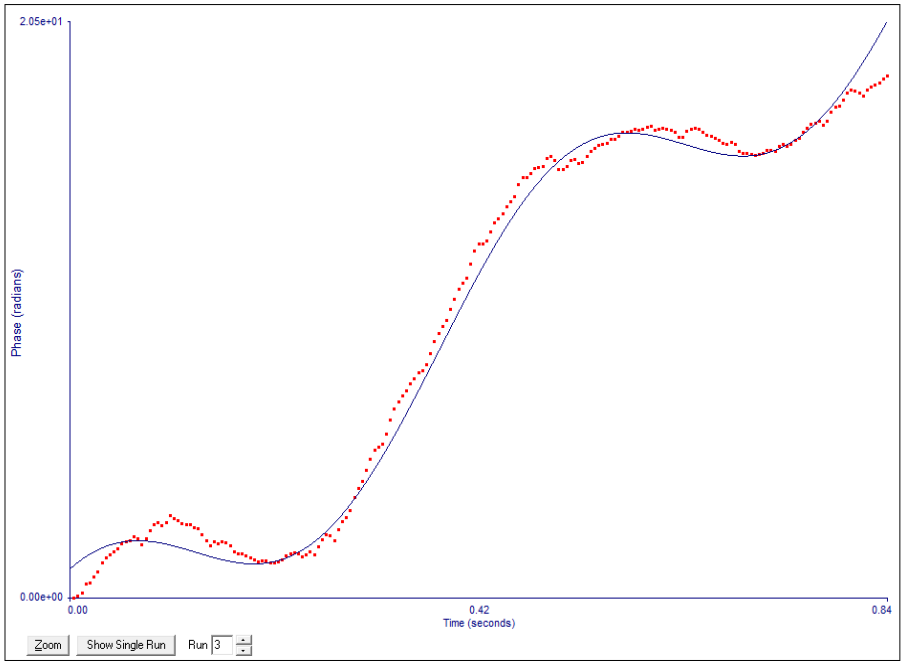

Figure 14: Zeta potential results for head sample of a solution with hydrazine added.

For this system, the zeta potential was only taken for one singular solution. The reason for this is that the Malvern zeta measuring system was not prepared for this system when this set of experiments were being conducted. A ZetaPal instrument was used for this data point. The result of -19.18 mV shows that the zeta potential of this head solution is incipiently stable which

indicates that some coagulation is occurring which is also evident by the visual inspection of the solution, since the sample taken was a head sample. The sample that was run in the analysis was taken from the head solution, but, due to the transport of the solution, the head solution became mixed with the precipitated and coagulated part of the solution which would account for that incipient result.

3.2. Secondary Gold Chloride System

3.2.1. Synthesis

All solutions were mixed according to the methods previously described. The solutions ranged from clear to slightly yellow due to the low gold concentration in the solutions. Because no tin precipitated in the solutions, the solutions did not appear purple as the name Purple of Cassius suggests. Examples of the solutions can be seen in Figure 15.

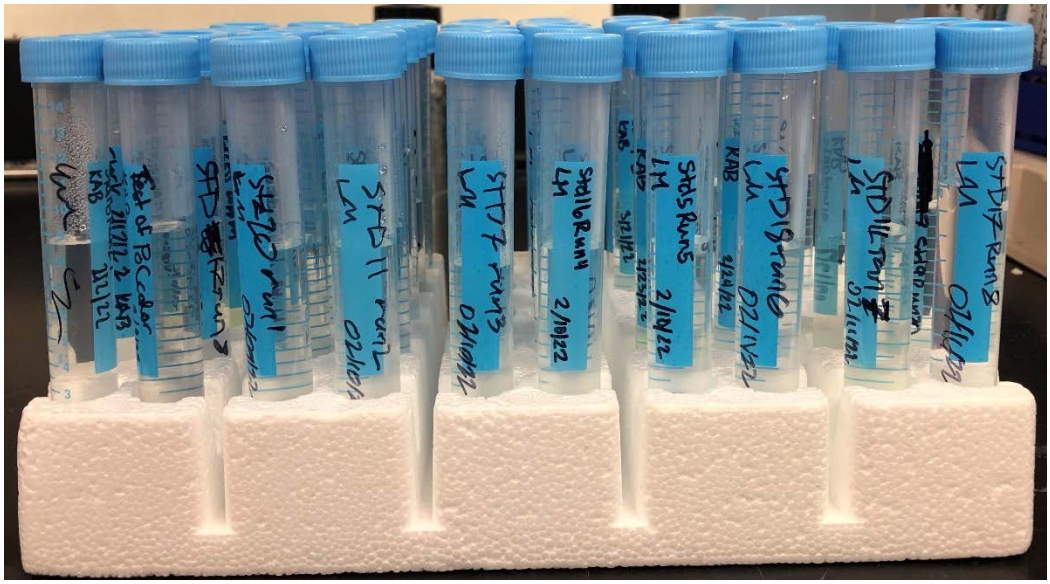

Figure 15: Image of secondary gold chloride system experimental solutions.

Because of the low concentrations of gold in the solutions, the solutions appeared clear with visual inspection. In the 20-ppm solution, the color of the solution exhibited a bit of the yellow color that was present in the initial system's pH 0 solutions. The lack of tin oxide

precipitate simplified analysis of the solution in the subsequent steps of Malvern Zetasizer and FESEM analysis.

3.2.2. Design of Experiments

3.2.2.1. Size Model

Malvern Zetasizer size peaks for each experiment were averaged and input into the Design Expert modeling software. The analysis was run, and reruns for outlier points were completed. The ANOVA analysis for the model can be seen in Table VII. It can be seen from Table VII that all of the factors included in the table were significant except for the individual thiol concentration factor, which was kept in the model due to the significant interaction parameter. With a p-value of 0.0082, the model was also shown to be significant.

Table VII: ANOVA table showing secondary gold chloride system size response model statistics.

Source	Sum of Squares	df	Mean Square	F-Value	p-Value
Model	87619.66	4	21904.92	5.7200	0.0082
A-Au Conc. [ppm]	29496.17	1	29496.17	7.7100	0.0168
B-Temperature [°C]	11554.93	1	11554.93	3.0200	0.1079
C-Thiol Conc.	3797.64	1	3797.64	0.9923	0.3389
AC	22986.95	1	22986.95	6.0100	0.0306
Residual	45927.34	12	3827.28		
Lack of Fit	16197.32	8	2024.67	0.2724	0.9445
Pure Error	298730.02	4	7432.51		
Cor Total	1.34E+05	16			

Figure 16 and Figure 17 shows the model results for all three factor interactions. The model found that gold concentration, temperature, and thiol concentration are factors that are significant within the system, either independently or as an interaction parameter. Figure 16 shows that gold concentration has no effect on the size of the nanoparticle when at 10 times thiol concentration. This is due to a connection between the anionic MPS attaching to multiple particles and drawing them together to form a larger agglomerate. The data also shows that there is a significant overlap between the error bars for both the low temperature (black lines) and high

temperature (red lines). Although there is not much difference in the temperature dependence of system, the higher temperature does give slightly smaller particles, which is due to nucleation in the system. At higher temperatures, the nucleation process has more energy and more interaction in the system; thus, particles do not grow as large and overall smaller particles are produced.

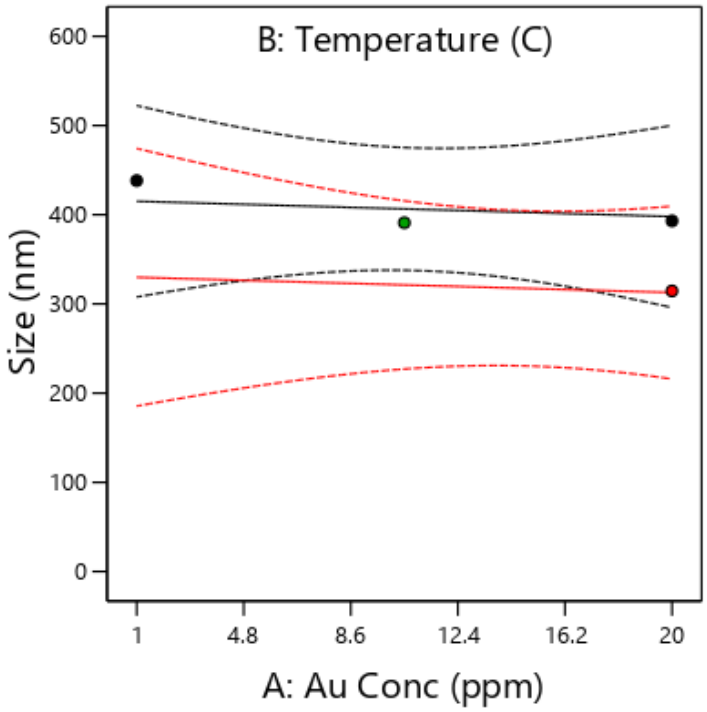

Figure 16: Secondary gold chloride system temperature and gold concentration interaction at 10 times thiol concentration.

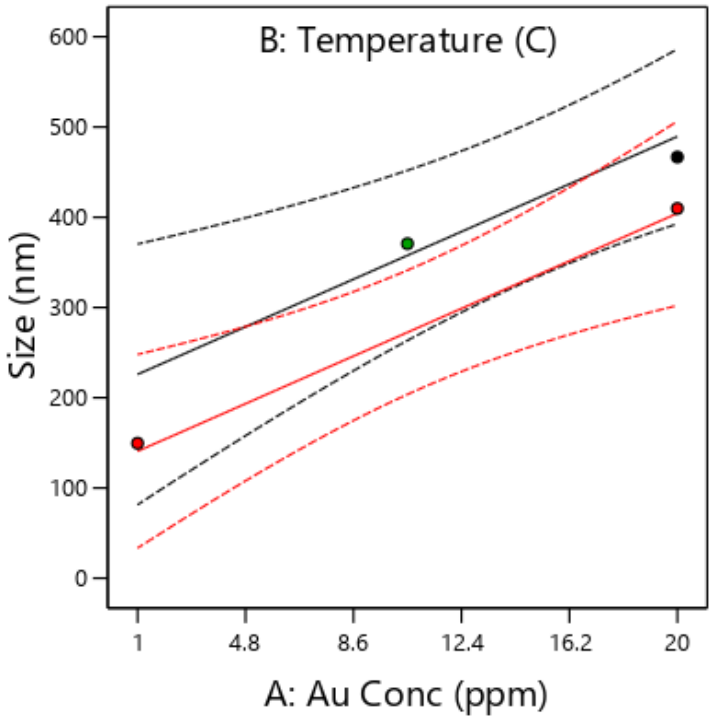

Figure 17: Secondary gold chloride system temperature and gold concentration interaction at no thiol concentration.

Figure 17 shows that gold concentration influences the size of the nanoparticles when thiol is not present in the solution. At 1 ppm gold concentrations and at high temperatures (red lines), the size of the particles is minimized. Because there is less total concentration in the solution at 1 ppm, the overall size of the particle is smaller. The particle cannot grow as large due to the lower amount of gold present in the area. At higher concentration, there is a higher concentration in the solution, which allows for a higher probability of gold in a given space. So, the particles are able to grow larger within this small range of concentration differences. This result is possible since there is no stabilizer present in the solution to inhibit the growth of the AuNPs, and the low concentration ranges of this system.

Figure 18 shows the transition point between no thiol present and ten times thiol concentration. In this regard, the effects at 5 times thiol concentration are revealed. The results

show the change from a positive slope in Figure 17 to a negative slope in Figure 16. Additional model graphs can be seen in Appendix A.

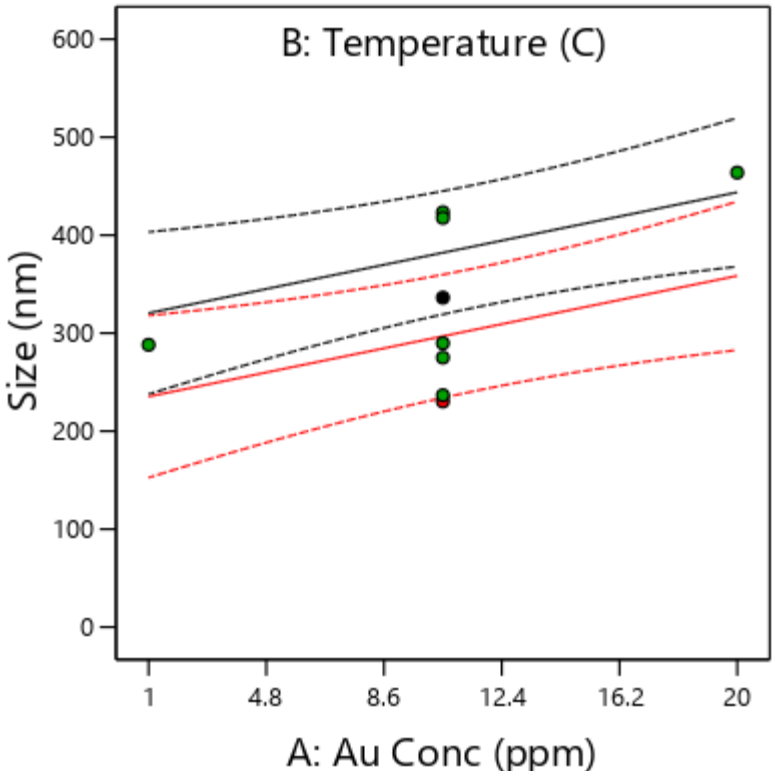

Figure 18: Secondary gold chloride system temperature and gold concentration interaction at 5 times thiol concentration.

The fit statistics for the size model can be seen in Table VIII. From this table, it can be seen that the fit statistics are fairly high for the model. Two confirmation test points were run, and both were within the boundaries predicted by the model, as can be seen in Table IX. From both the test points and the fit statistics, it can be said that the model has predictive power.

Table VIII: Design Expert secondary gold chloride system size model fit statistics.

R^2	0.6561
Adjusted R^2	0.5415
Predictive R^2	0.5194
Adequate Precision	10.3979

Table IX: Secondary gold chloride system confirmation points for the size response that shows the conditions and responses for the experiments.

System and Test Point	Response	Predicted Mean	Predicted Median	Standard Deviation	n	SE Pred.	95% PI Low	Data Mean	95% PI High	Au Conc. [ppm]	Temp. [°C]	Thiol Conc.
Secondary Chloride 1	Size	363.4080	363.4080	61.8650	1	65.8530	219.9270	475.2000	506.8900	16	50	3
Secondary Chloride 2	Size	343.0010	343.0010	61.8650	1	65.5050	200.2780	402.9000	485.7240	7	40	7

3.2.2.2. Zeta Potential Model

The zeta potential model used three runs from each Malvern analysis set and the averaged data was used in the model. The model was shown to be significant in a 90% interval instead of the standard 90% interval, as can be seen in the ANOVA data in Table X. All of the factors seen in Table X, except the individual gold concentration factor, were shown to be significant in the model. Even though the individual gold concentration factor was not significant, it had to be kept in the model since the squared gold concentration factor was significant.

Table X: ANOVA table showing secondary gold chloride system zeta potential response model statistics.

Source	Sum of Squares	df	Mean Square	F-Value	p-Value
Model	637.58	4	159.4	2.5	0.0981
A-Au Conc. [ppm]	43.75	1	43.75	0.6865	0.4235
C-Thiol Conc.	224.74	1	224.74	3.53	0.0849
A^2	256.41	1	256.41	4.02	0.068
C^2	302.26	1	302.26	4.74	0.0501
Residual	764.8	12	63.73		
Lack of Fit	620.81	8	77.6	2.16	0.2389
Pure Error	143.99	4	36		
Cor Total	1402.38	16			

Figure 19 shows that the zeta potential changed slightly between the lowest and highest gold concentrations. The zeta potential was most negative at a gold concentration of 10.5 ppm. The difference across the model is very minimal between the gold concentrations, but, overall, shows the ideal concentration required to get the most stable solution. When no thiol is present (black line), the zeta potential was higher. At ten times thiol concentration (red line), the zeta potential was more negative. This is due to the thiol creating a more negatively charged surface on the particle. Consequently, the more thiol that was present, the more stable the solution becomes because of this negatively charged surface. Additional model graphs can be seen in Appendix A.

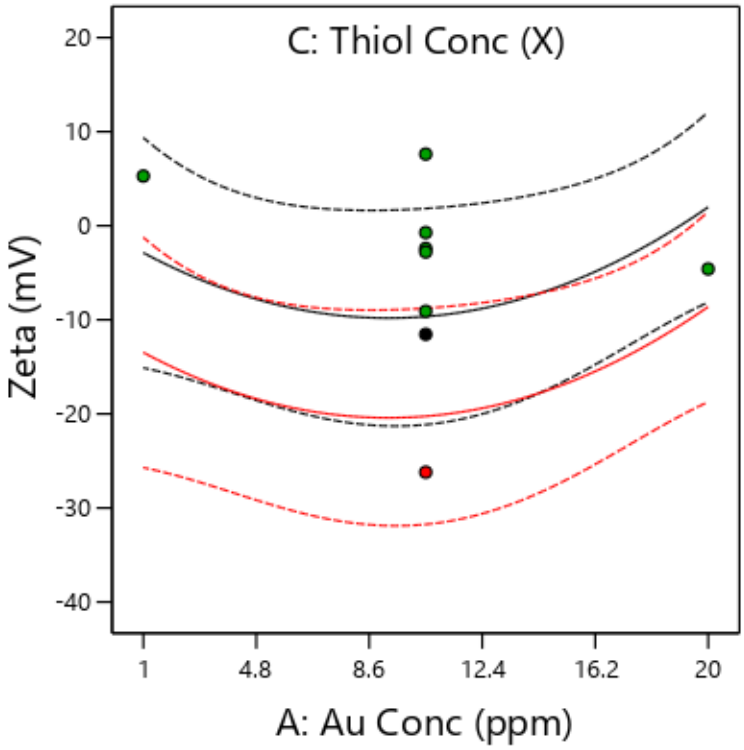

Figure 19: Secondary gold chloride system gold concentration and thiol concentration interaction.

The fit statistics for the model can be seen in Table XI. From this table, it can be seen that the fit statistics are low for the model. Two confirmation test points were run, and one were within the boundaries predicted by the model, as can be seen in Table XII. From this, it can be said that the model has predictive power.

Table XI: Design Expert secondary gold chloride system zeta potential model fit statistics.

R^2	0.4542
Adjusted R^2	0.2729
Predictive R^2	0.0176
Adequate Precision	6.2224

Table XII: Secondary gold chloride system confirmation points for the zeta potential response that shows the conditions and responses for the experiments.

System and Test Point	Response	Predicted Mean	Predicted Median	Standard Deviation	n	SE Pred.	95% PI Low	Data Mean	95% PI High	Au Conc. [ppm]	Temp. [°C]	Thiol Conc.
Secondary Chloride 1	Zeta	0.0625	0.0625	7.9833	1	8.5252	-18.5122	-18.6800	18.6372	16	50	3
Secondary Chloride 2	Zeta	-8.3156	-8.3156	7.9833	1	8.4889	-26.8113	-2.3190	10.1802	7	40	7

3.2.3. Dynamic Light Scattering Size Analysis

Malvern Zetasizer results showed there were one or two peaks for each run of the machine within the detectable regions of the instrument. The results showed some nanoscale particles, near-nanoscale particles, and agglomerates. Sizing data for this set of experiments showed that the gold chloride system can produce individual AuNPs, but not consistently throughout all the experiments. The data that was utilized in the design of experiments for the size model included the AuNPs in the total average size of the particles since the data for this secondary system had data that was near nanosized and smaller sized agglomerates overall. The peaks that were not within the limits of the detectable region were excluded from the overall size average for each experiment. Figure 20 shows an example of the Malvern Zetasizer data output for the size distribution.

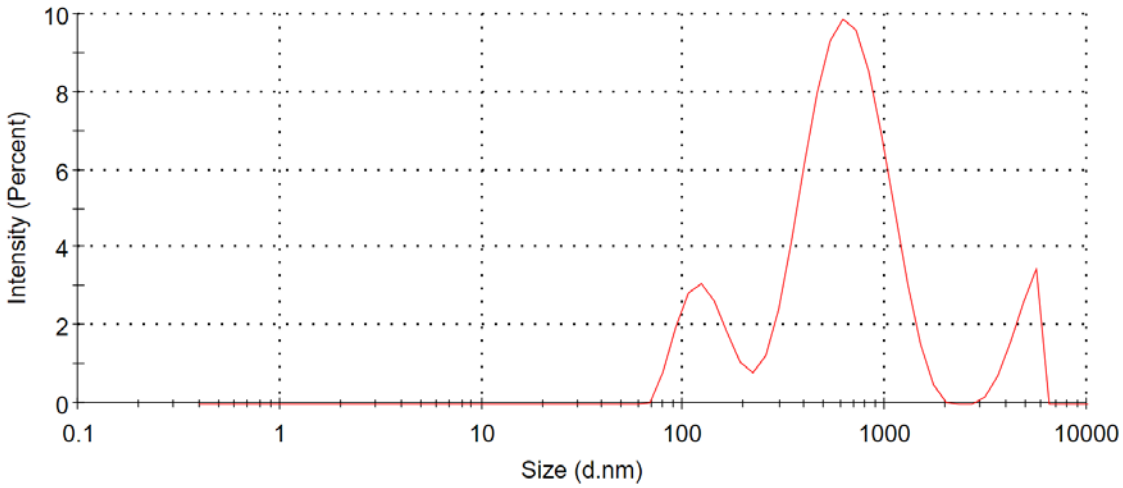

Figure 20: STD18Run6 record 3 Malvern Zetasizer size data

3.2.4. Field Emission Scanning Electron Microscopy

The AuNPs were able to be visualized, but the edge imagery of the particles was not clearly visible. Various shapes and sizes of nanoparticles were visible on the samples. With the FESEM imaging, the sizes observed mostly matched up with the data from the Malvern Zetasizer, but, occasionally, gold particles were larger than what the Malvern Zetasizer data indicated. Some images support the explanation that the nanoparticles were being connected by the anionic MPS and growing in conjunction with the connection. The Malvern Zetasizer analysis data also shows wide size peaks, meaning that the visualized sizes within the samples varied around a central size that was taken as the average size for that peak.

Some of the interparticle ripening that has been seen before in systems was observed on these AuNPs. Although the particles still tended to be mostly spherical, some of the particles had other shapes attached to the spherical particle. Figure 21 is an example of what was seen within these samples, with globular and spiked edges off a spherical AuNP. Figure 22 shows the spherical particles were also commonly found within this secondary gold chloride experiments.

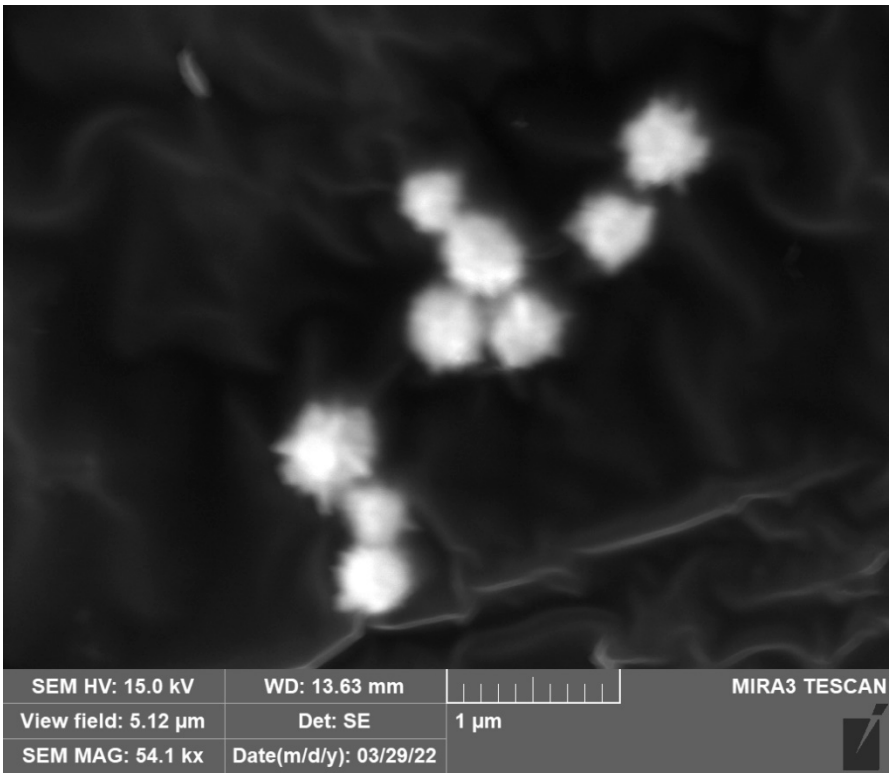

Figure 21: STD2Run10 image 1 SE showing examples of spherical particles with spikes attached.

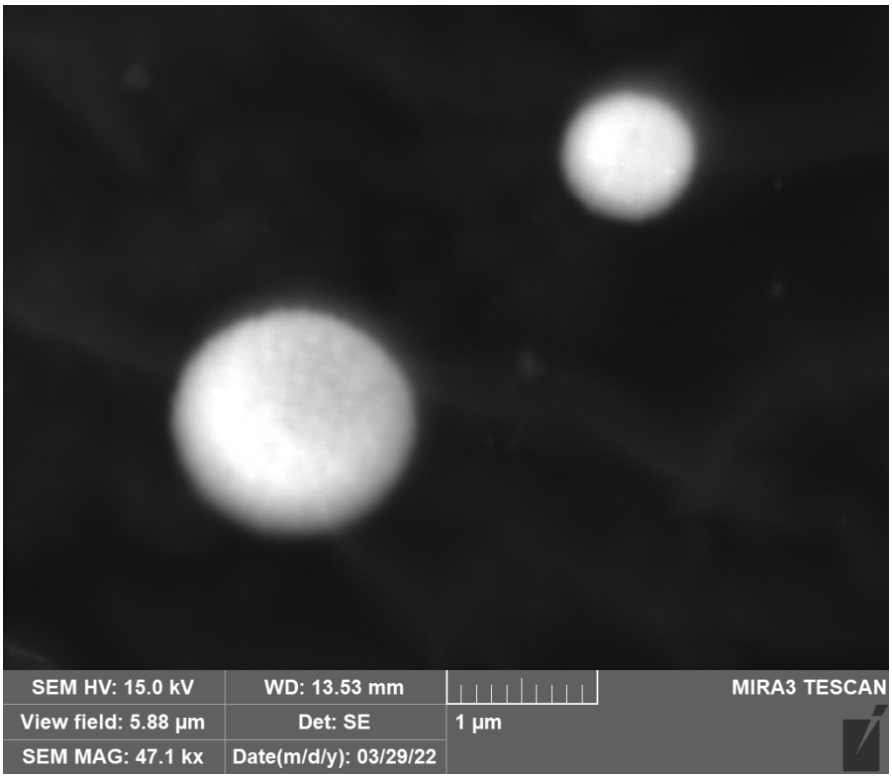

Figure 22: STD10Run17 image 2 SE showing spherical particles.

Some of the particles within the system did not give results that matched up with the particles found in the FESEM imaging. Figure 22, for instance, shows a particle over a micron in diameter, while the average size for that STD10Run17 was 463.9 nm. The reason for this discrepancy appears to be the wide peaks given from the Malvern Zetasizer analysis, as well as the reported particle size being an average across the peak. The other particle in Figure 22 is about 600 nm which is much closer to the average size from the Malvern Zetasizer. Additional images of this system can be found in Appendix C.

Typically, transmission electron microscopy (TEM) is recommended for nanosized particles due to its imaging range, but due to equipment limitations at the time of experimentation, the TEM was not utilized.

3.2.5. Zeta Potential Analysis

Zeta potential data for this secondary system gave results that fluctuated between positive and negative values. The average of the three data points were used for the zeta potential statistically designed model. Because of this analysis methodology, the average reflected both the positive and negative values gathered during analysis. The fluctuation is seemingly due to the surface charge of the particles changing due to how much thiol is attached to each particle.

3.3. Gold Cyanide System

3.3.1. Synthesis

Resulting solutions during these tests were clear suggesting that the AuNPs were suspended. Examples of the color of these solutions can be seen in Figure 23. Parafilm was used over the top of solutions to ensure that the solution did not evaporate while at the temperature requirement. The solutions did not have any particular problems with synthesis and no

coagulation was visible even after a few days or months. This could be due to the small gold concentration amount in these samples.

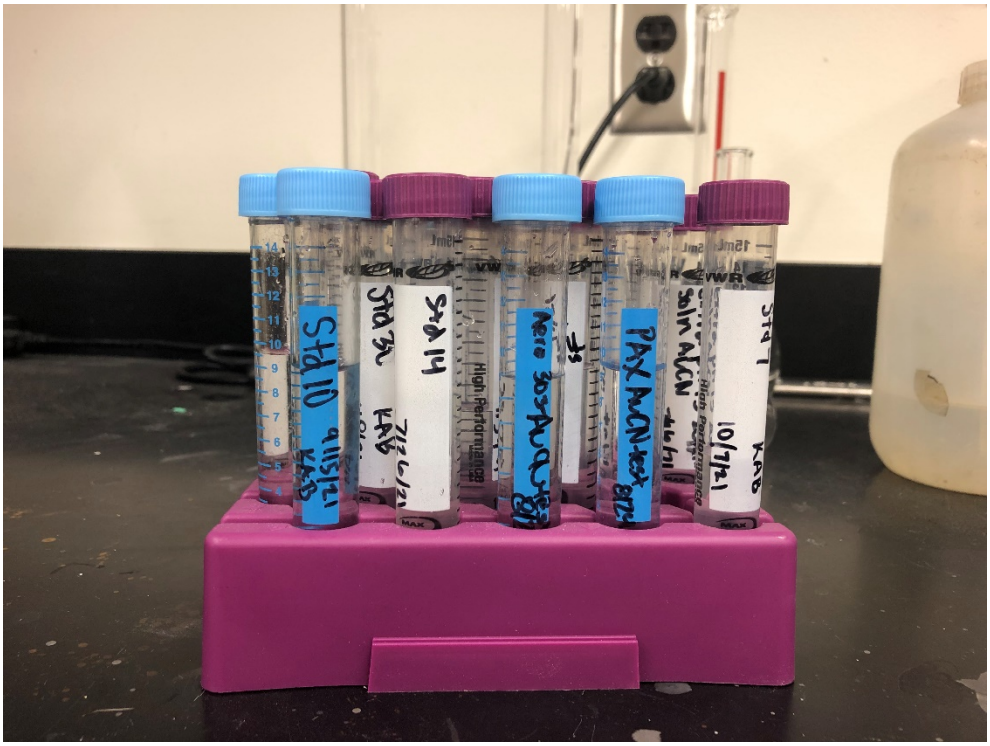

Figure 23: Examples of the clear solutions from the gold cyanide system.

3.3.2. Design of Experiments

3.3.2.1. Size Model

A few outliers within the system were tested again. Average sizes of the particles from the Malvern Zetasizer data were calculated and input into the Design Expert model. The average included only the agglomerate data, meaning the data ranged from 101-999 nm. The nanoscale size particles were not used in the design because of their effect on the averages since the presence of nanoscale particles was inconsistent. Not including these nanosized particles in the average size data input into the model was purely to understand how the solutions were producing a majority of the particles, and not the experiments that contained the outlier of a nanoscale particle. The ANOVA analysis for the model can be seen in Table XIII, where the pH

factor as well as all the squared factors shown were significant. Even though the gold concentration and thiol concentration factors were not individually significant, they had to be included in the model because the squared factors of gold concentration and thiol concentration were significant. The model overall was shown to be significant with a p-value of 0.0005.

Table XIII: ANOVA table showing gold cyanide system size response model statistics.

Source	Sum of Squares	df	Mean Square	F-Value	p-Value
Model	1.16E+05	6	19264.12	6.3100	0.0005
A-Au Conc. [ppm]	311.31	1	311.31	0.1019	0.7524
C-pH	43595.21	1	43595.21	14.2700	0.0010
D-Thiol Conc.	3222.87	1	3222.87	1.0500	0.3150
A^2	12711.14	1	12711.14	4.1600	0.0530
C^2	23828.48	1	23828.48	7.8000	0.0103
D^2	36732.56	1	36732.56	12.0200	0.0021
Residual	70262.49	23	3054.89		
Lack of Fit	58403.81	18	3244.66	1.3700	0.3905
Pure Error	11858.68	5	2371.74		
Cor Total	1.86E+05	29			

Figure 24, Figure 25, and Figure 26 show the low, middle, and high point conditions, respectively, with the corresponding size model results. Temperature was shown to not be included within the model; therefore, the sizing data has no variation across the entire range. Gold concentration, pH and thiol concentration all had similar trends which only shifted the graph up or down based on the set point of the conditions.

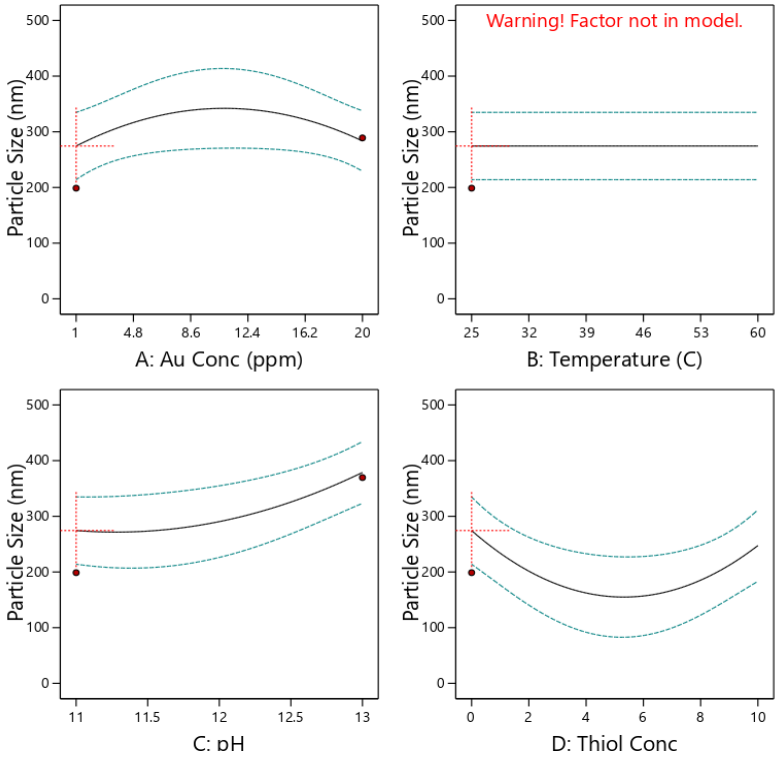

Figure 24: Design Expert all factor responses for size at low point conditions.

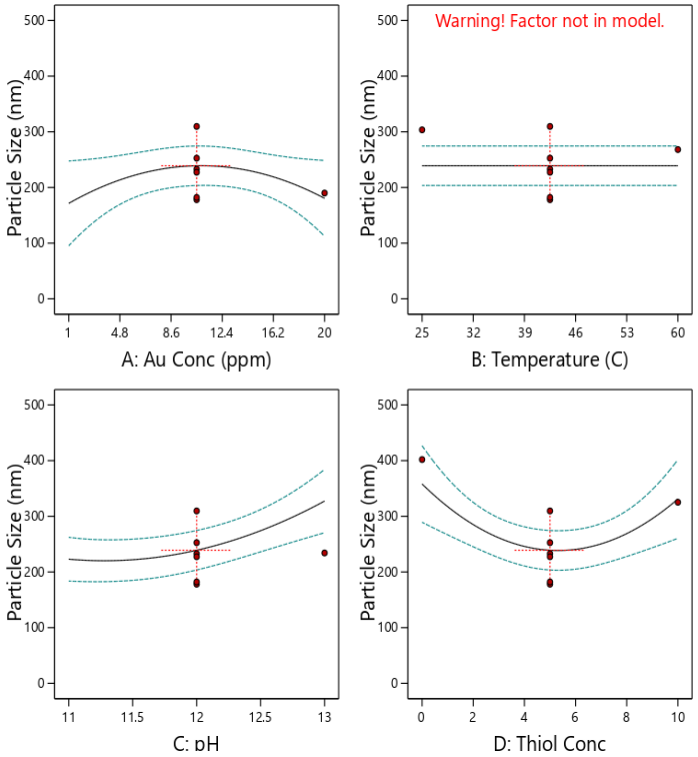

Figure 25: Design Expert all factor responses for size at midpoint conditions

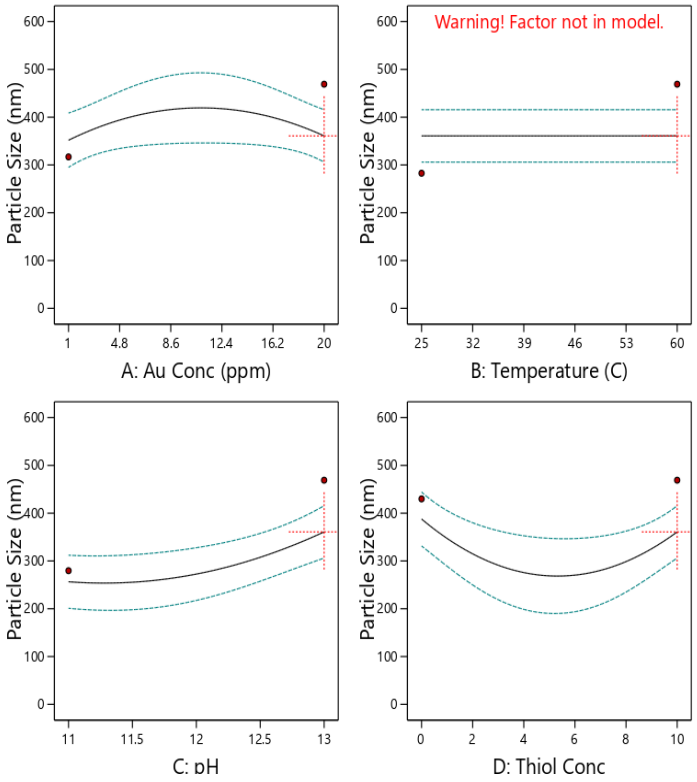

Figure 26:Design Expert all factor responses for size at high point conditions.

Based on the model, the AuNPs are agglomerated with sizes exhibiting a minimum at both the highest and the lowest concentrations. This has been determined to be from the fluctuation in the sample from the competing nucleation sites. It is a very minimal shift, but the competition of particles at the lowest concentration of 1 ppm gives a particle size of roughly 180 nm. A gold concentration of 20 ppm also gives a similar result of about 190 nm. The midpoint of 10.5 ppm has the local maximum of roughly 220 nm. It is hypothesized that this small fluctuation is due to the 20 ppm experiments having relatively more competing nucleation sites than the 10.5 ppm samples, thus making each individual particle smaller overall. The downward trend of size after 10.5 ppm means that after this point, competing nucleation points is no longer the driving factor when determining particle size. The gold concentration in the solution is so sparse that the gold particles stay a smaller size overall.

The pH was a factor that did influence the system. As pH increased, the particle size also increased. It was determined that this appears to be because of competing reactions on the site of the particles. As pH increases, there is more cyanide ions and hydronium ions present in the solution. The increase in this particle size of about 310 nm on the higher pH values means that the outer surface of the gold particles is being surrounded by anions in the solution instead of the potentially present thiol in some of the solutions. Lower pH values gave an average particle size of about 220 nm. Overall, the trend increases across the pH.

Thiol concentration was another factor that did have an effect on the system. The local minimum for this factor is at the midpoint of five times thiol concentration at an average particle size of about 250 nm. With no thiol present, the largest agglomerates are at about 370 nm in size. Large sizes on the extreme ends of the graph make sense because there is no stabilizer present to inhibit the growth of the particles. At the maximum thiol concentration of ten times the required stoichiometric amount, there is also a larger average particle size than the midpoint, at a roughly 330 nm size. The reasoning for this is seemingly due to the competition of the thiol for different areas on the particles which could affect the overall growth of the particles. High concentrations of thiol could also be causing a coagulation effect in the solution with the anionic structure of the thiol providing two sites that can attach to particles. This could mean that both ends attach to different particles, and cause coagulation of the particles, similar to how polymeric chains effect solutions to flocculate particles.

Gold concentration, pH, and thiol concentration factors all interact with each other causing the particle size to fluctuate within these described boundaries depending on the exact numbers for each factor. The model has predictive power as shown by the statistics that can be seen in Table XIV, with the predictive R2 being positive and within a reasonable range to the

adjusted R2. Two confirmation points were experimented, and neither point was within the 95% confidence interval, as can be seen in Table XV. This implies that overall, the system has very little predicative power.

Table XIV: Design Expert gold cyanide system size model fit statistics.

R^2	0.6219
Adjusted R^2	0.5233
Predictive R^2	0.3698
Adequate Precision	8.7059

Table XV: Gold cyanide system confirmation points for the size response that shows the conditions and responses for the experiments.

System and Test Point	Response	Predicted Mean	Predicted Median	Standard Deviation	n	SE Pred.	95% PI Low	Data Mean	95% PI High	Au Conc. [ppm]	Temp. [°C]	pH	Thiol Conc.
Cyanide 1	Size	208.8220	208.8220	55.2711	1	59.6796	83.5366	461.0200	332.2790	18	50	11.04	3
Cyanide 2	Size	272.6650	272.6650	55.2711	1	58.5182	151.6110	415.5200	393.7200	8	30	12.16	8

3.3.2.2. Zeta potential model

A response was applied in Design Expert for the zeta potential results for each experiment. An average of the three runs for each experiment was input into the program to create the model. The ANOVA statistics stable can be seen in Table XVI, which shows that squared interaction parameters as well as the individual parameters in the model were significant, except for the individual thiol concentration factor. Even though individually the thiol concentration factor was not significant, it had to be included because the squared thiol concentration factor was significant. ANOVA analysis also showed that the model was significant overall, with a p-value of less than 0.0001.

Table XVI: ANOVA table showing gold cyanide system zeta potential response model statistics.

Source	Sum of Squares	df	Mean Square	F-Value	p-Value
Model	2341.90	7	334.56	9.5500	<0.0001
A-Au Conc. [ppm]	127.01	1	127.01	3.6300	0.0700
B-Temperature [°C]	153.63	1	153.63	4.3900	0.0480
C-pH	331.88	1	331.88	9.4700	0.0055
D-Thiol Conc.	18.38	1	18.38	0.5248	0.4764
B^2	1228.47	1	1228.47	35.0700	<0.0001
C^2	470.55	1	470.55	13.4300	0.0014
D^2	400.77	1	400.77	11.4400	0.0027
Residual	770.60	22	35.03		
Lack of Fit	600.98	18	33.39	0.7873	0.6819
Pure Error	169.62	4	42.41		
Cor Total	3112.50	29			

Figure 27, Figure 28, and Figure 29 show the low, middle, and high points conditions, respectively, of the system and the corresponding zeta potential results. The zeta potential model for the gold cyanide system showed that all four factors of gold concentration, temperature, pH, and thiol concentration, were significant either through interaction parameters or individually, as shown in Table XVI. The zeta potential gets more negative as the gold concentration increases in the system. This finding can be attributed to the nucleation sites increasing as the gold concentration increases. With more nucleation sites, the solution maintains more of a charge overall.

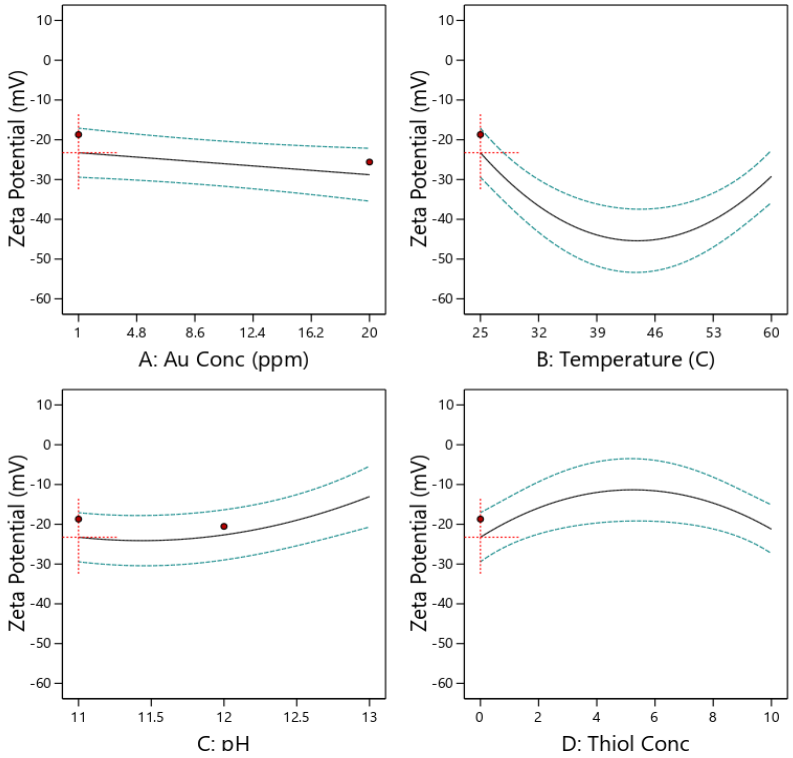

Figure 27: Design Expert all factor responses for zeta potential at low point conditions.

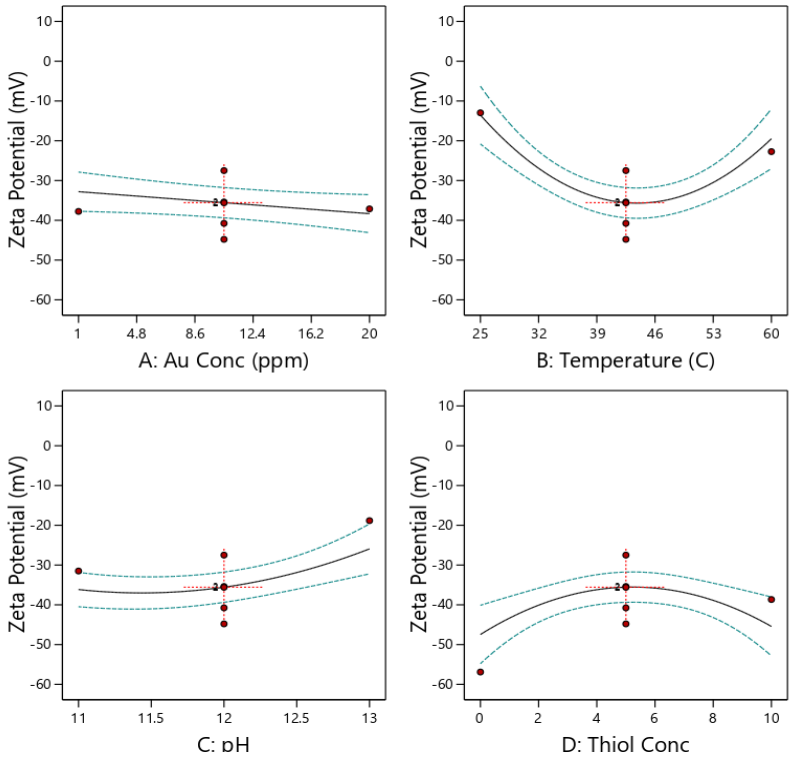

Figure 28: Design Expert all factor responses for zeta potential at midpoint conditions.

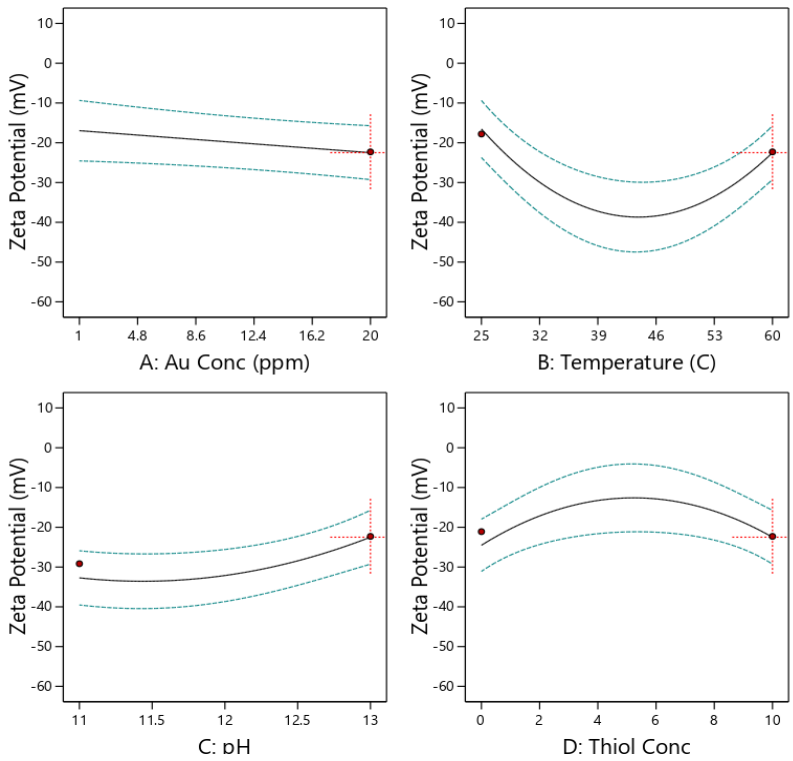

Figure 29: Design Expert all factor responses for zeta potential at high point conditions.

The temperature effect on the system shows a local minimum at the midpoint of 42.5°C at about -35 mV. In this regard, the effect of temperature on the system indicates that there is a temperature dependence, and the optimal temperature is around the midpoint. The most logical reason for this is that the solution has a need to be at that midpoint to maximize the stability of the solution. The solution vaporizes more readily at higher temperatures, and the parafilm becomes less effective in keeping the solution volume the same. It appears to be that this has contributed to the temperature effect observed in the model. A watch glass or another more solid lid would be more effective in keeping the solution volume constant.

Zeta potential generally became less negative as the pH increased. This is a similar trend for the pH as what was seen for the gold cyanide size Design Expert model. It is hypothesized that the reason for this is similar to that of the size model. There are competing reactions at the site of the particles. As the pH increases, there is more cyanide ions and hydronium ions present

in the solution. The change in the zeta potential to roughly -25 mV on the upper pH end means that the outer surface of the gold particles is being surrounded by these cyanide and hydronium ions instead of the potentially present thiol in some of the solutions. At the lower pH end, the data gives an average zeta potential of about -35 mV and is more negative due to less competition for space on the particle surface with the cyanide and the hydronium ions. Overall, the trend increases across the pH range tested.

The thiol concentration of the system has the least negative point at the midpoint of five times the stoichiometric requirement for the gold concentration. The zeta potential is most negative when no thiol is present in the solution with a zeta potential value of about -48 mV. So, the gold particles have some stability without the effect of the thiol stabilizer. As the surface is covered with more thiol, the charge in the system becomes less negative. In this regard, the solution becomes less stable since the particles are being covered by the thiol and do not have their natural stability as they have with no thiol. At ten times thiol concentrations, the zeta potential yet again becomes more negative. This could be due to a grouping effect where the thiol is attaching to multiple particles. Table XVII shows that the model has predictive power as shown by the statistics that can be seen in. With the predictive R^2 being positive and within a reasonable range to the adjusted R^2, it can be said that the system has predicative power. Two confirmation points were experimented, and both points were within the 95% confidence interval. This implies that overall, the system has predicative power.

Table XVII: Design Expert gold cyanide system zeta potential model fit statistics.

R^2	0.7524
Adjusted R^2	0.6736
Predictive R^2	0.5219
Adequate Precision	11.3529

Table XVIII: Gold cyanide system confirmation points for the zeta potential response that shows the conditions and responses for the experiments.

System and Test Point	Response	Predicted Mean	Predicted Median	Standard Deviation	n	SE Pred.	95% PI Low	Data Mean	95% PI High	Au Conc. [ppm]	Temp. [°C]	pH	Thiol Conc.
Cyanide 1	Zeta	-38.3046	-38.3046	5.9184	1	6.4196	-51.6180	-31.1333	-24.9912	18	50	11.04	3
Cyanide 2	Zeta	-25.3668	-25.3668	5.9184	1	6.2396	-38.3069	-37.3000	-12.4267	8	30	12.16	8

3.3.3. Dynamic Light Scattering Size Analysis

Results from the Malvern Zetasizer were obtained for all experiments. The Malvern Zetasizer parameters were set to the same settings that have been used for previous Purple of Cassius research. Three size distribution records were taken for each solution. The average of the three records was taken as the size of the AuNPs and gold agglomerates for that experiment.

Size data from the Malvern for this system showed that the samples mostly had one or two size peaks, and occasionally a third peak within the boundaries of the detectable regions of the systems. Extraneous results outside the boundaries of the system were ignored when averaging the size data, such as above 1000 sized peaks. Very few particles in the micrometer range were seen in the FESEM results; therefore, these results were deemed to be from error within the system from overlapping particles on the DLS. Malvern Zetasizer sizing data had AuNPs present in some of the experiments but not in all of them. The nanoparticle data was not included in the average size used for the design of experiments modelling. Figure 30 shows an

example of the Malvern Zetasizer size distribution data from the gold cyanide system. The nanosized and the near nanosized size distribution can be seen in this image.

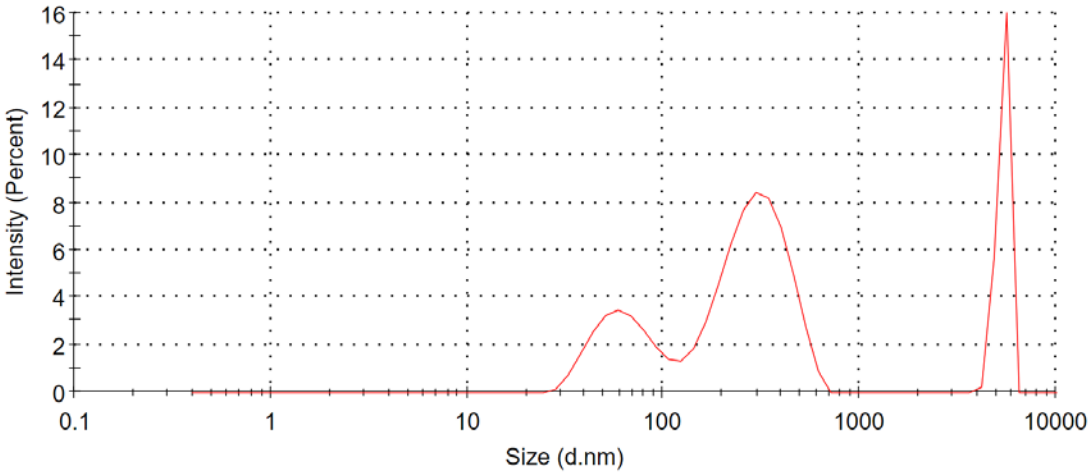

Figure 30: STD2Run30 record 1 Malvern Zetasizer data

3.3.4. Field Emission Scanning Electron Microscopy

Only some of the samples showed individual AuNPs and agglomerates. Some examples of this can be seen in Figure 31, Figure 32, Figure 33, and Figure 34. Figure 31 and Figure 32 show the direct difference between using the no MPS and MPS, respectively. The two images are at the same magnification and demonstrate the agglomerates are smaller with the MPS added to the otherwise same experiment conditions.

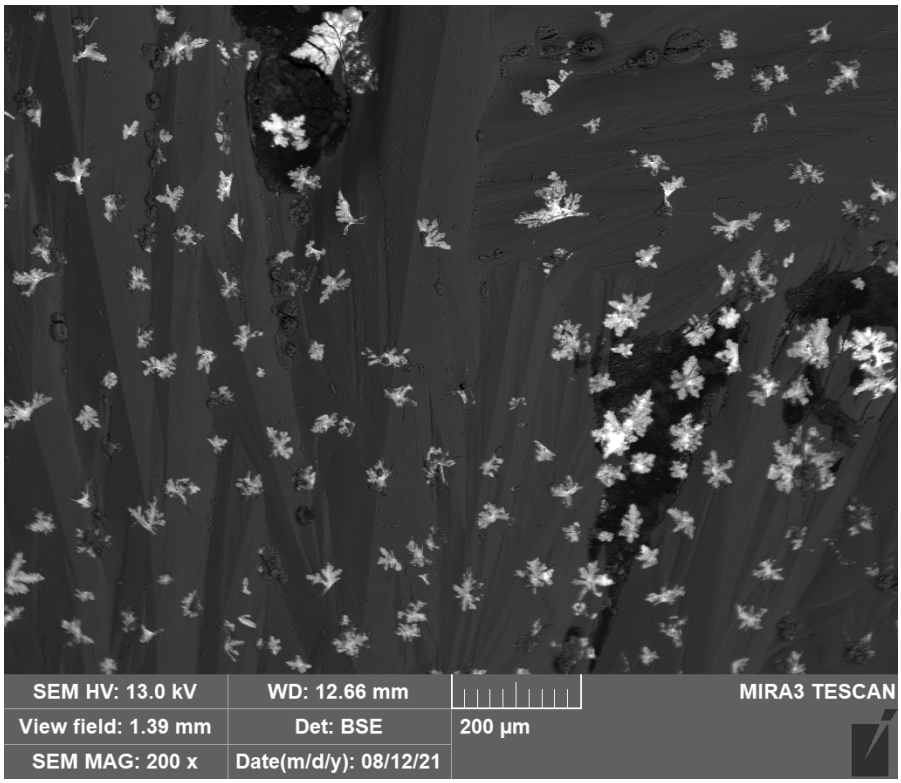

Figure 31: Conditions of 20 ppm, 13 pH, no thiol added, and 25°C produced snowflake like structures.

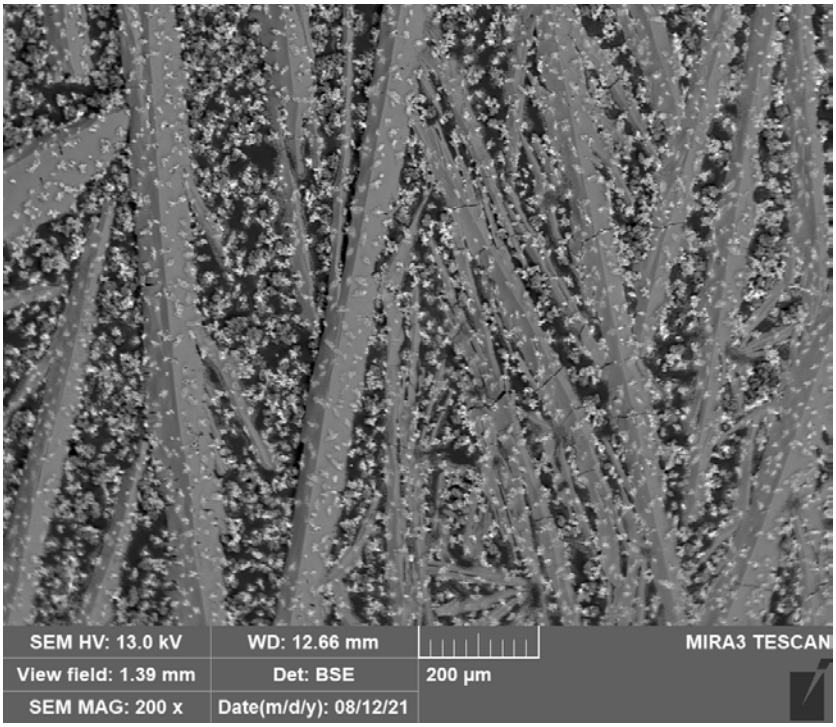

Figure 32: Conditions of 20 ppm, 13 pH, 10X stoichiometric value thiol added, and 25°C produced snowflake like structures.

Figure 33 shows a few individual AuNPs that are about 100-200 nm in diameter. The image was taken using BSE, so the salt substrate that is dried on the surface impedes the imaging from having clear edges. Various techniques to clear up these edges were used to create images like this one.

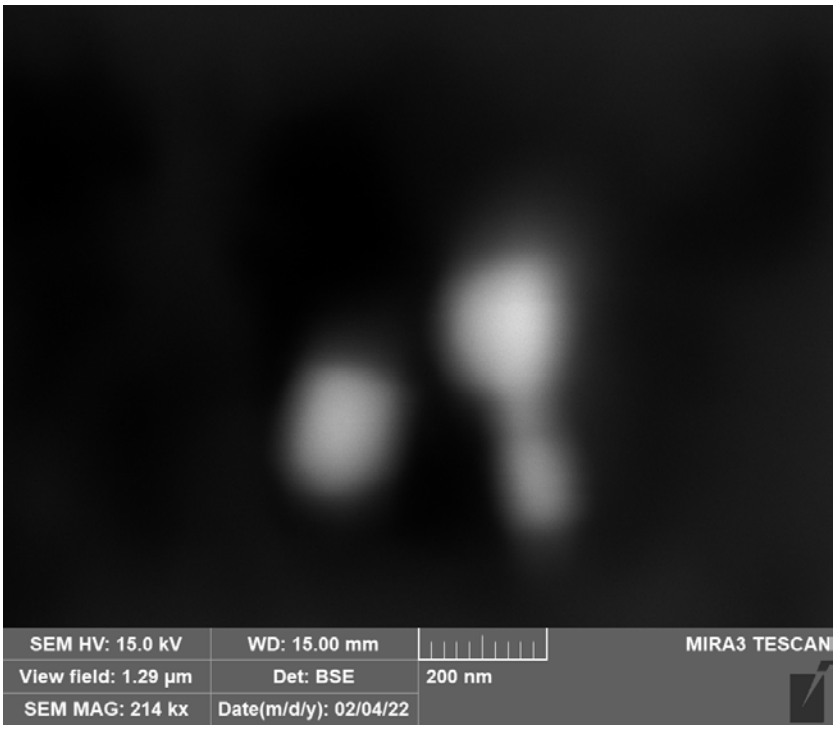

Figure 33: Conditions of 10.5 ppm, 12 pH, 10X stoichiometric value thiol added, and 42.5°C produced nanoparticles.

Figure 34 shows a few AuNPs that are outlined in red circles, as well as an agglomerate that is in the upper half of the image. The edge clarity on these images is poor, but many efforts were taken to increase the clarity of the particles to this level.

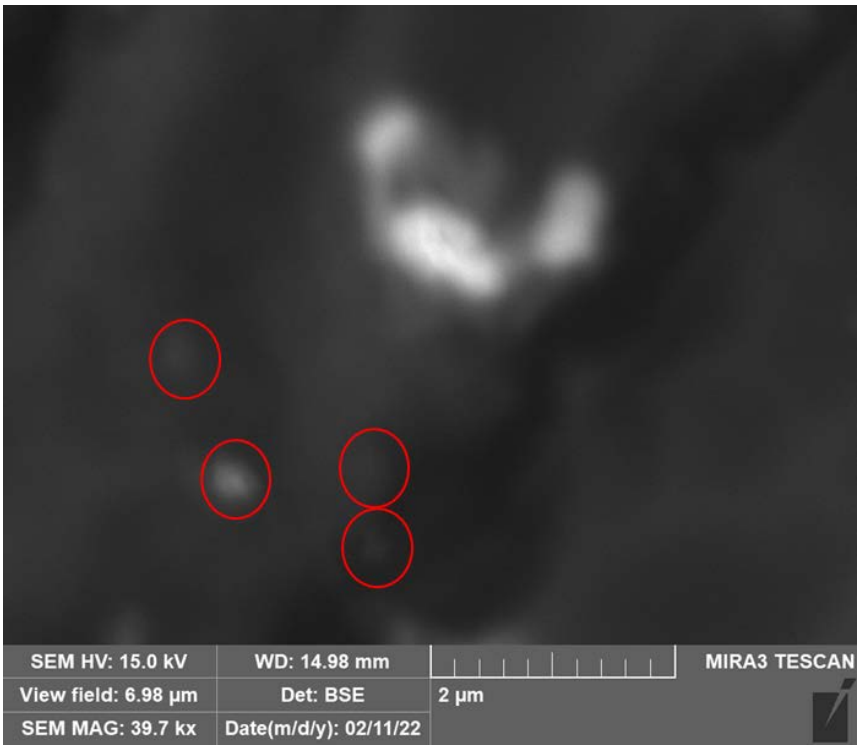

Figure 34: Conditions of 20 ppm, 11 pH, 10X stoichiometric value thiol added, and 25°C produced nanoparticles and agglomerates.

FESEM images for this system showed that some samples did have nanoscale particles which concurs with the results from the Malvern. The AuNPs do have some level of variation once dried on the SEM stub, so the comparison unfortunately is not 1:1. The Malvern uses an overall average of the data in the region of the peak, meaning there is some variation within the width of those peaks.

Some samples were not able to be imaged for several reasons including the dried solution creating salts covering the gold particles, the particles being washed off by the washing technique, and the gold concentrations being so low that the samples had virtually no gold particles on them. The washing technique was only used when the solution could not be imaged as is. Washing continued until it was determined that no particles could be found on the sample.

The samples that were imaged agreed with other samples in the size and shape of the particles. Most of the particles found were spherically shaped.

Some impurities were found on the samples depending on their composition. One potential source of these impurities includes the temperature probe that was used for the experiment which was made of stainless steel. This probe corroded after being introduced to the highly basic solution in this system, as well as the highly acidic solutions in the gold chloride system. Another potential source of these impurities is the general laboratory glassware and equipment. Many precautions were taken to avoid contamination of the solutions including using equipment separate from the rest of the general laboratory equipment. Given that these solutions are at such low concentrations, it is not surprising that contamination did occur in some of the samples. None of the contaminants found were determined to be consequential in the synthesis of the AuNPs or gold agglomerates. Additional images of this system can be found in Appendix D.

Typically, transmission electron microscopy (TEM) is recommended for nanosized particles due to its imaging range, but due to equipment limitations at the time of experimentation, the TEM was not utilized for any of the systems.

3.3.5. Zeta Potential Analysis

Zeta potential results for the gold cyanide system showed consistently negative results. The parameters were set to the same settings that have been used for previous Purple of Cassius research. Three zeta potential records were taken for each solution. The average of the three records was taken as the overall zeta potential of the solution for that experiment.

Zeta potential data for this system had a number of peaks, all of which were negative. The average of the three runs for each experiment was used for the design of experiments model

for the zeta potential response. The data generally was within a close range of each other and so the averages were within reasonable agreement with the initial data.

3.3.6. Other Stabilizer Trials

Other chemicals were tested as stabilizers due to their similar structure to the MPS. Two such chemical were potassium ethyl xanthate (KEX) and potassium amyl xanthate (PAX). Figure 35 shows the agglomerate shape that the PAX produced in the solution. This agglomerate is quite large at roughly 40 micrometers wide, with smaller particles within the agglomerate. The general shape of the agglomerate is a snowflake structure with individual sections growing off from a central point. The individual particles within the agglomerate are generally spherically shaped.

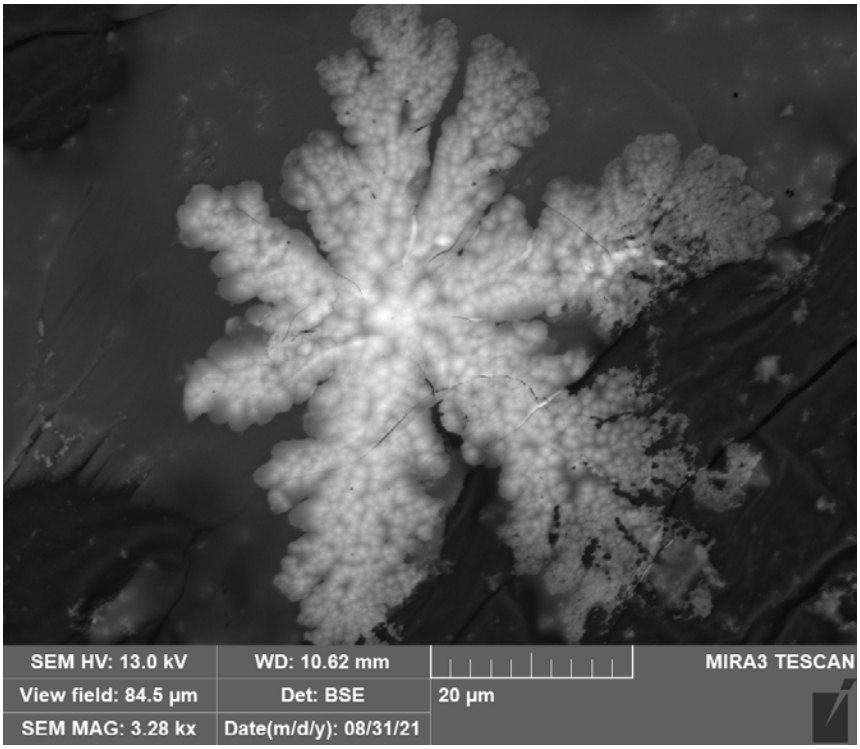

Figure 35: PAX added to 20 ppm gold cyanide solution.

Figure 36 shows the result of using the KEX as a stabilizer in a 20-ppm gold cyanide solution. The particles are generally spherical within a cauliflower like structure. Individual

AuNPs can been seen on the right side of the figure on the carbon tape. The KEX overall produced smaller sized agglomerates than the PAX. Neither stabilizer produced solely AuNPs.

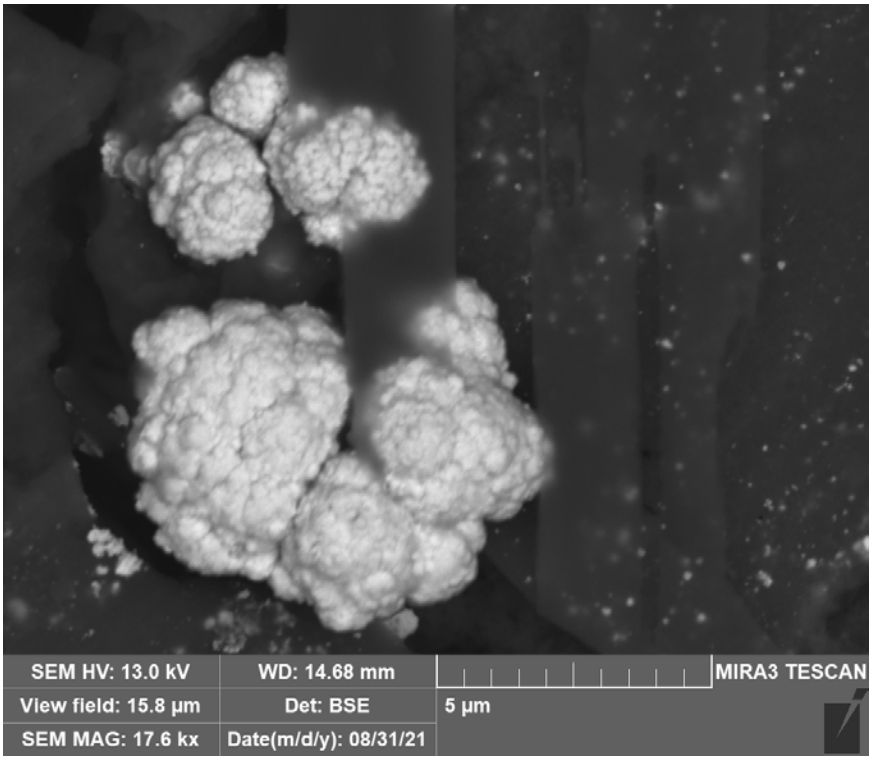

Figure 36: KEX added to 20 ppm gold cyanide solution.

One more alternate stabilizer, Orfom D8, was tested at five times and ten times stoichiometric requirements to account for all gold in the solution. Because Orfom D8 comes in a diluted aqueous form, the total volume of the solution changes drastically. Orfom D8 was tested a number of times and produced some interesting results. The solutions had both 1-10 nm sized data as well as 700 nm sized particles. This mismatch between the sizes led to doing more tests at various other concentrations of Orfom D8 within the solution.

The color of the solution for the D8 experiments also drastically changes from the clear color normally seen with the gold cyanide system due to the orange color that the D8 solution has independently. Malvern Zetasizer results gave results of around 1 and 700-4000 nm for the various Orfom D8 experiments. The particles that were able to be imaged were better visualized

using the BSE instead of the SE, since the particles were encapsulated in the dried Orfom D8 solution matrix that turned gel like. An example of the difference between the BSE and SE detector clarity on the particles can be seen in Figure 37 and Figure 38, respectively.

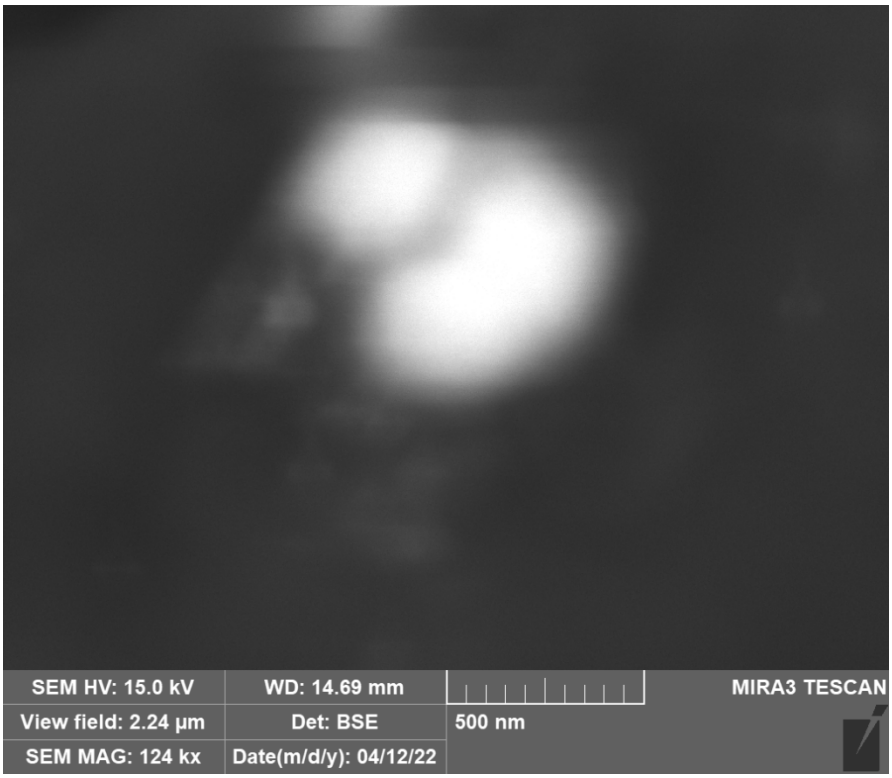

Figure 37: Globular gold particle agglomerate imaged in an Orfom D8 experiment with BSE detector.

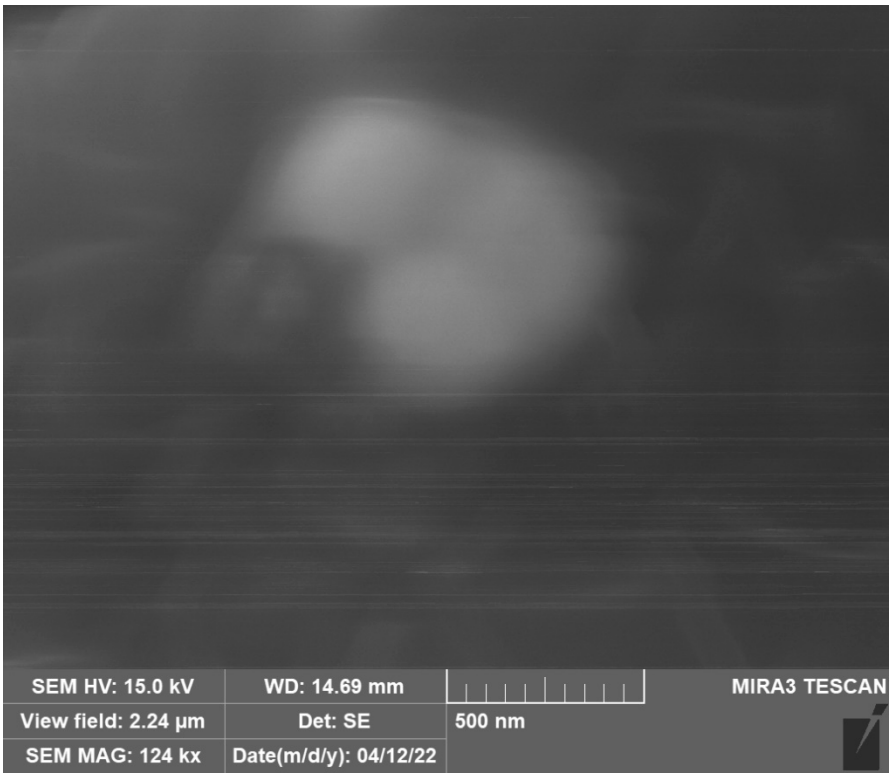

Figure 38: Globular gold particle agglomerate imaged from Orfom D8 experiment using SE detector.

Another example of the gold particles produced using Orfom D8 as the stabilizer can be seen in Figure 39 and Figure 40 with the BSE and SE detectors, respectively.

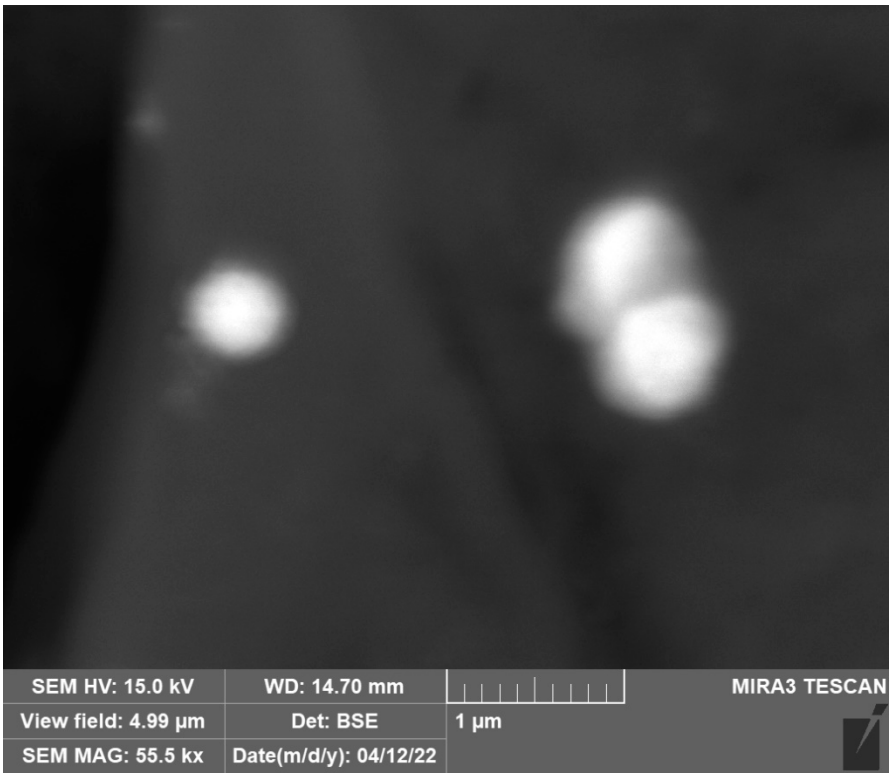

Figure 39: Gold particles from Orfom D8 experiments showing three separate particles with BSE detector.

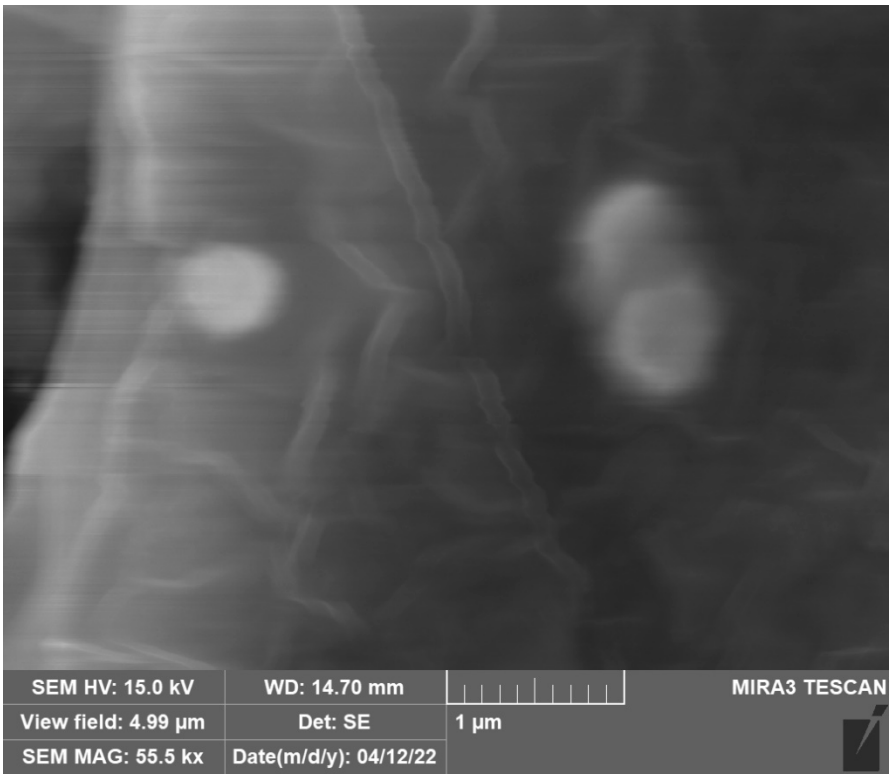

Figure 40: Gold particles from Orfom D8 experiments showing three separate particles with SE detector.

3.4. Comparison

3.4.1. Gold Chloride to Gold Cyanide System

Overall, the gold cyanide system generally gave more samples with individual AuNPs in comparison to the gold chloride system, as can been seen within the tables in Appendix E. The gold chloride system was able to produce smaller particles once the gold concentration in the system was decreased from the 5-500 ppm to 1-20 ppm. All three models still showed that the overall average of the gold particles was well above nanoscale. Within all three experimental models, the nucleation sites of the particles were an overarching factor. At higher temperatures for the gold chloride system, the particles were smaller in size. The gold cyanide system did not have temperature as a contributing factor of the size of the gold particles. In the gold cyanide system, the smallest particles were achieved at five times thiol concentration, but the secondary gold chloride system had the smallest particles at a 1ppm gold concentration and no thiol present. The thiol addition in the gold chloride system at a ten times concentration made the size difference between the different gold concentrations negligible.

Overall, the gold chloride system showed having less stable solutions as per the zeta potential results in comparison to the gold cyanide system. Also, the gold cyanide systems are more stable because they are negatively charged particles in solution with an anionic thiol (MPS) attached to the particles which induces a more negative charge on the particle. The gold cyanide system in return is more stable over time than the gold chloride system, which was evident by the comparison of the initial gold chloride system to the gold cyanide system.

3.4.2. Gold Chloride and Gold Cyanide Systems to Literature

The gold chloride system shows results that are consistent with the nucleation processes that happen at lower pH ranges but creates more agglomerates than seen in literature (Ji et al.,

2007). The gold cyanide system produces particles that look like the same slow growing nucleation process that happens at higher pH ranges (Ji et al., 2007). Both systems were able to produce some AuNPs consistent with regular sized nanoparticles found in the literature, but not always. The reproducibility of the gold chloride and gold cyanide system results is not reliable. From the experimentation within this document, the systems tended to have bimodal size distributions from the hydrodynamic size analysis from the Malvern ZetaSizer. The FESEM showed that the hydrodynamic size analysis did not always match up with the Malvern Zetasizer in the secondary gold chloride and the gold cyanide systems. Part of this could be due to AuNPs that are made within water tend to be less high quality and consistent in size in comparison to seeded growth of AuNPs (Jana et al., 2001; Ji et al., 2007; Nguyen et al., 2010).

Typically, the size of the AuNPs in most research is shown to be consistently in the nano range. For instance, the AuNPs from a gold (III) chloride and glucose system produced were on the range of 16.3 to 84.6 nm, with most of the results between 20 and 30 nm in diameter (Pacławski et al., 2012). In a gold chloride and citrate system, the size of the AuNPs ranged from about 15-60 nm in diameter and when using a revised method that range narrows down to 20-40 nm (Ji et al., 2007). Research on the gold chloride and tin chloride system produced AuNPs on the range of 5-30 nm within the colloidal solution (Vaskelis et al., 2007). The solution, in this case, did maintain both the AuNPs as well as the tin (IV) oxide precipitate (Vaskelis et al., 2007). Some of the particles in the initial gold chloride, secondary gold chloride, and gold cyanide systems had some AuNPs near this range but most of were in the larger size range of 200-900 nm.

Overall, the particles made in this research were less dependable for both size and shape in comparison to the gold chloride systems traditionally used. These gold chloride and citrate

systems are widely researched and have an abundance of kinetic, sizing, shape, and customization data available.

4. Conclusions

4.1. Initial Gold Chloride System

The size of the AuNPs was found to be dependent on both the temperature and the gold concentration. Within this system, the pH of the solution is not a contributing factor but does determine if tin oxide precipitates from the solution. Overall, the system did not produce many individual AuNPs but did produce agglomerates with AuNPs within the agglomerates. Consequently, the size of the nanoparticle agglomerates was found to be on the range on 300-1000 nm, whereas the individual nanoparticles were typically found to be on the range of 20-400 nm. Most of the nanoparticle structures had only spherical particles, with a few particles that exhibited some deformations that created edges or oval shaped particles.

4.2. Secondary Gold Chloride System

After refining the parameters from the initial system, the sizing data was generally smaller than the initial system. Results from this system showed that individual AuNPs were created, but not always below 100 nm. The particles showed signs of interparticle ripening when imaged using the FESEM. Two statistically designed models were created. The size model showed that the gold concentration, temperature, and thiol concentration were all contributing factors for the size of the gold particles. Contrastingly, the zeta potential model showed that only two of the variables, gold concentration and thiol concentration, were contributing factors to the zeta potential of the solution.

4.3. Gold Cyanide System

The gold cyanide system was found to create both AuNPs and gold agglomerates. The size Design Expert model determined that the gold concentration, pH, and thiol concentration were all contributing factors. Also, the zeta potential Design Expert model determined that all

four factors, gold concentration, temperature, pH, and thiol concentration, were contributing factors. Each of the factors interact with one another which also affects the overall AuNP size and zeta potential of the solutions. Both the size and zeta potential models have predictive power which means they can be used to predict another point within the boundaries of the system. The system produced generally spherical particles with some of them also being deformed with edges or more oval-like shapes.

5. Future Work

There is some future work that should be completed on both of these systems. Both systems should have TEM analysis completed on the samples, as well as UV-vis spectroscopy analysis completed to better understand the shape, size, and kinetics of the systems. Both systems should also be studied further to understand how the MPS is attaching to the AuNPs. This would lead to potentially understanding how to decrease the overall size of these gold particles produced in both the gold chloride and gold cyanide systems. A future possibility for the gold chloride with tin chloride system is to recycle the tin oxide precipitate through solvent extraction or ion exchange processes.

Longer experimentation should occur for the gold cyanide system to determine if longer reaction periods would decrease the variation in the size distributions of the particles. Methods such as flow microreactor systems have shown promise in controlling the size distributions of particles in a gold (III) chloride and glucose systems stabilized with polyvinylpyrrolidone (PVP) (Pacławski et al., 2012). The gold cyanide system was clearly shown to yield AuNPs and should therefore be examined in more detail. Also, the gold cyanide system should have further studies on using Orfom D8 and other froth flotation chemicals as stabilizers. The potential in this area is vast for using different stabilizers in these alkaline systems.

Bibliography

Acharya, D., Mohanta, B., Deb, S., & Sen, A. K. (2018). Theoretical prediction of absorbance spectra considering the particle size distribution using Mie theory and their comparison with the experimental UV–Vis spectra of synthesized nanoparticles. *Spectroscopy Letters*, *51*(3), 139–143. https://doi.org/10.1080/00387010.2018.1442351

Amendola, V., & Meneghetti, M. (2009). Size evaluation of gold nanoparticles by UV-vis spectroscopy. *Journal of Physical Chemistry C*, *113*(11), 4277–4285. https://doi.org/10.1021/jp8082425

Fisher Scientific. (n.d.-a). *Potassium Amylxanthate 97.0%*. https://www.fishersci.com/shop/products/potassium-amylxanthate-tci-america/A046125G

Fisher Scientific. (n.d.-b). *Potassium ethyl xanthate, 97%*. https://www.fishersci.com/shop/products/potassium-ethyl-xanthate-97-thermo-scientific/AAA1145036?searchHijack=true&searchTerm=potassium+ethyl+xanthat&searchType=RAPID&matchedCatNo=potassium+ethyl+xanthat

Habashi, F. (2016). Purple of Cassius: Nano Gold or Colloidal Gold? *European Chemical Bulletin*, *5*(10), 416–419. https://doi.org/10.17628/ECB.2016.5.416

Heiligtag, F. J., & Niederberger, M. (2013). The fascinating world of nanoparticle research. In *Materials Today* (Vol. 16, Issues 7–8, pp. 262–271). https://doi.org/10.1016/j.mattod.2013.07.004

Hughes, C. (2021). *Synthesis of Nano-Au from Potassium Gold Cyanide Conc.*

Jana, N. R., Gearheart, L., & Murphy, C. J. (2001). *Wet Chemical Synthesis of High Aspect Ratio Cylindrical Gold Nanorods*. 4065–4067.

Ji, X., Song, X., Li, J., Bai, Y., Yang, W., & Peng, X. (2007). Size control of gold nanocrystals in citrate reduction: The third role of citrate. *Journal of the American Chemical Society*, *129*(45), 13939–13948. https://doi.org/10.1021/ja074447k

Kestell, A. E., & DeLorey, G. T. (2010). *Nanoparticles: Properties, Classification, Characterization, and Fabrication* (A. E. Kestell & G. T. DeLorey (eds.); 1st ed.). Nova Science Publisher, Inc.

Kumar, A., & Dixit, C. K. (2017). 3-Methods for characterization of nanoparticles. *Advances in Nanomedicine for the Delivery of Therapeutic Nucleic Acids*, 43–58.

Lata, K., Jaiswal, A. K., Naik, L., & Sharma, R. (2015). Gold Nanoparticles: Preparation,

Characterization and Its Stability in Buffer. *Nano Trends: A Journal of Nanotechnology and Its Applications*, *17*(1), 1–10.

Mikhlin, Y., Karacharov, A., Likhatski, M., Podlipskaya, T., Zubavichus, Y., Veligzhanin, A., & Zaikovski, V. (2011). Submicrometer intermediates in the citrate synthesis of gold nanoparticles: New insights into the nucleation and crystal growth mechanisms. *Journal of Colloid and Interface Science*, *362*(2), 330–336. https://doi.org/10.1016/j.jcis.2011.06.077

Moir, J. (1910). Colloidal gold and "purple of cassius." *Transactions of the Royal Society of South Africa*, *2*(1), 203–204. https://doi.org/10.1080/00359191009519376

Nguyen, D. T., Kim, D. J., So, M. G., & Kim, K. S. (2010). Experimental measurements of gold nanoparticle nucleation and growth by citrate reduction of HAuCl4. *Advanced Powder Technology*, *21*(2), 111–118. https://doi.org/10.1016/j.apt.2009.11.005

Nobbmann, U. (2014). *How important is the refractive index of nanoparticles?* Malvern Analytical. materials-talks.com/faq-how-important-are-refractive-index-absorption-for-nanoparticles/

Pacławski, K., Streszewski, B., Jaworski, W., Luty-Błocho, M., & Fitzner, K. (2012). Gold nanoparticles formation via gold(III) chloride complex ions reduction with glucose in the batch and in the flow microreactor systems. *Colloids and Surfaces A: Physicochemical and Engineering Aspects*, *413*, 208–215. https://doi.org/10.1016/j.colsurfa.2012.02.050

Panariello, L., Radhakrishnan, A. N. P., Papakonstantinou, I., Parkin, I. P., & Gavriilidis, A. (2020). Particle size evolution during the synthesis of gold nanoparticles using in situ time-resolved UV−Vis spectroscopy: An experimental and theoretical study unravelling the effect of adsorbed gold precursor species. *Journal of Physical Chemistry C*, *124*(50), 27662–27672. https://doi.org/10.1021/acs.jpcc.0c07405

Park, M., Deng, S., & Advincula, R. C. (2004). *pH-Sensitive Bipolar Ion-Permselective Ultrathin Films*. 13723–13731.

Polte, J., Erler, R., Thu, A. F., Sokolov, S., Ahner, T. T., Rademann, K., Emmerling, F., & Kraehnert, R. (2010). Nanoparticles Studied via in situ Small. *ACS Nano*, *4*(2), 1076–1082.

Porcaro, F., Battocchio, C., Antoccia, A., Fratoddi, I., Venditti, I., Fracassi, A., Luisetto, I., Russo, M. V., & Polzonetti, G. (2016). Synthesis of functionalized gold nanoparticles capped with 3-mercapto-1-propansulfonate and 1-thioglucose mixed thiols and "in vitro" bioresponse. *Colloids and Surfaces B: Biointerfaces*, *142*, 408–416.

https://doi.org/10.1016/j.colsurfb.2016.03.016

Rose, T. K. (1906). *Metallurgy of Gold* (Fifth). Charles Griffin and Company, Limited.

Suherman, A. L., Zampardi, G., Kuss, S., Tanner, E. E. L., Amin, H. M. A., Young, N. P., & Compton, R. G. (2018). Understanding gold nanoparticle dissolution in cyanide-containing solution: Via impact-chemistry. *Physical Chemistry Chemical Physics*, *20*(44), 28300–28307. https://doi.org/10.1039/c8cp05154b

Thanh, N. T. K., Maclean, N., & Mahiddine, S. (2014). Mechanisms of nucleation and growth of nanoparticles in solution. *Chemical Reviews*, *114*(15), 7610–7630. https://doi.org/10.1021/cr400544s

The Editors of Encyclopaedia Britannica. (n.d.). *Thiol*. Encyclopaedia Britannica. Retrieved April 7, 2022, from https://www.britannica.com/science/thiol

Tscharnuter, W. (2000). Photon Correlation Spectroscopy in Particle Sizing. *Encyclopedia of Analytical Chemistry*, 5469–5485. https://doi.org/10.1002/9780470027318.a1512

Turkevich, J., Stevenson, P. C., & Hillier, J. (1951). A study of the nucleation and growth processes in the synthesis of colloidal gold. *Discussions of the Faraday Society*, *11*(c), 55–75. https://doi.org/10.1039/DF9511100055

Vaskelis, A., Tarozaite, R., Jagminiene, A., Tamasiunaite, L. T., Juskenas, R., & Kurtinaitiene, M. (2007). Gold nanoparticles obtained by Au (III) reduction with Sn (II): Preparation and electrocatalytic properties in oxidation of reducing agents. *Electrochimica Acta*, *53*, 407–416. https://doi.org/10.1016/j.electacta.2007.04.008

Venditti, I., Fontana, L., Fratoddi, I., Battocchio, C., Cametti, C., Sennato, S., Mura, F., Sciubba, F., Delfini, M., & Russo, M. V. (2014). Direct interaction of hydrophilic gold nanoparticles with dexamethasone drug: Loading and release study. *Journal of Colloid and Interface Science*, *418*, 52–60. https://doi.org/10.1016/j.jcis.2013.11.063

Young, C. A. (1987). *Nonstoichiometry of Chalcocite in Water/Xanthate Systems*.

Young, C. A., Das, A., LaDouceur, R., Timbillah, S., & Childress, S. (2022). Review of the Mechanism for Orfom D8 Depression of Chalcopyrite in Cu-Mo Separation during Cleaner Flotation. *International Journal of the Society of Materials Engineering for Resources*, *25*(1).

Young, C. A., & Huang, H.-H. (2019). Aqueous-Phase Redox Precipitation. In R. C. Dunne, S. K. Kawatra, & C. A. Young (Eds.), *SME Mineral Processing and Extractive Metallurgy*

Handbook (pp. 1411–1421). Society for Mining, Metallurgy & Exploration, Incorporated.

Zhou, J., Ralston, J., Sedev, R., & Beattie, D. A. (2009). Functionalized gold nanoparticles: Synthesis, structure and olloid stability. *Journal of Colloid and Interface Science, 331*, 251–262.

6. Appendix A: Design Expert Model Graphs

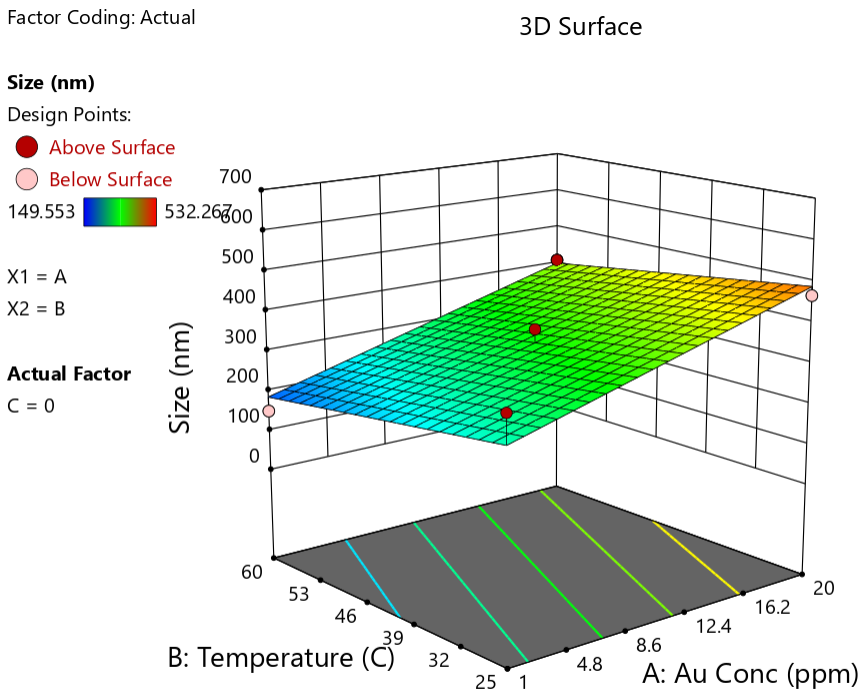

Figure 41: Secondary gold chloride system size 3D surface model at zero thiol concentration.

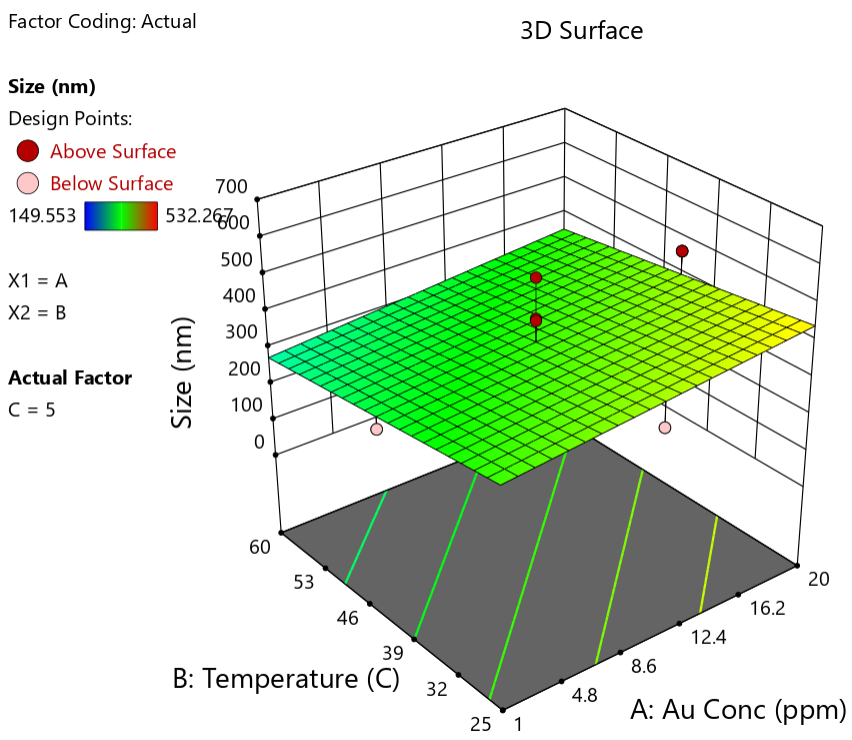

Figure 42: Secondary gold chloride system size 3D surface model at 5 times thiol concentration.

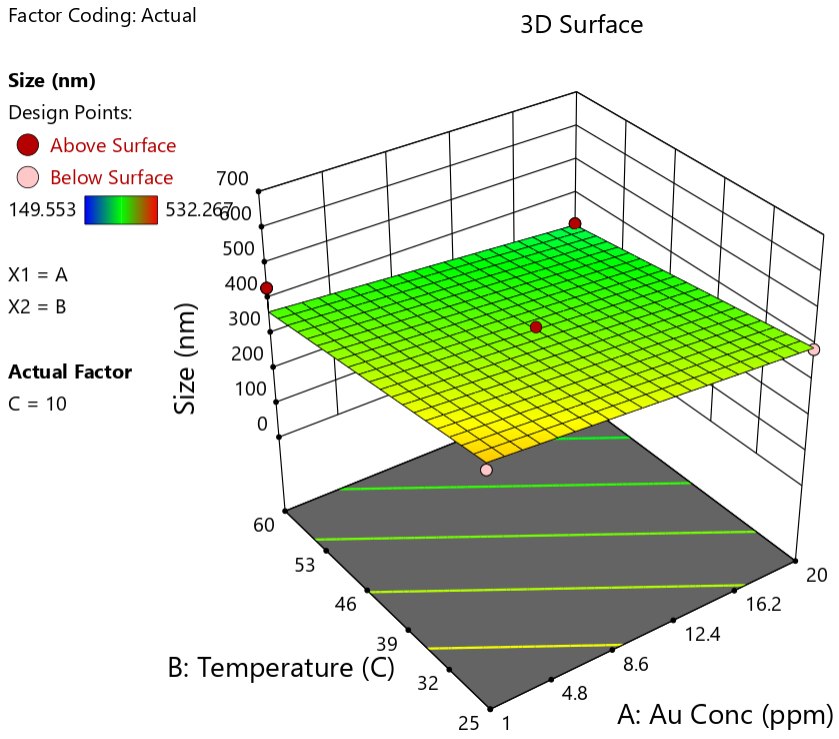

Figure 43: Secondary gold chloride system size 3D surface model at 10 times thiol concentration.

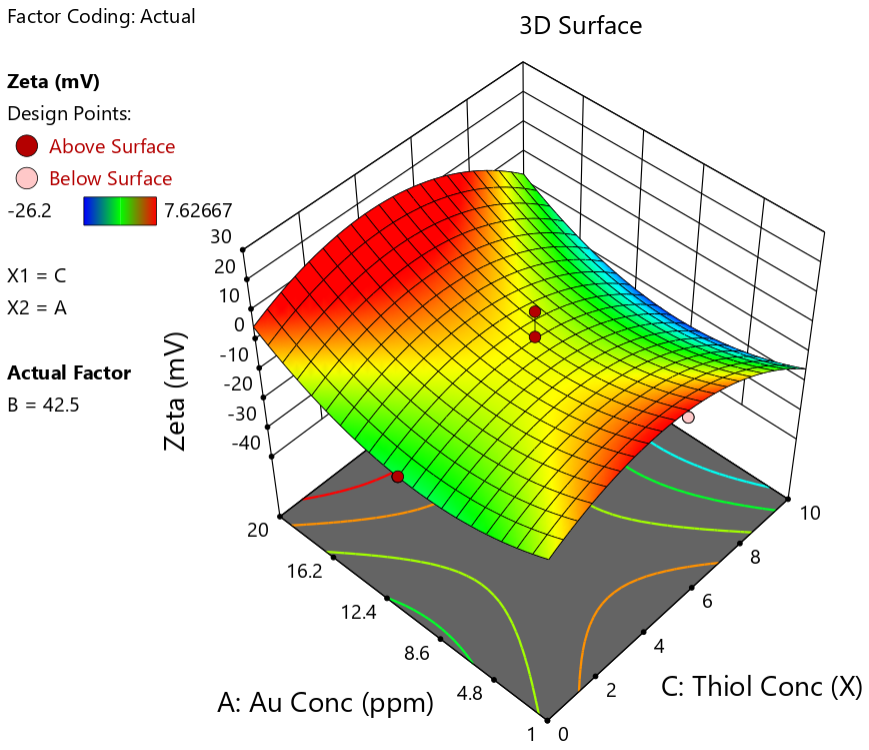

Figure 44: Secondary gold chloride system zeta potential 3D surface model.

7. Appendix B: FESEM Images of Initial Gold Chloride System

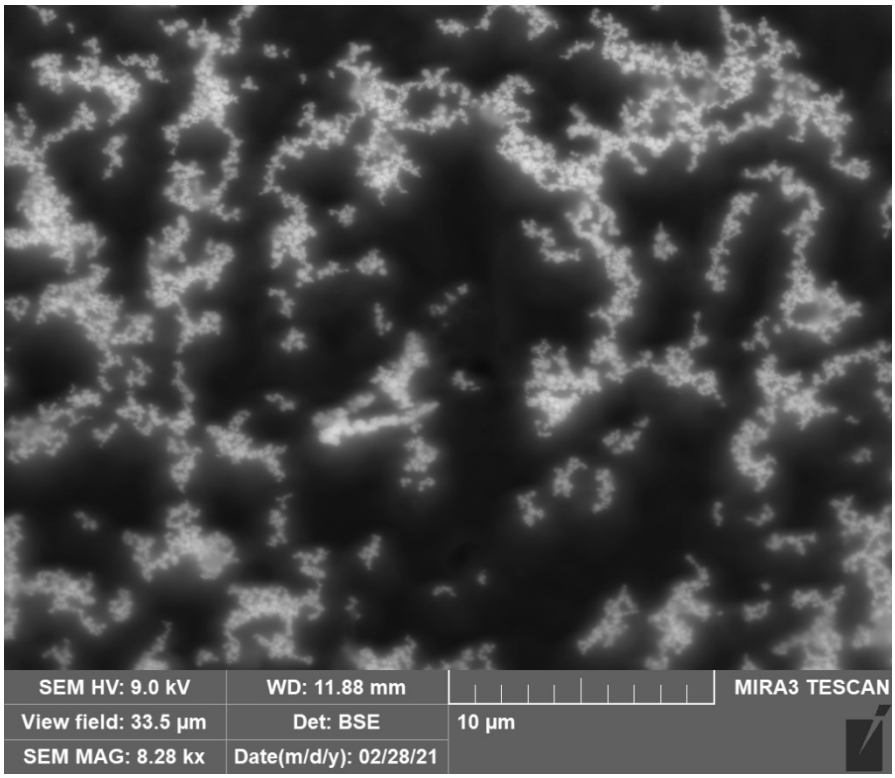

Figure 45: Run1 no hydrazine added image 4

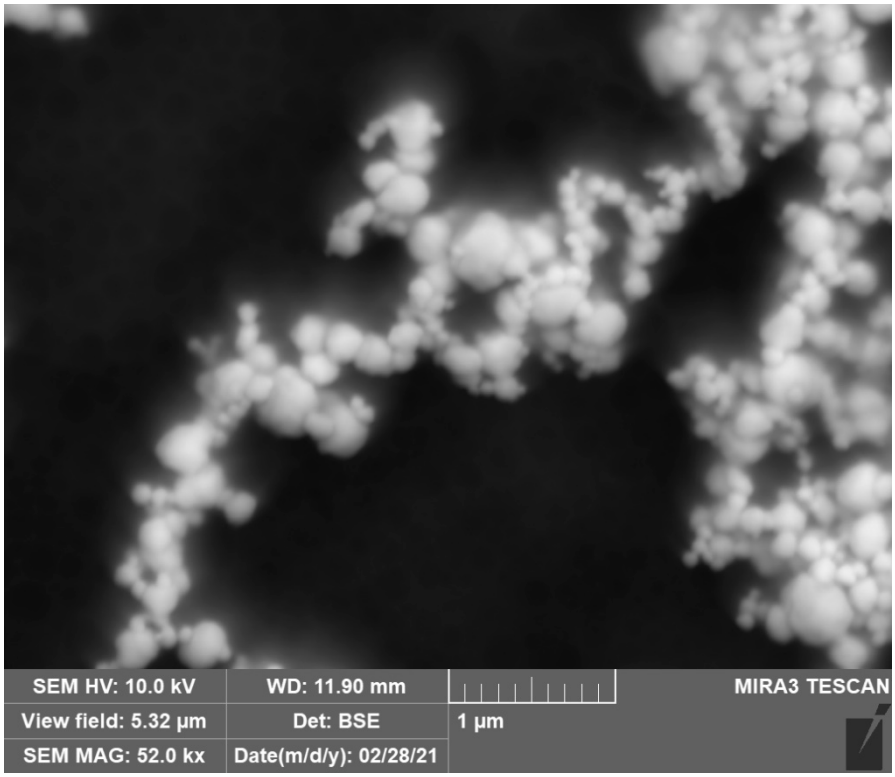

Figure 46: Run1 no hydrazine image 5

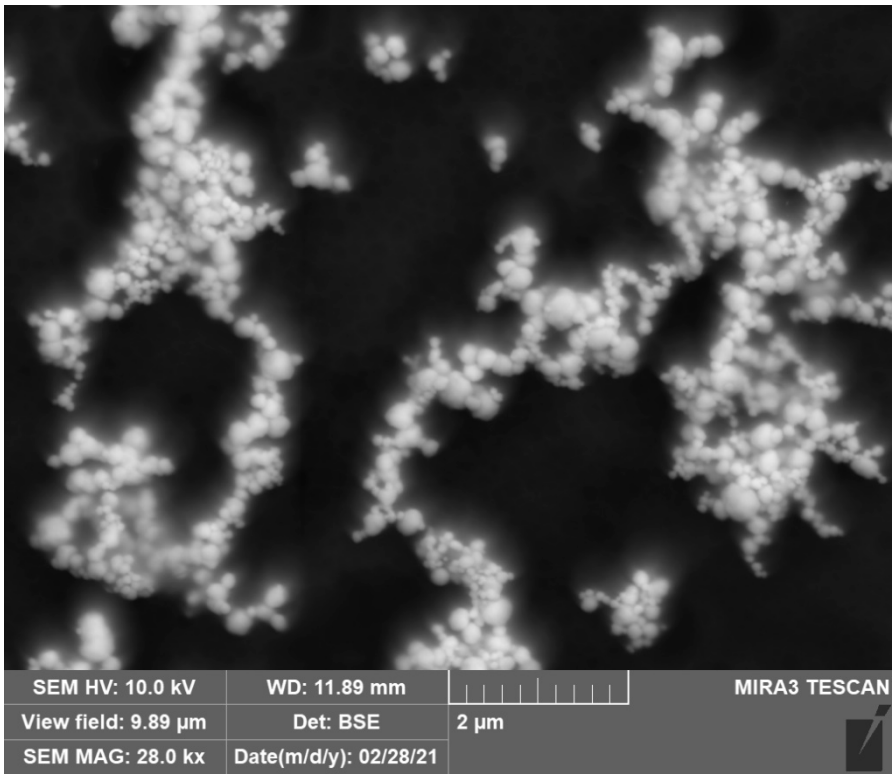

Figure 47: Run1 no hydrazine image 6

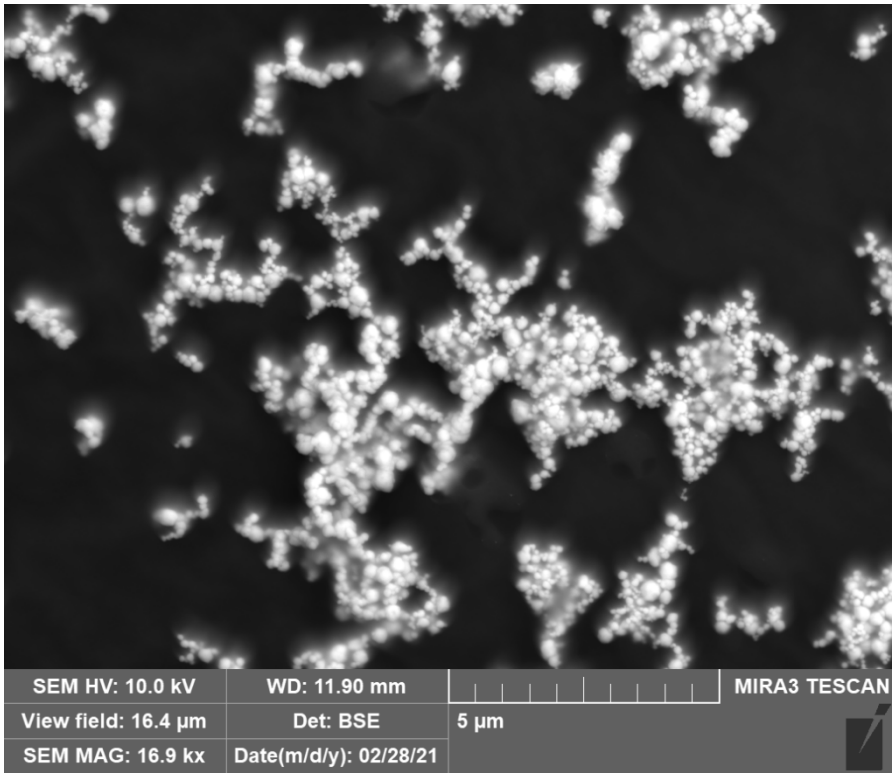

Figure 48: Run1 no hydrazine image 7

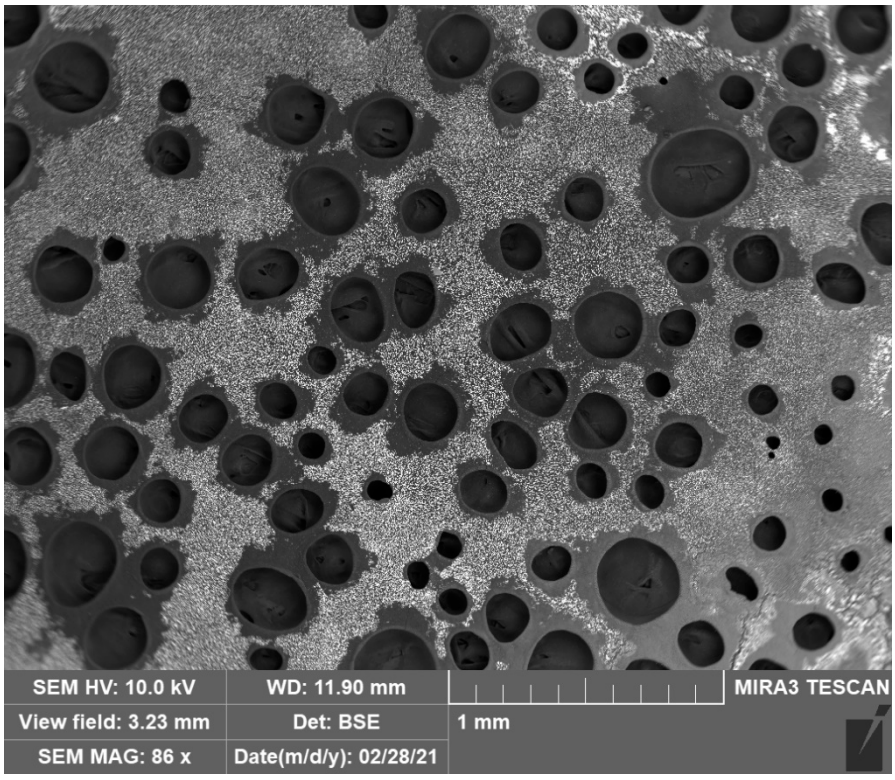

Figure 49: Run1 no hydrazine image 8

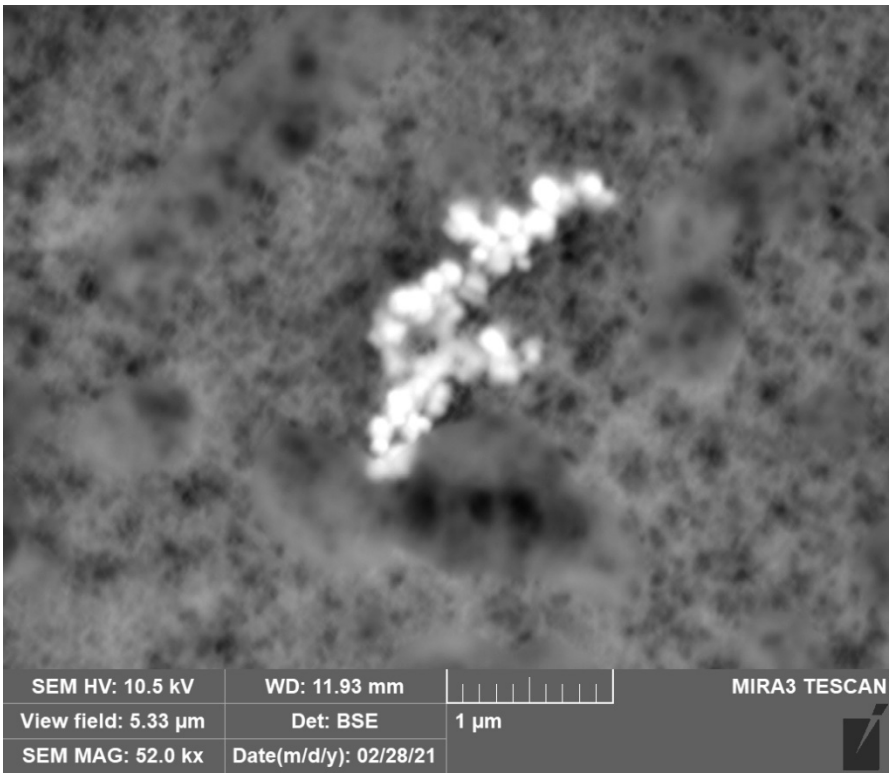

Figure 50: Run2 with hydrazine image 1

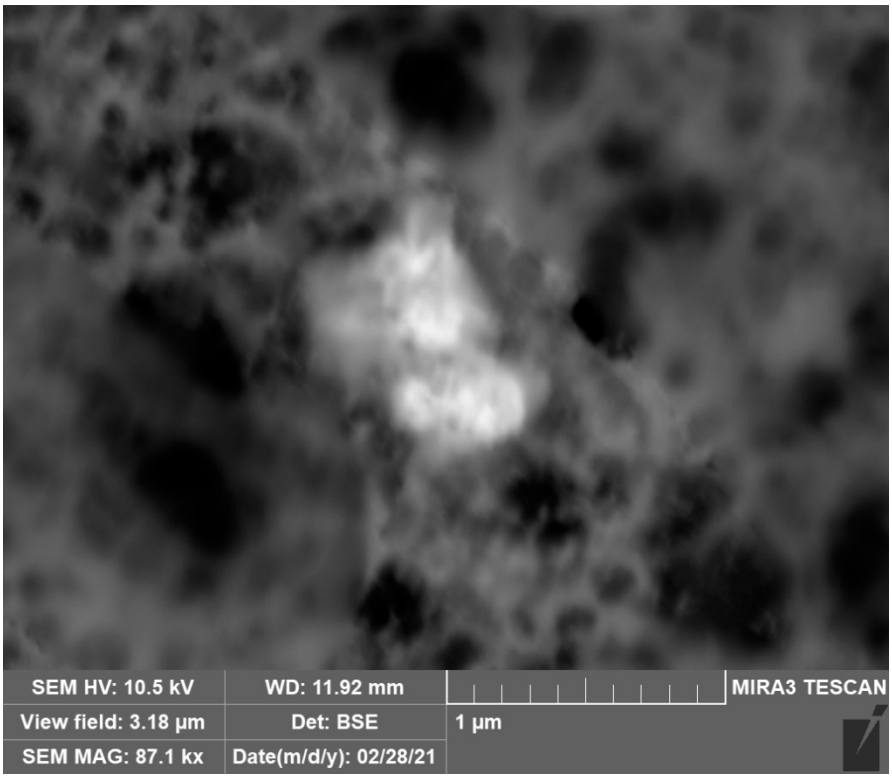

Figure 51: Run2 with hydrazine image 2

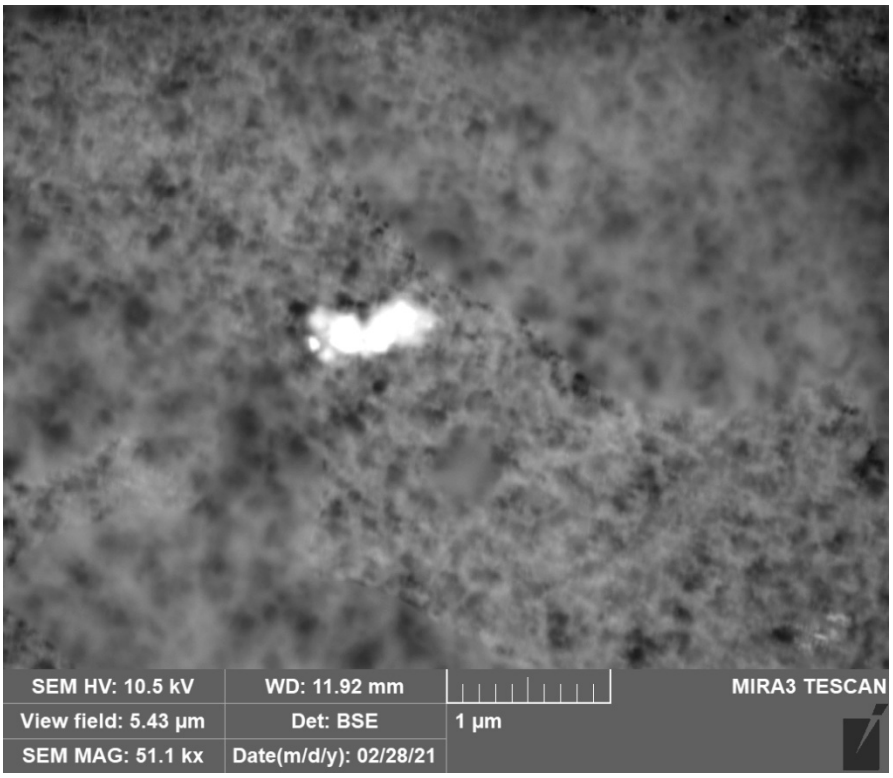

Figure 52: Run2 with hydrazine image 3

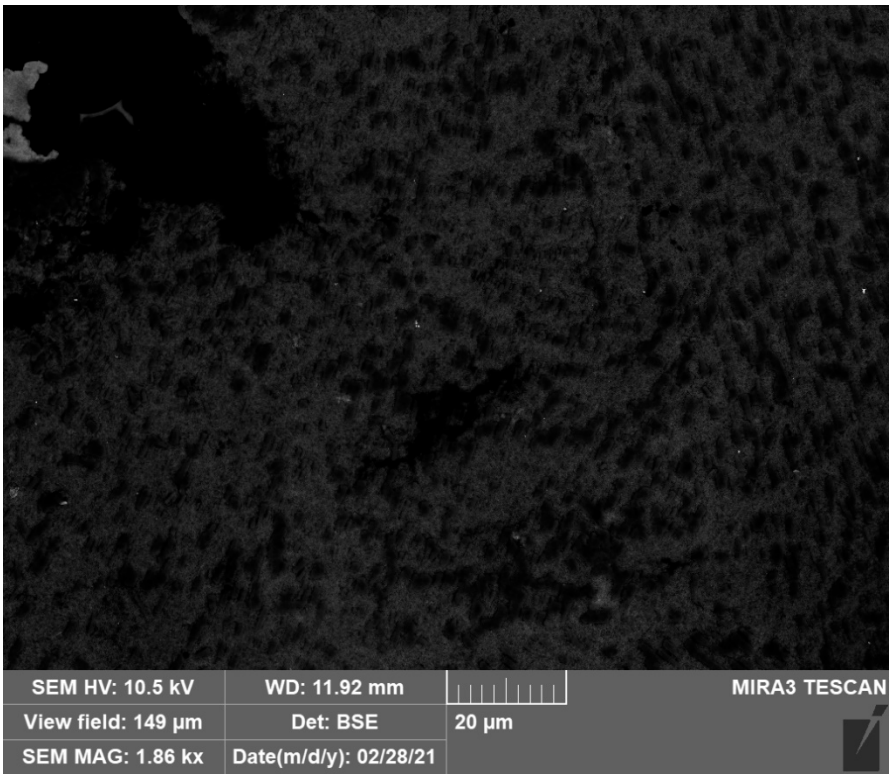

Figure 53: Run2 with hydrazine image 5

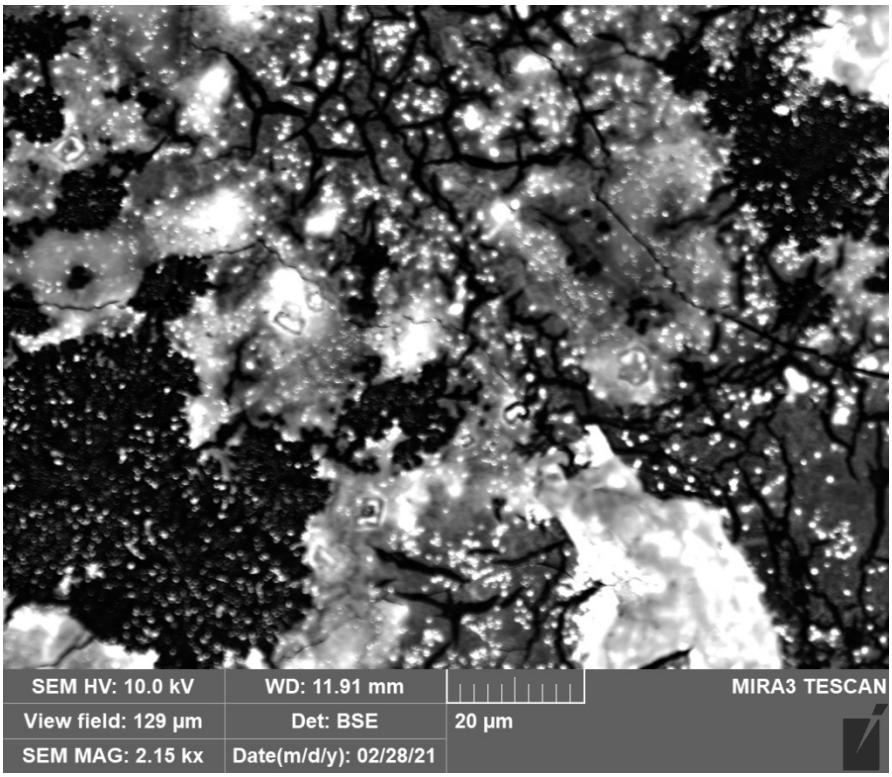

Figure 54: Run2 no hydrazine image 1

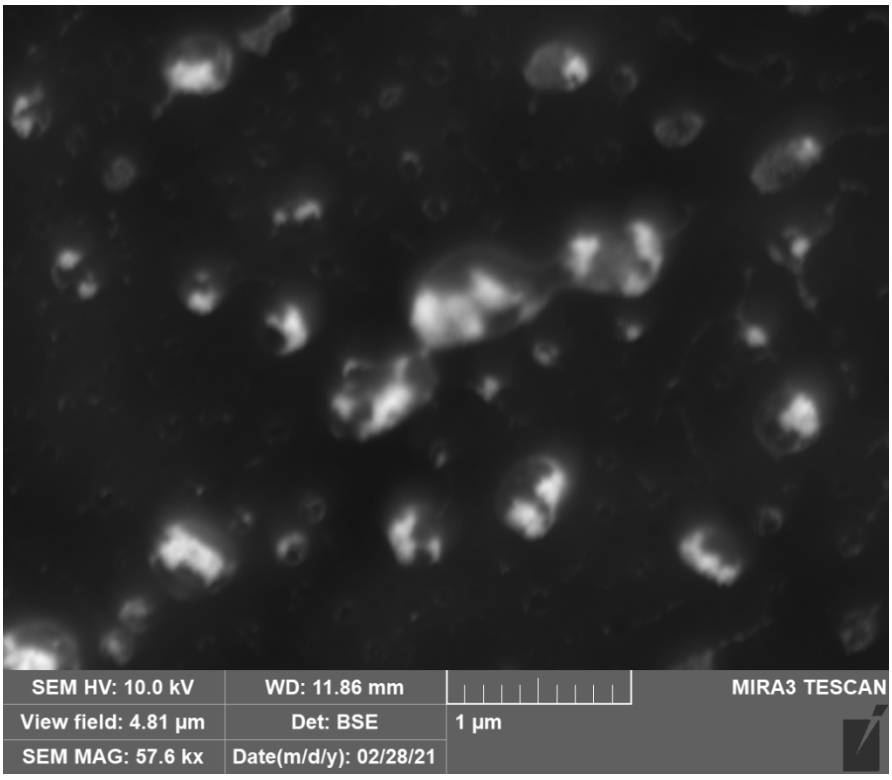

Figure 55: Run2 no hydrazine image 2

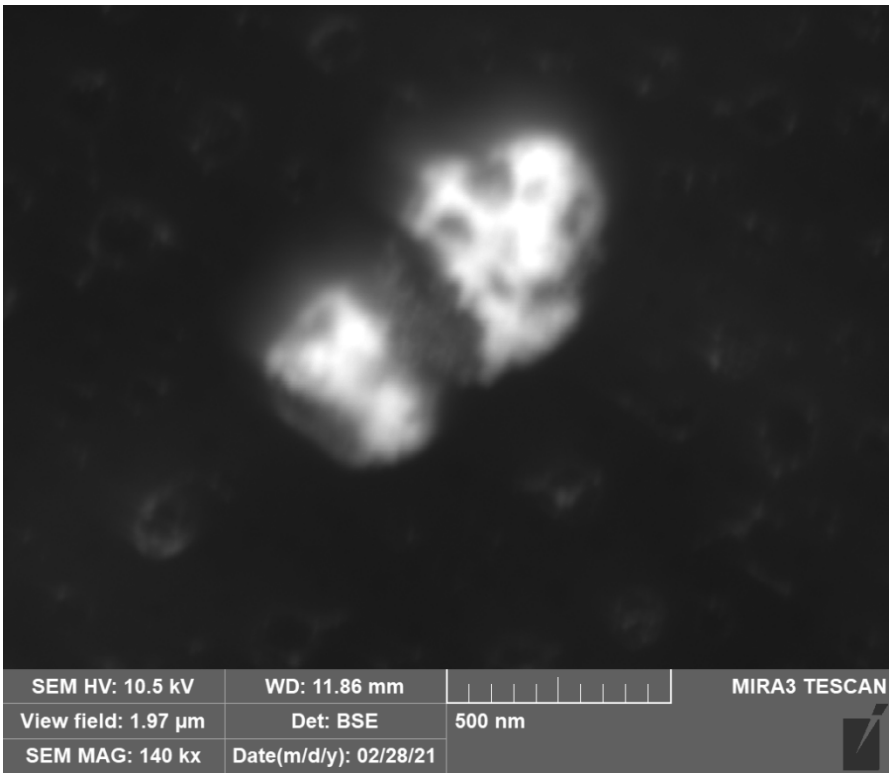

Figure 56: Run2 no hydrazine image 6

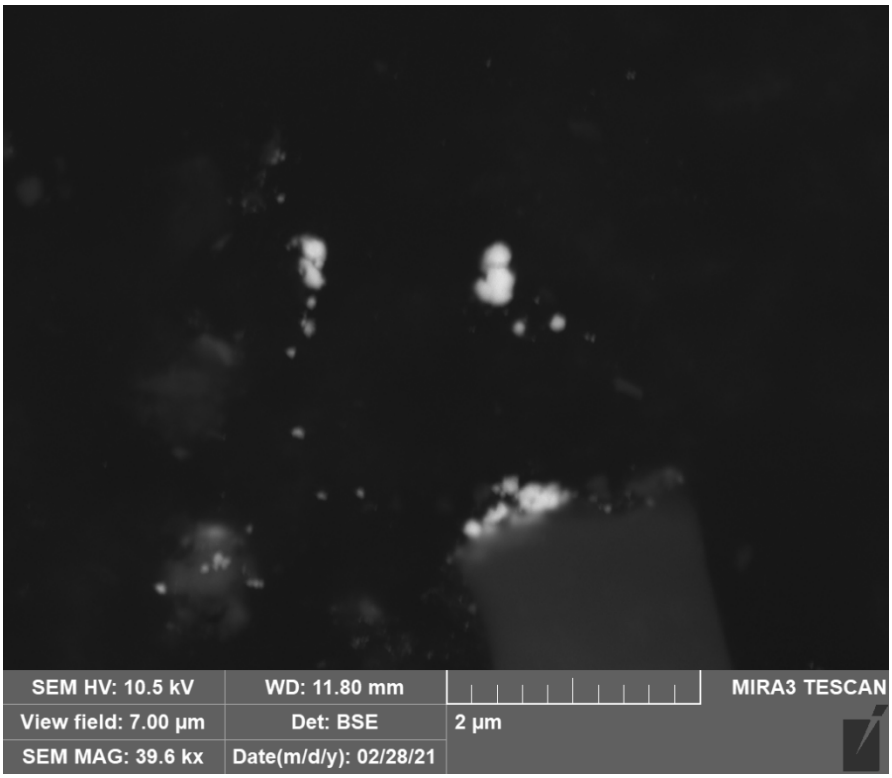

Figure 57: Run3 with hydrazine image 2

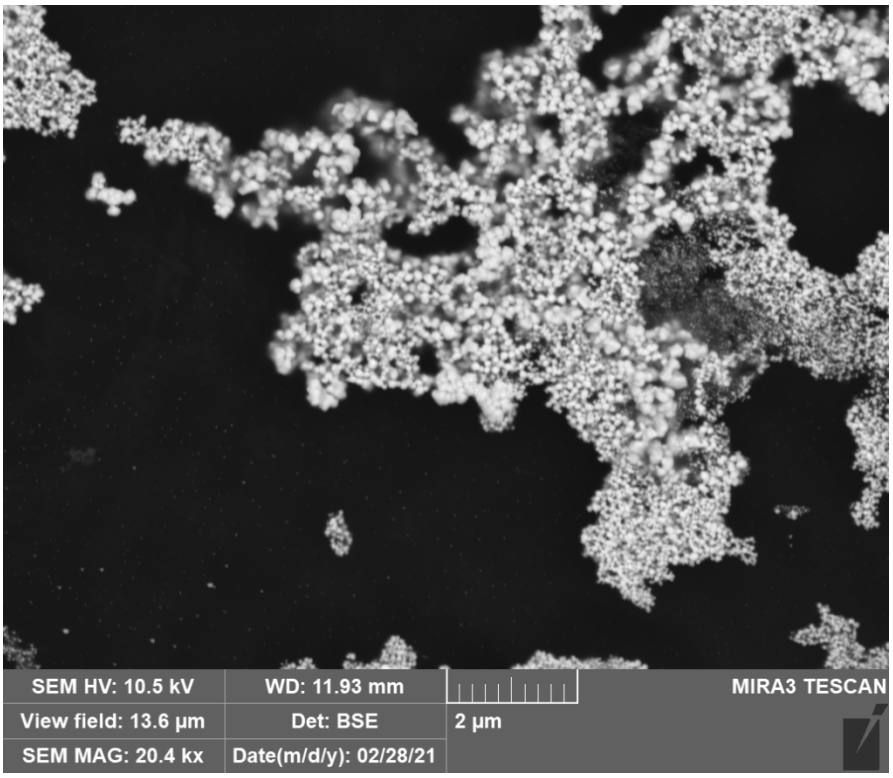

Figure 58: Run3 no hydrazine image 2

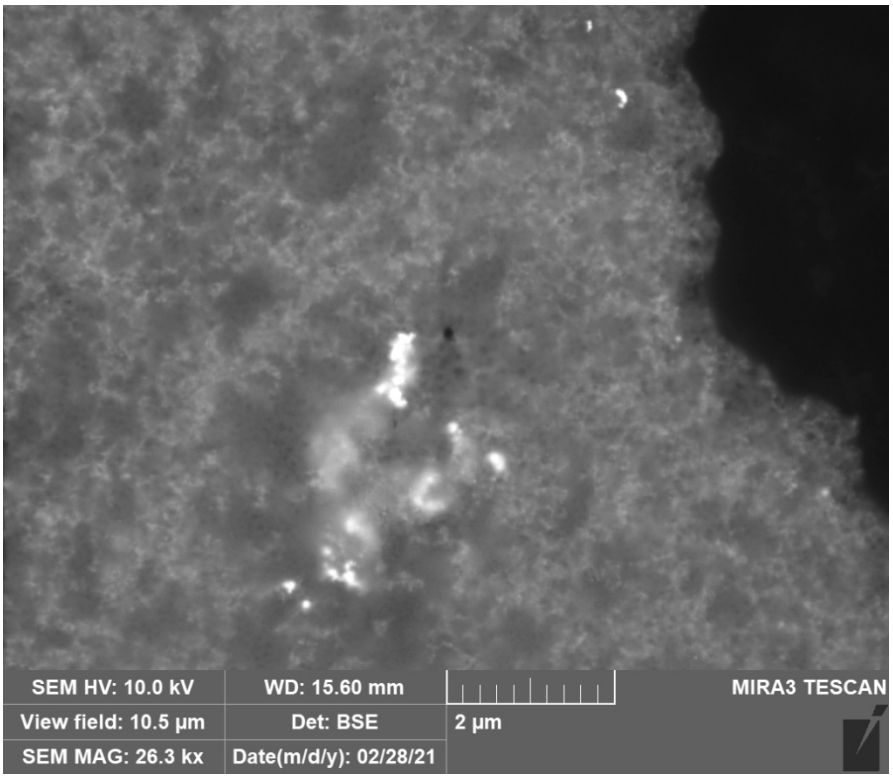

Figure 59: Run4 with hydrazine image 3

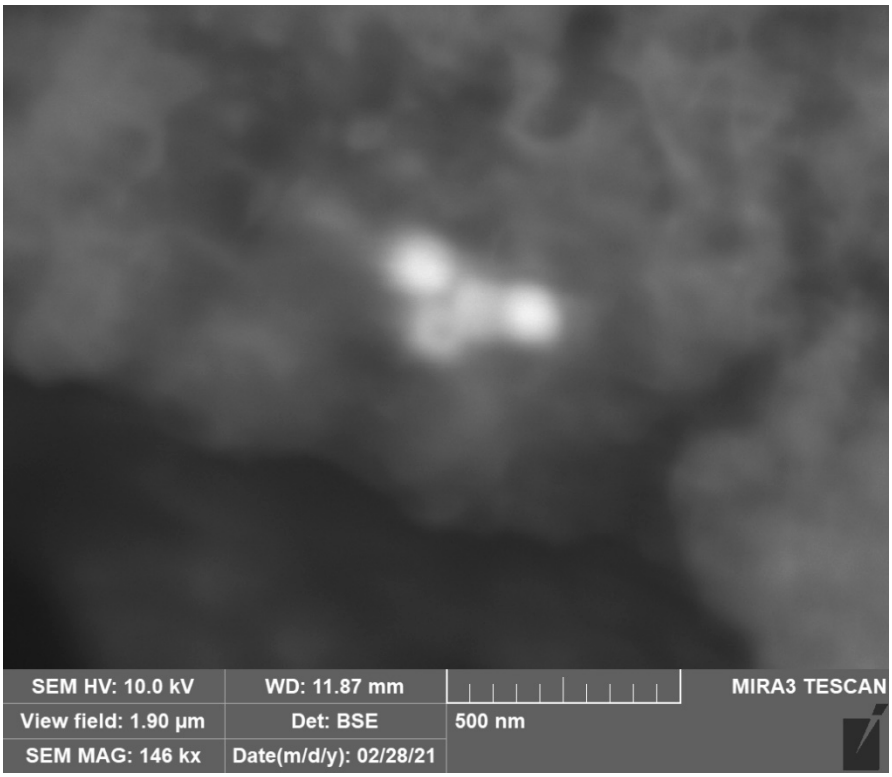

Figure 60: Run4 no hydrazine image 3

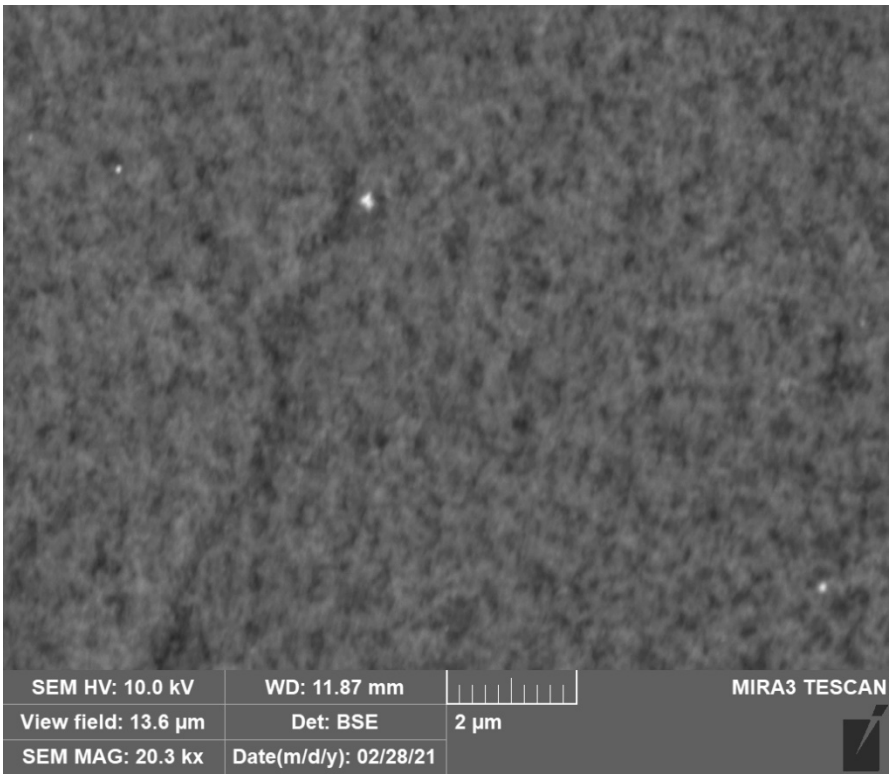

Figure 61: Run4 no hydrazine image 5

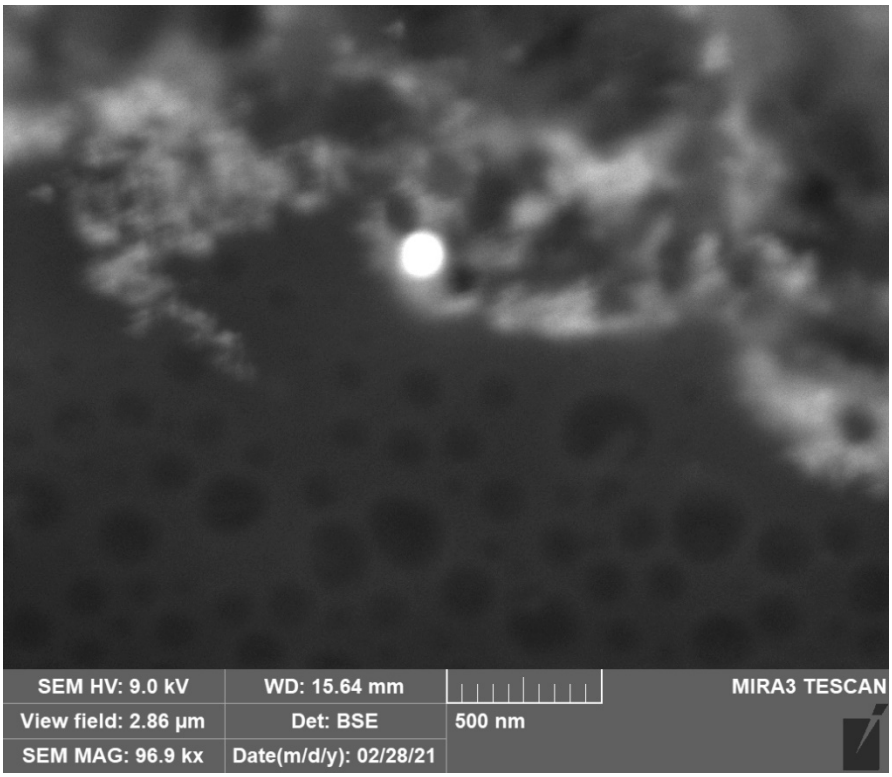

Figure 62: Run5 with hydrazine image 1

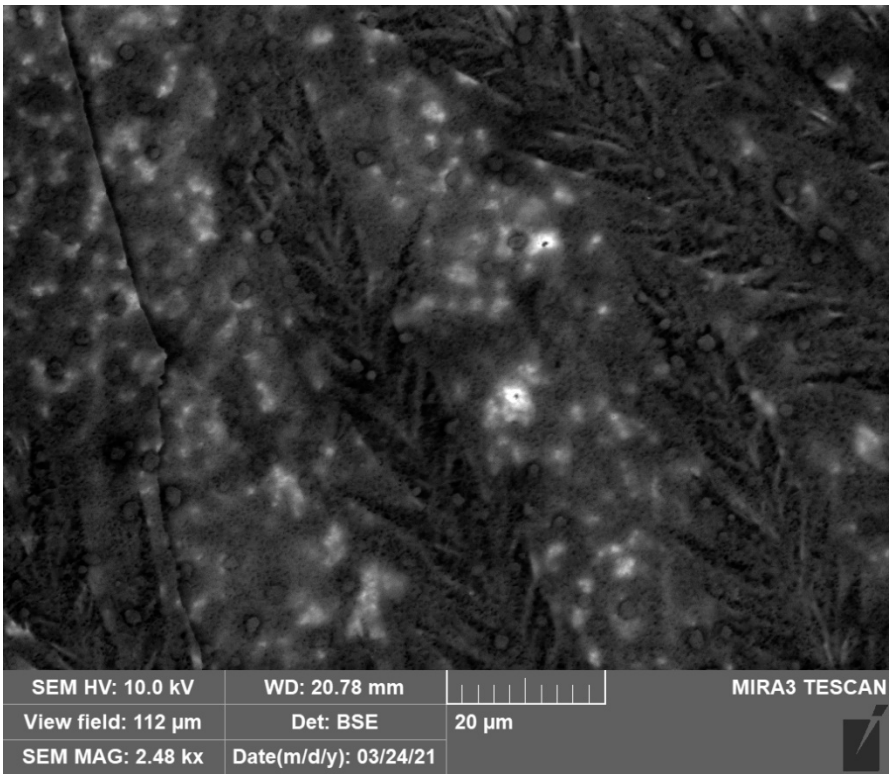

Figure 63: Run6 no hydrazine image 1

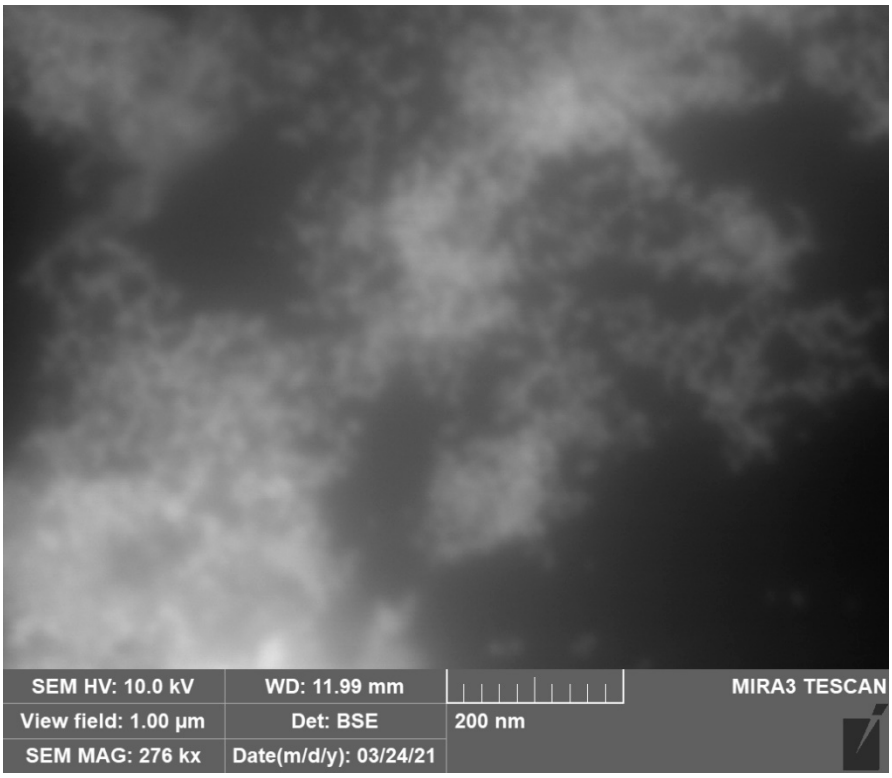

Figure 64: Run8 no hydrazine image 2

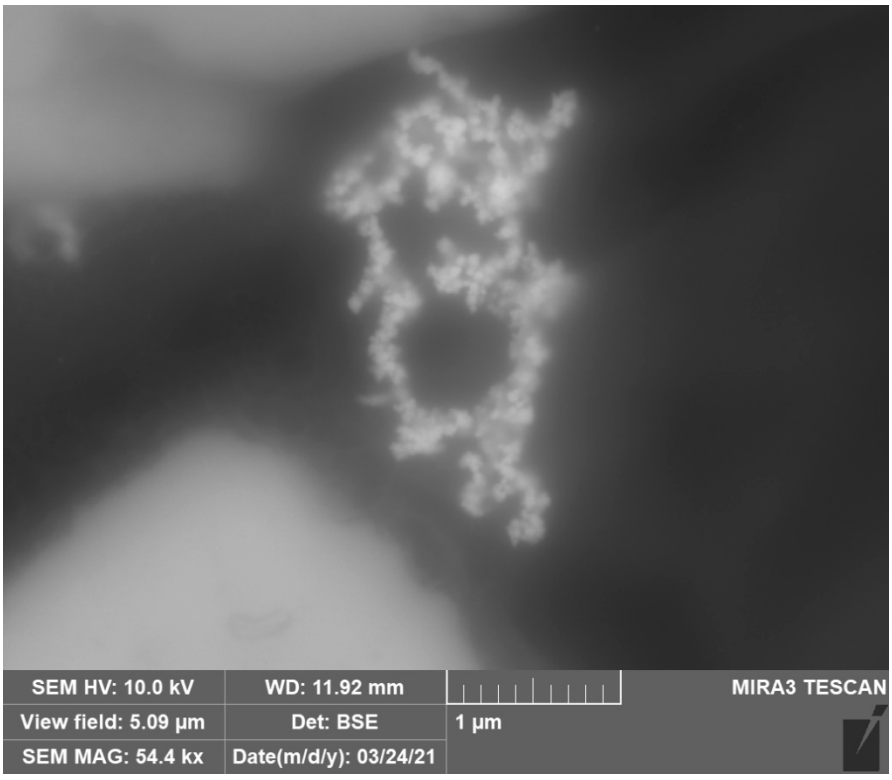

Figure 65: Run9 no hydrazine image 1

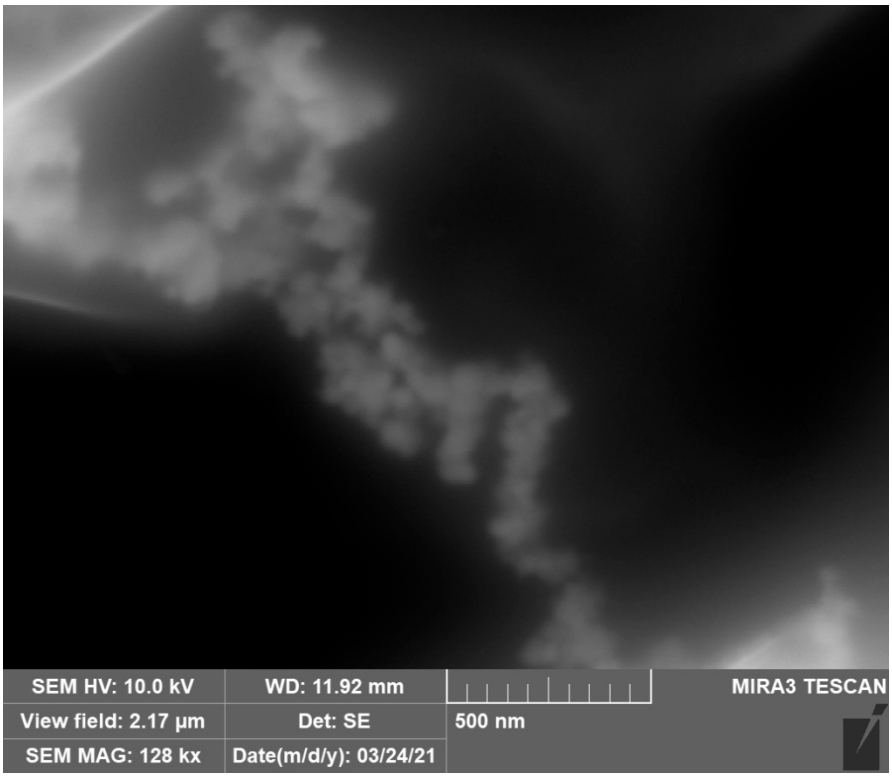

Figure 66: Run9 no hydrazine image 2

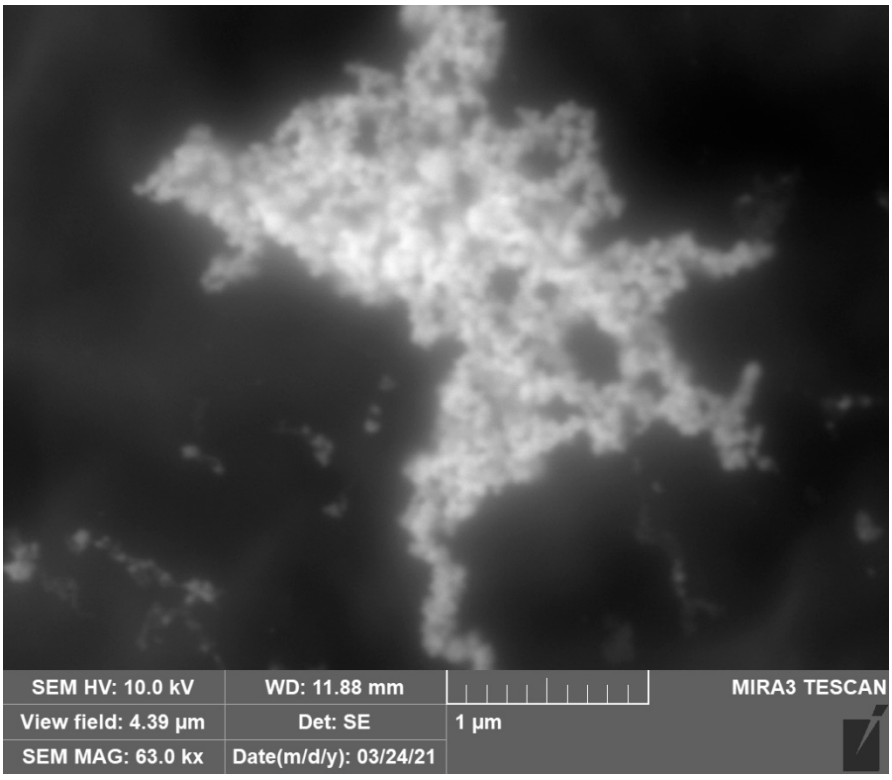

Figure 67: Run9 no hydrazine image 5

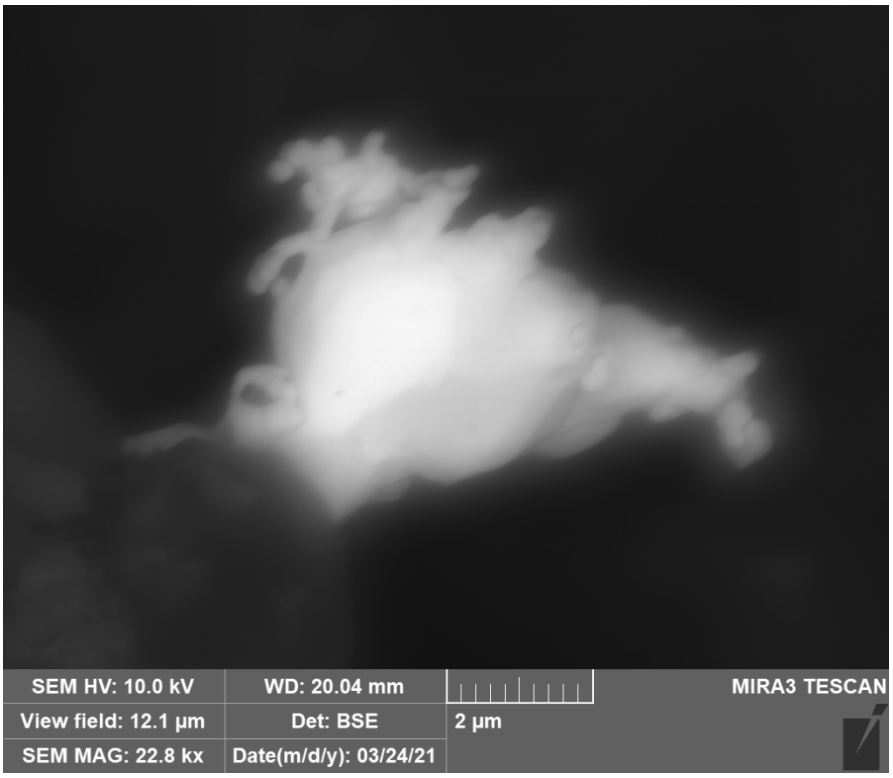

Figure 68: Run11 no hydrazine image 1

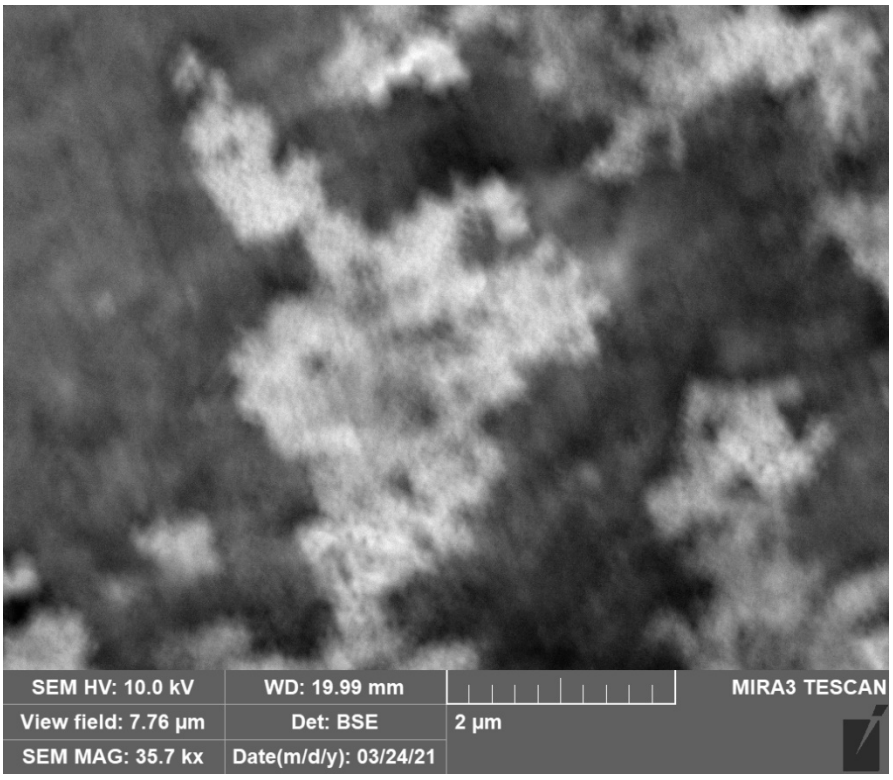

Figure 69: Run12 no hydrazine image 1

8. Appendix C: FESEM Images of Secondary Gold Chloride System

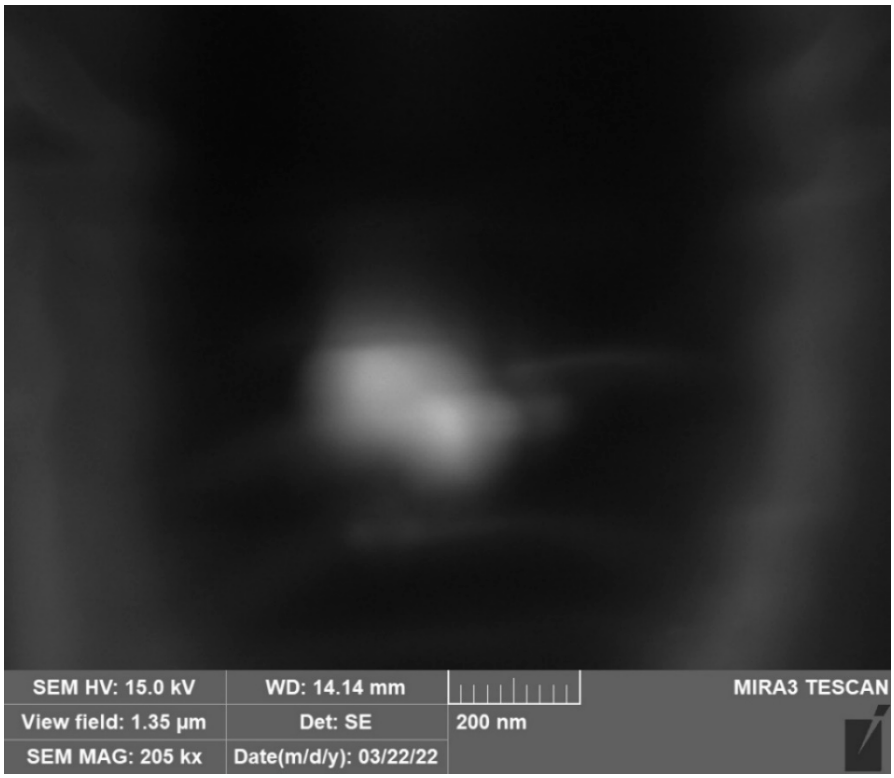

Figure 70: STD1Run14 Image 1 SE.

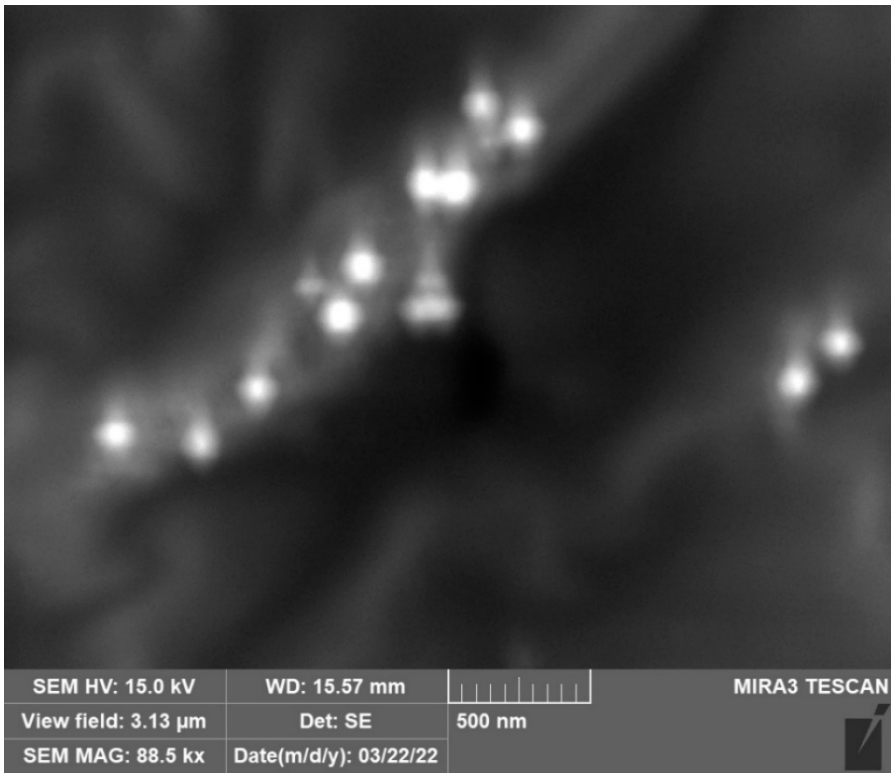

Figure 71: STD1Run14 Image 2 SE

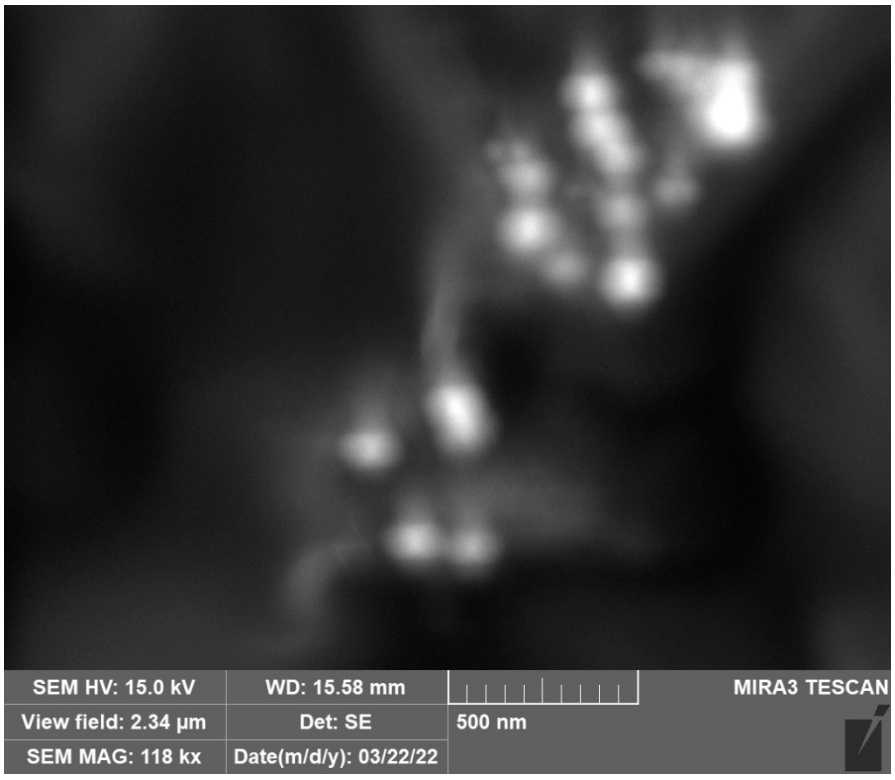

Figure 72: STD2Run10 Image 1 SE

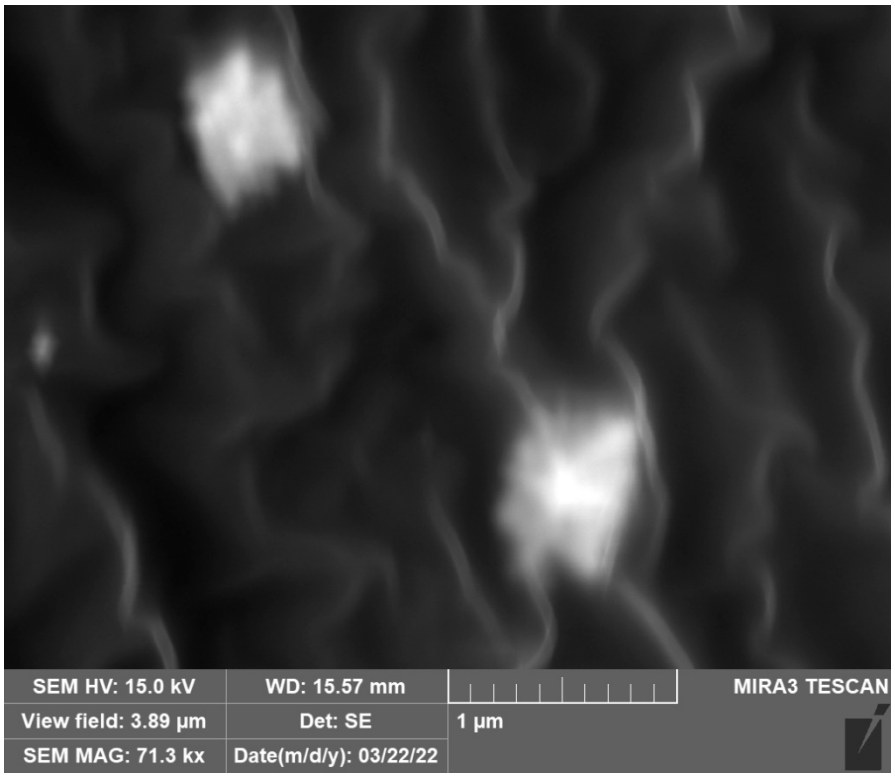

Figure 73: STD2Run10 Image 1 SE

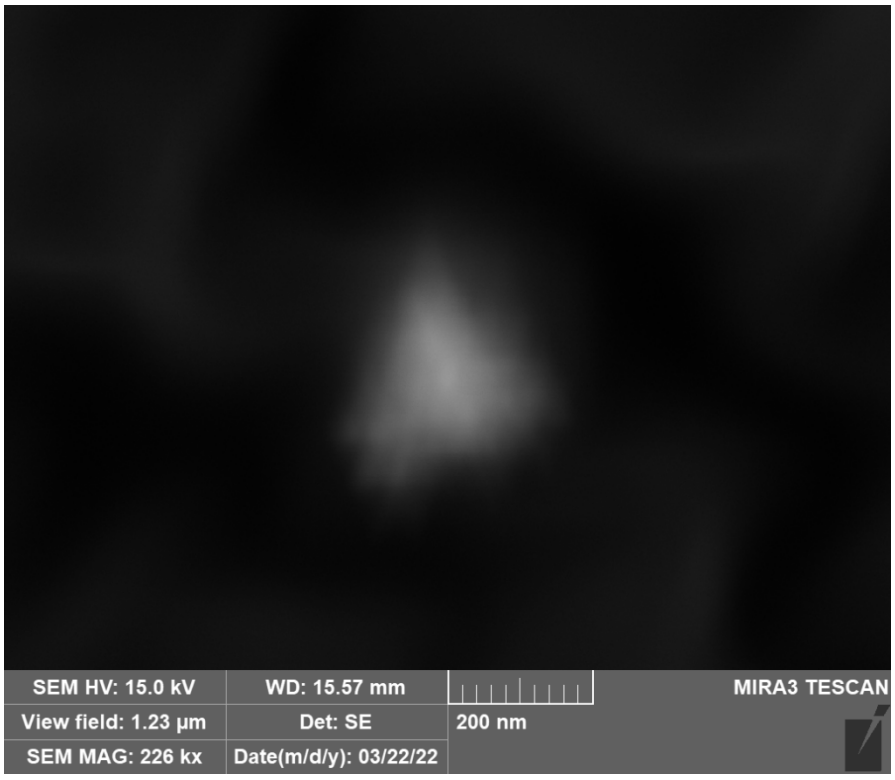

Figure 74: STD2Run10 Image 2 SE

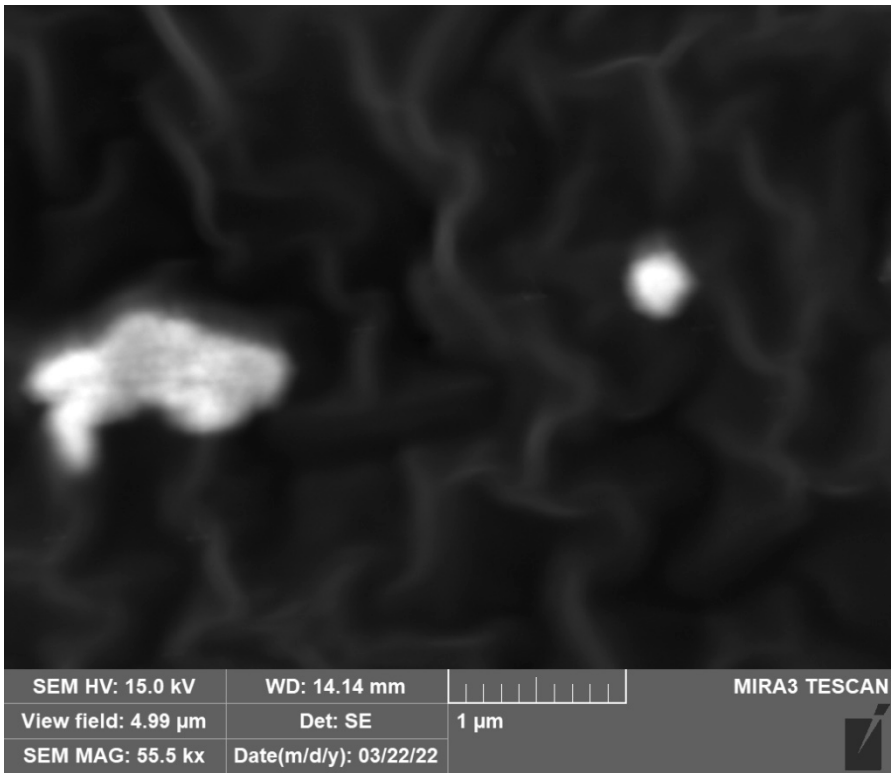

Figure 75: STD3Run11 Image 1 SE

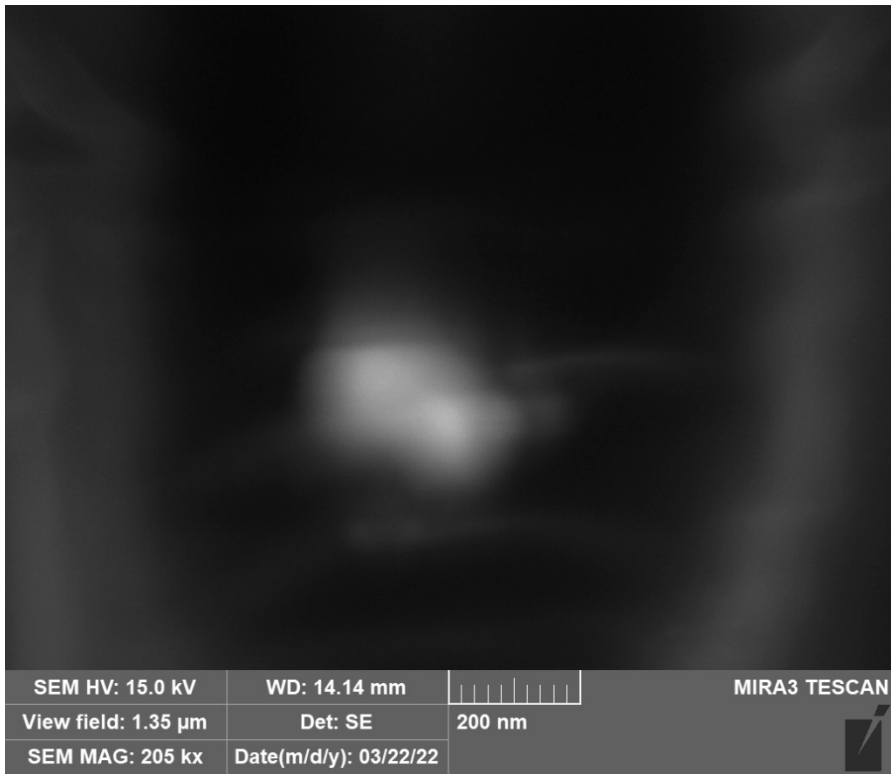

Figure 76: STD3Run11 Image 2 SE

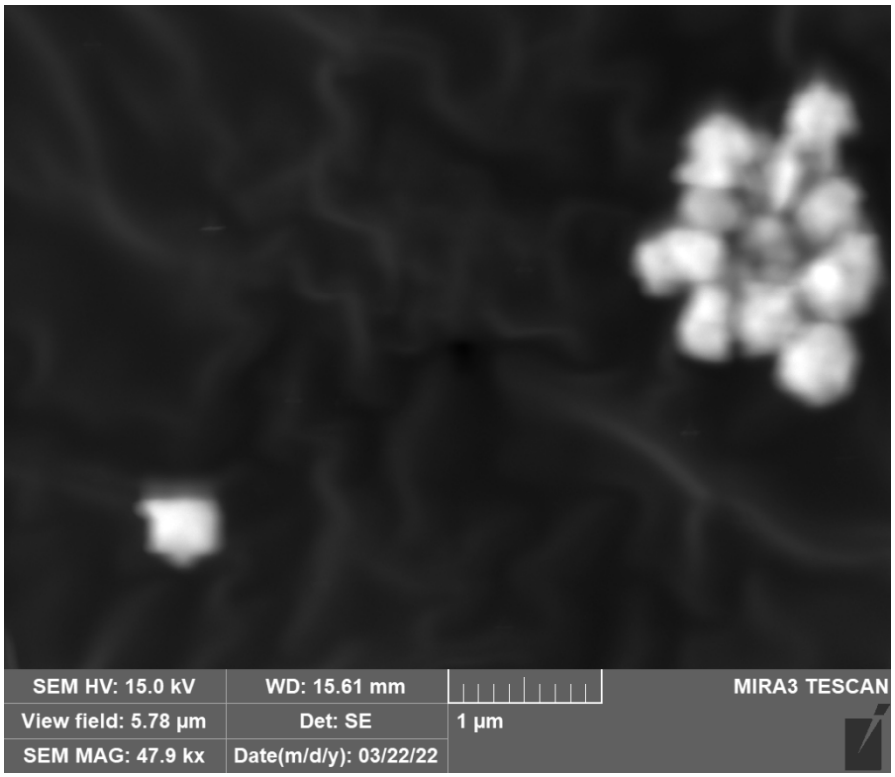

Figure 77: STD4Run9 Image 1 SE

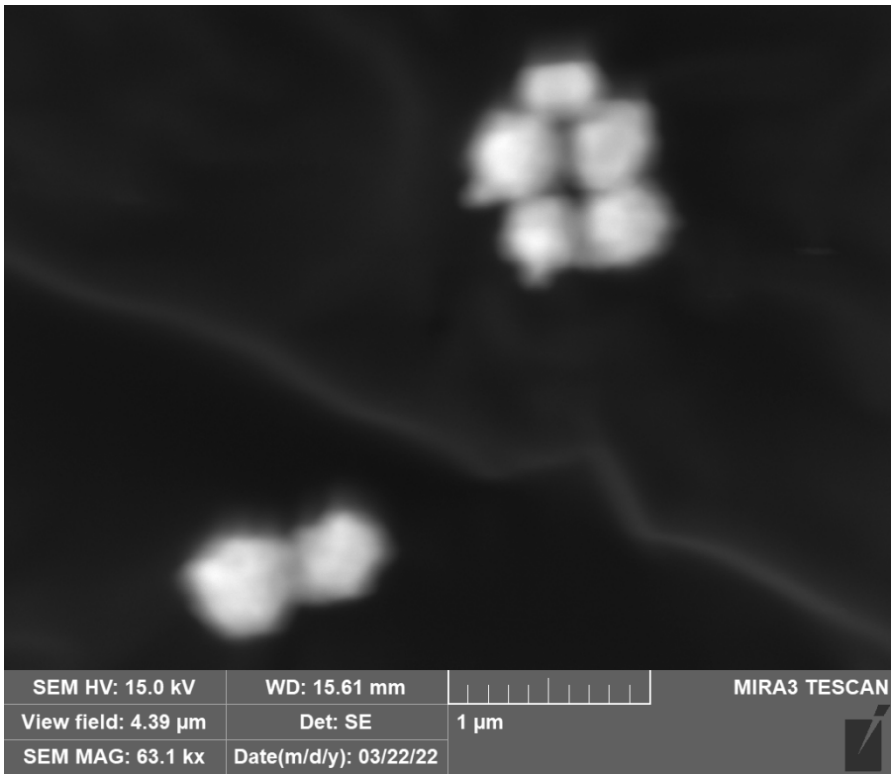

Figure 78: STD4Run9 Image 2 SE

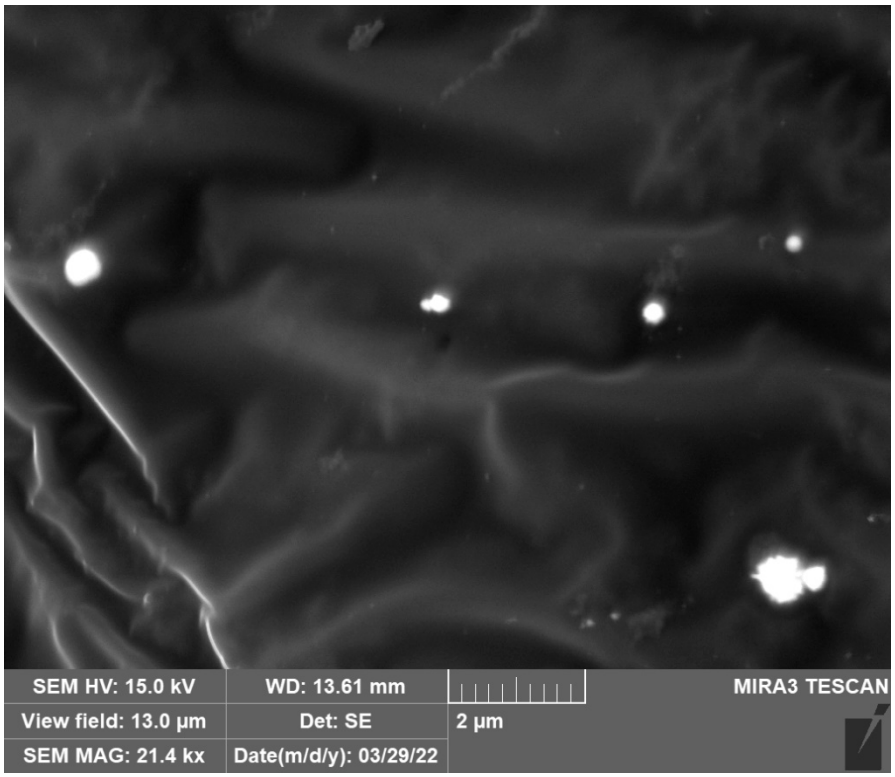

Figure 79: STD5Run5 Image 1 SE

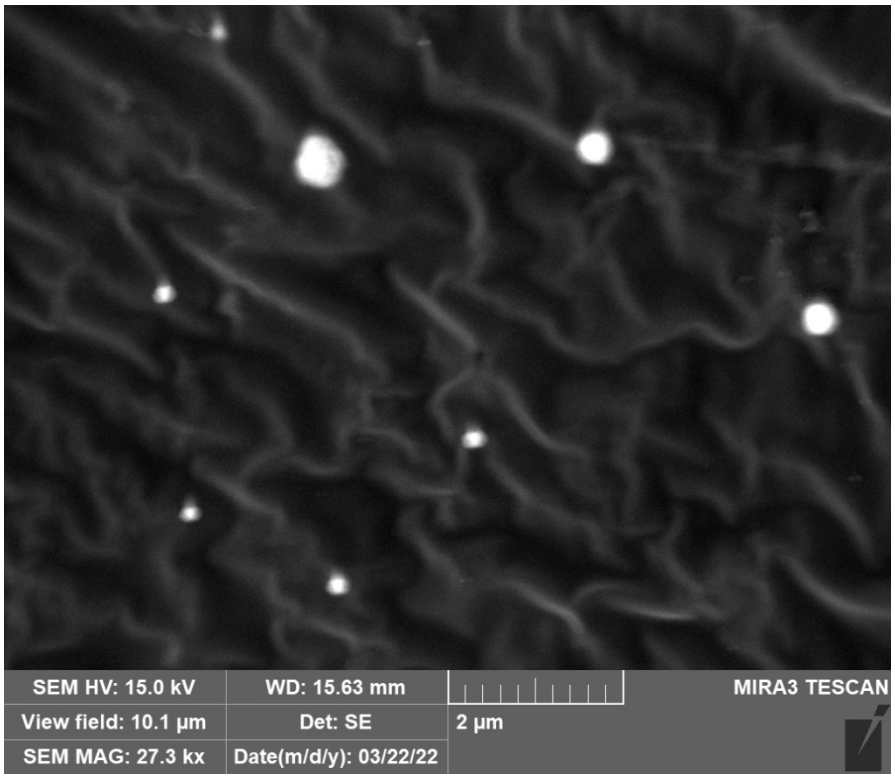

Figure 80: STD6Run12 Image 1 SE

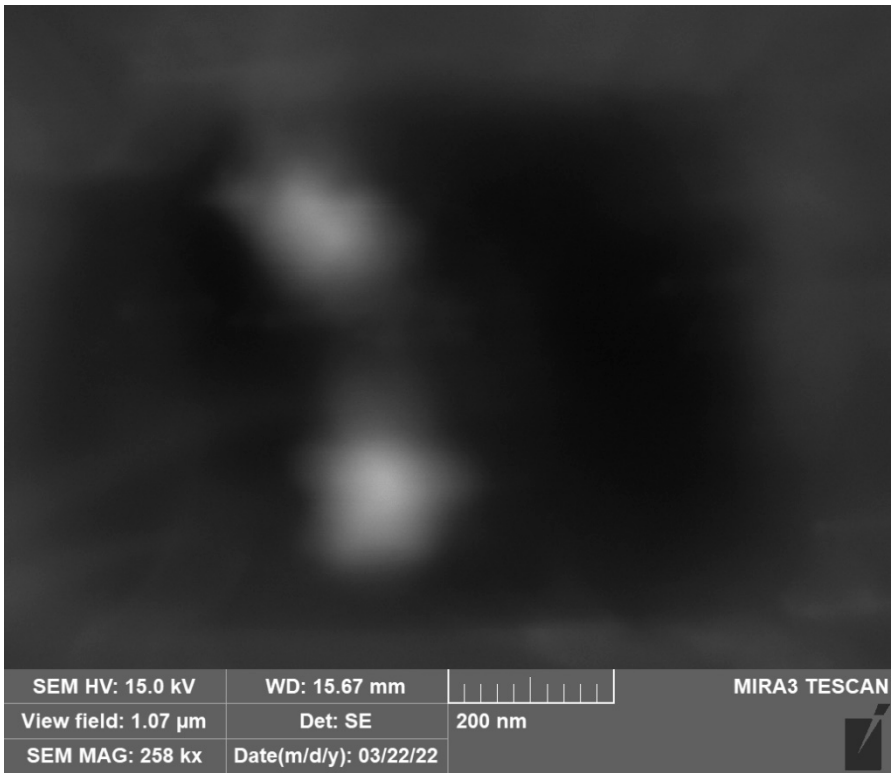

Figure 81:STD7Run3 Image 1 SE

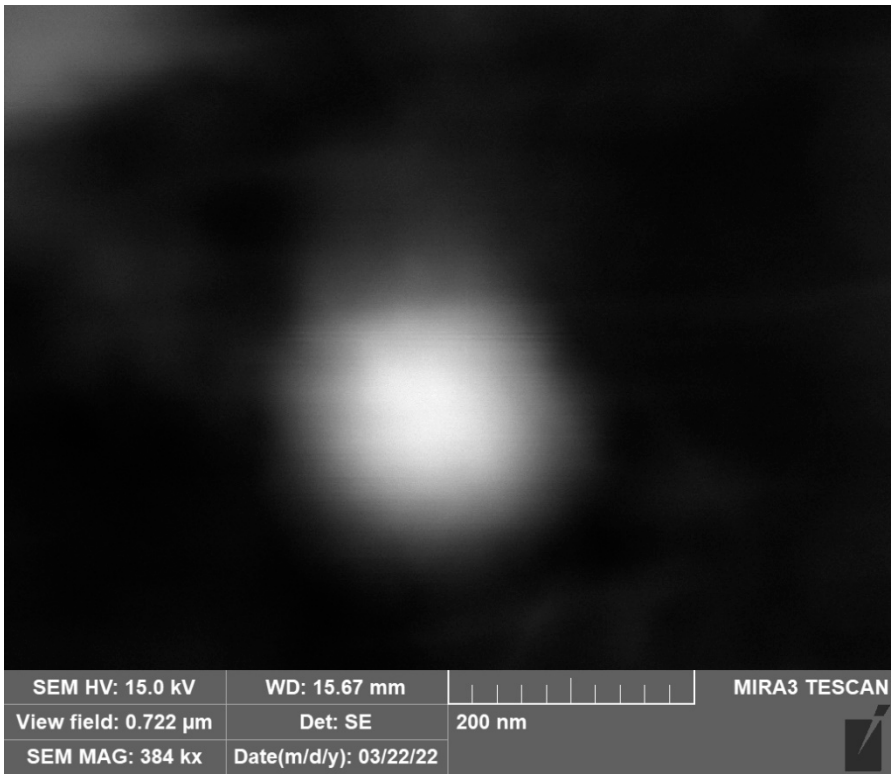

Figure 82: STD7Run3 Image 2 SE

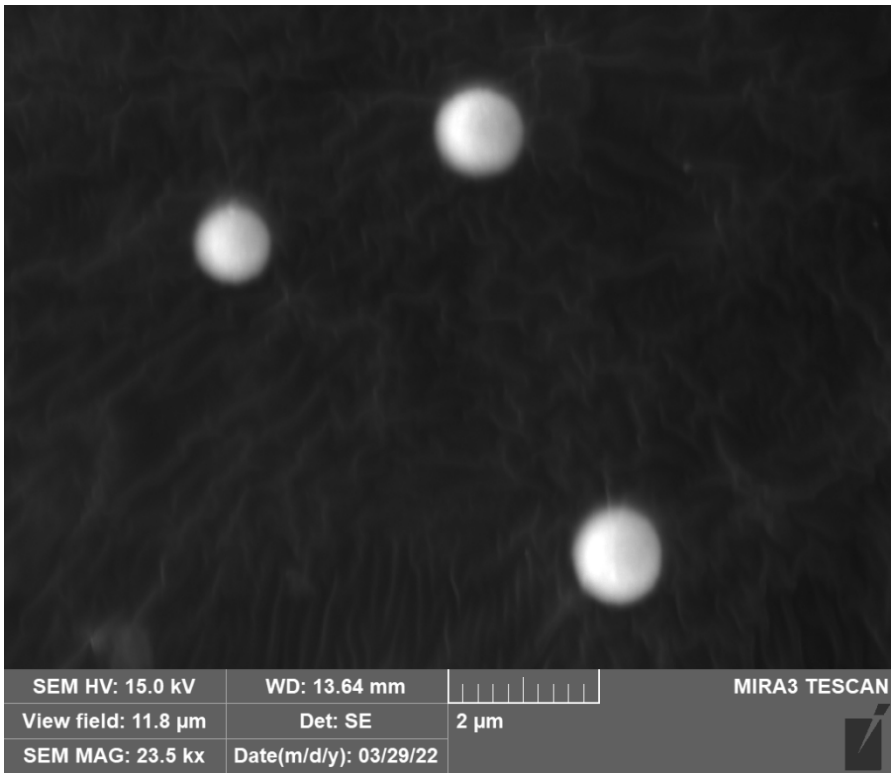

Figure 83: STD8Run16 Image 1 SE

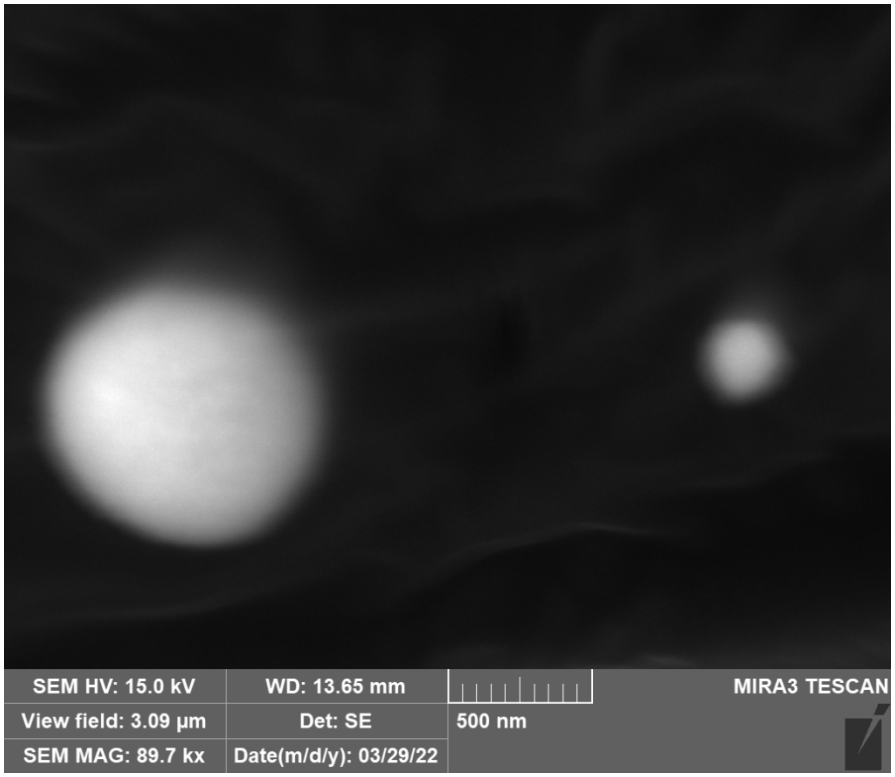

Figure 84: STD8Run16 Image 2 SE

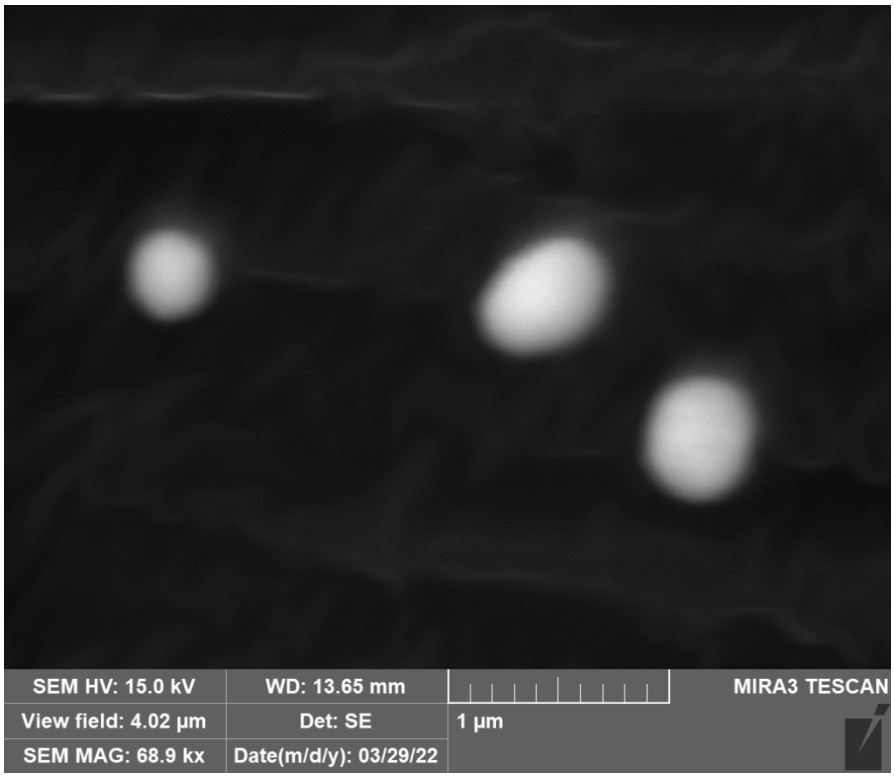

Figure 85: STD8Run16 Image 3 SE

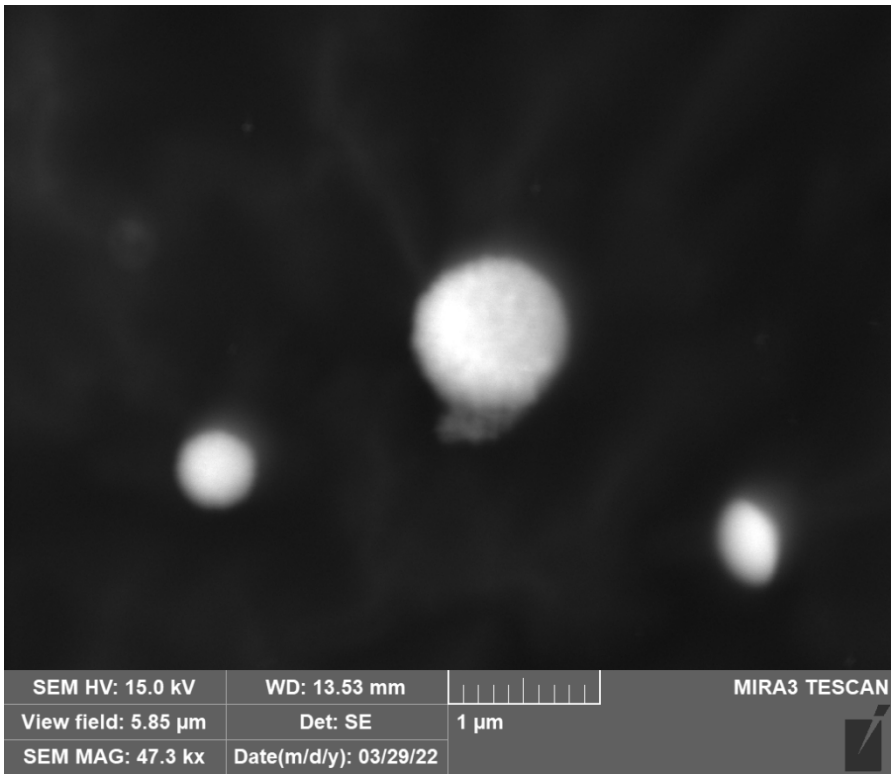

Figure 86: STD10Run17 Image 1 SE

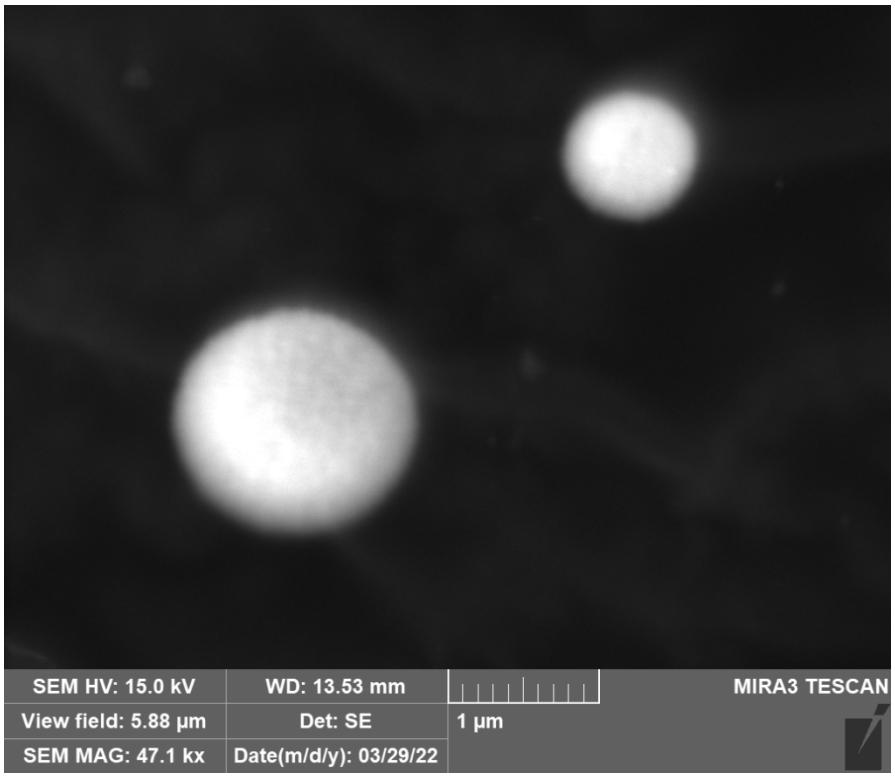

Figure 87: STD10Run17 Image 2 SE

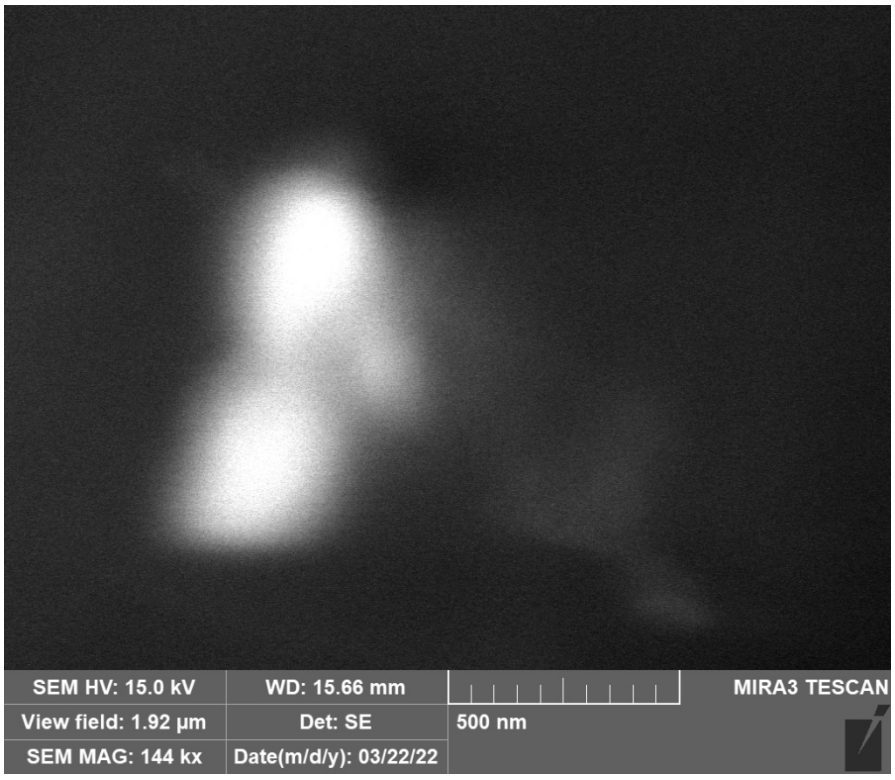

Figure 88: STD11Run2 Image 1 SE

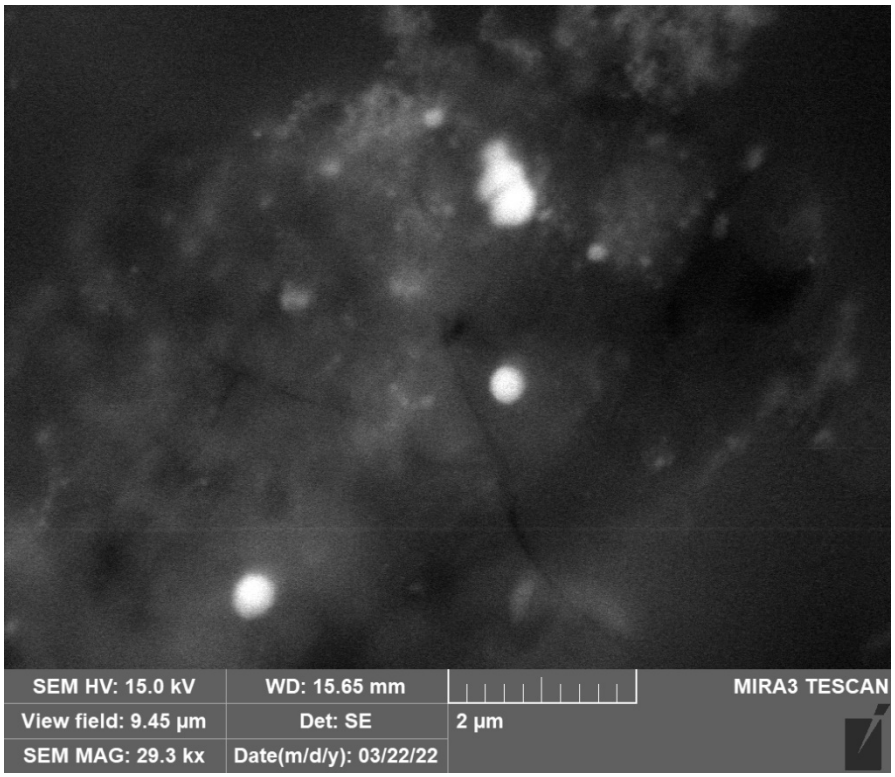

Figure 89: STD11Run2 Image 2 SE

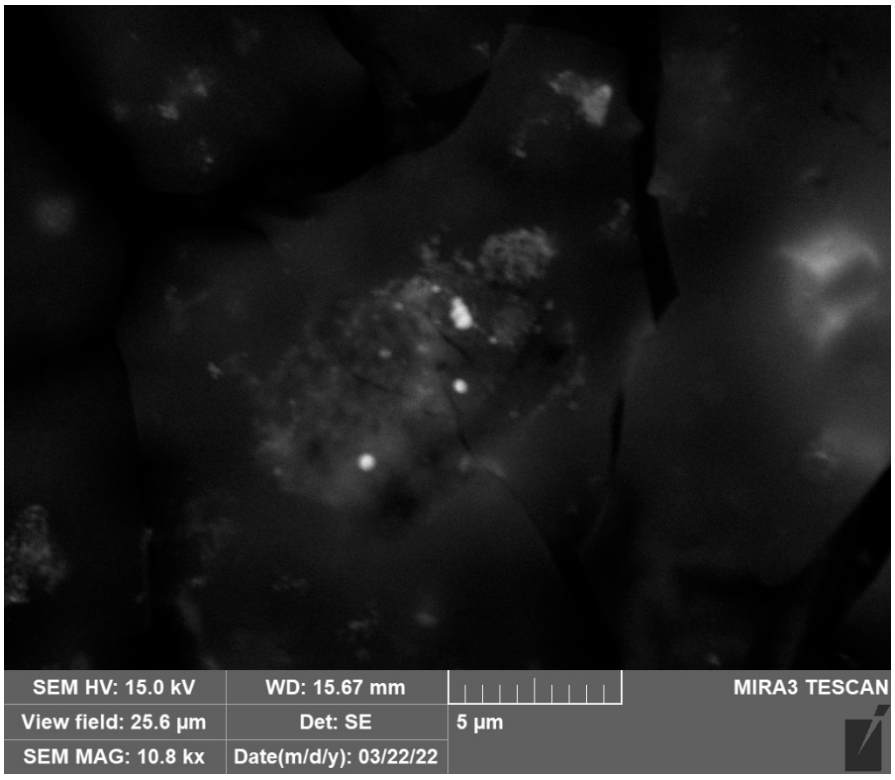

Figure 90: STD11Run2 Image 3 SE

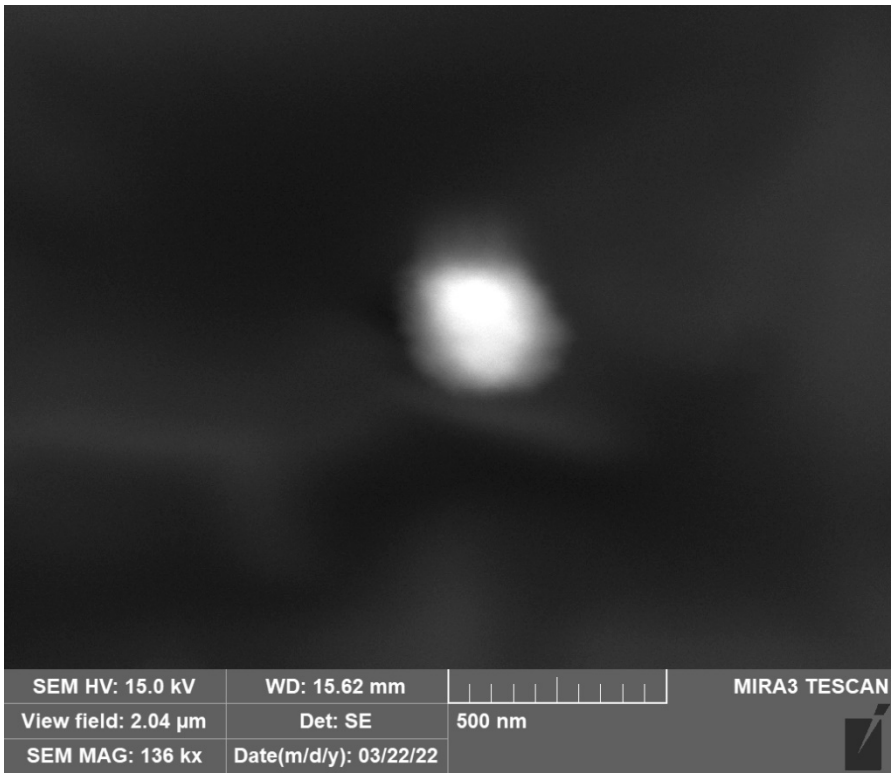

Figure 91: STD12Run13 Image 1 SE

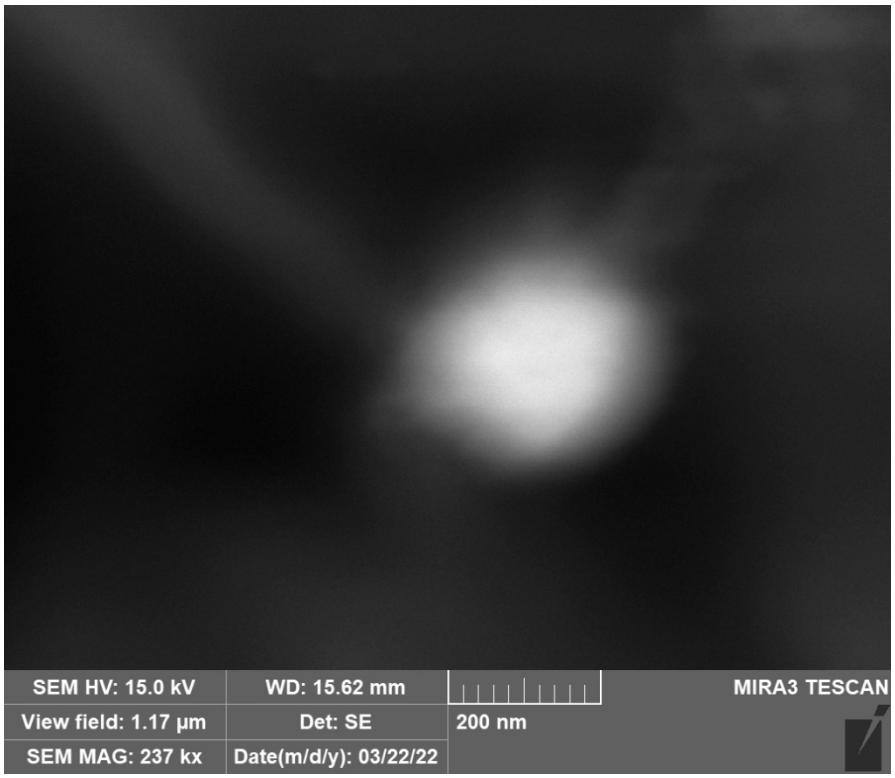

Figure 92: STD12Run13 Image 2 SE

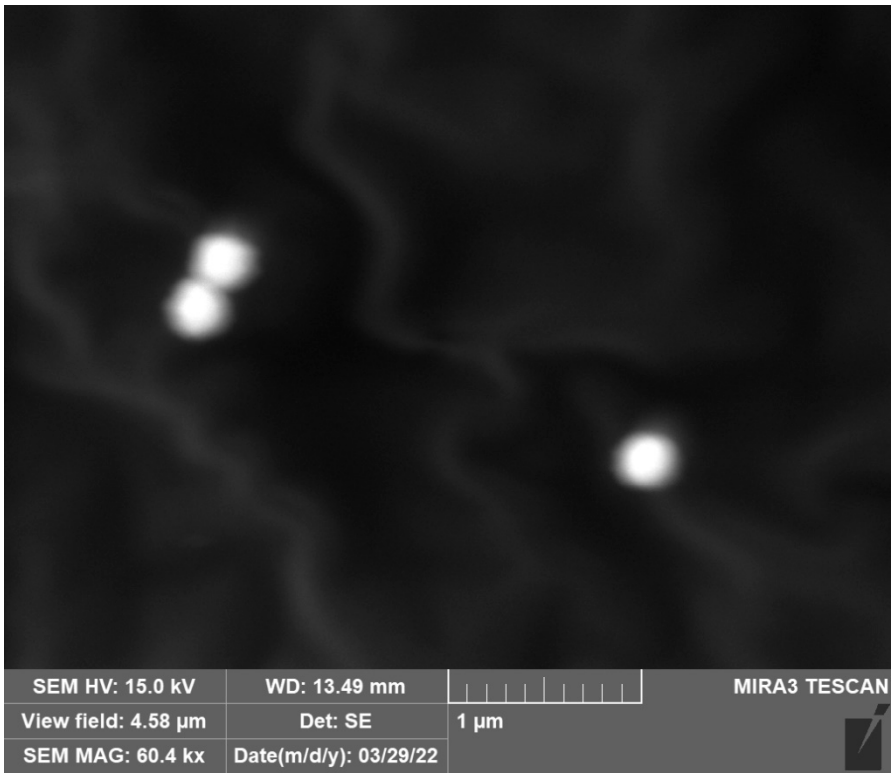

Figure 93: STD13Run18 Image 1 SE

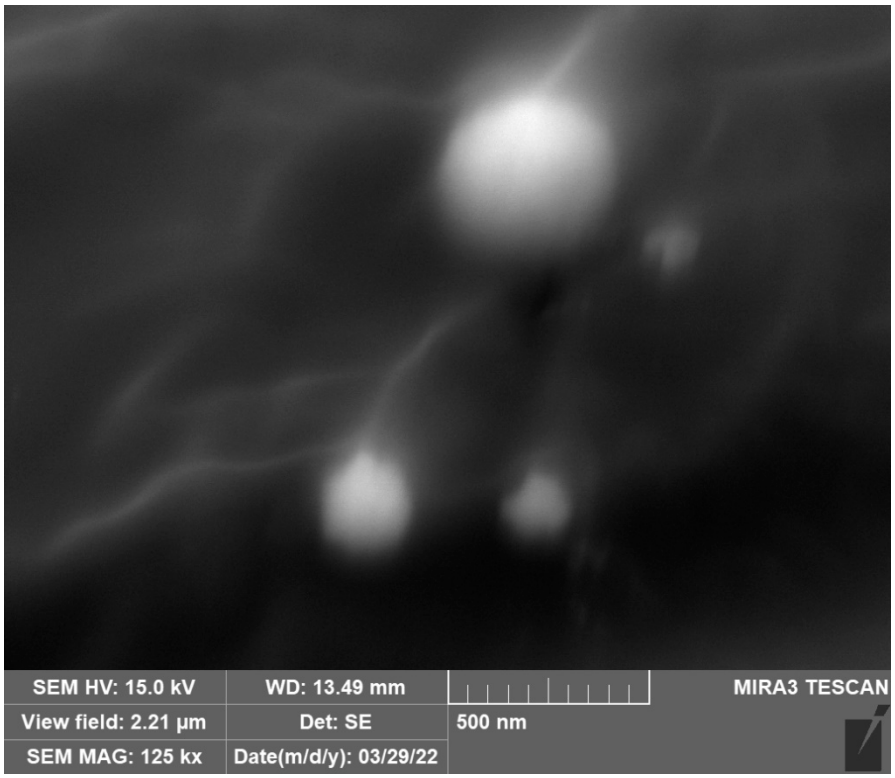

Figure 94: STD13Run18 Image 2 SE

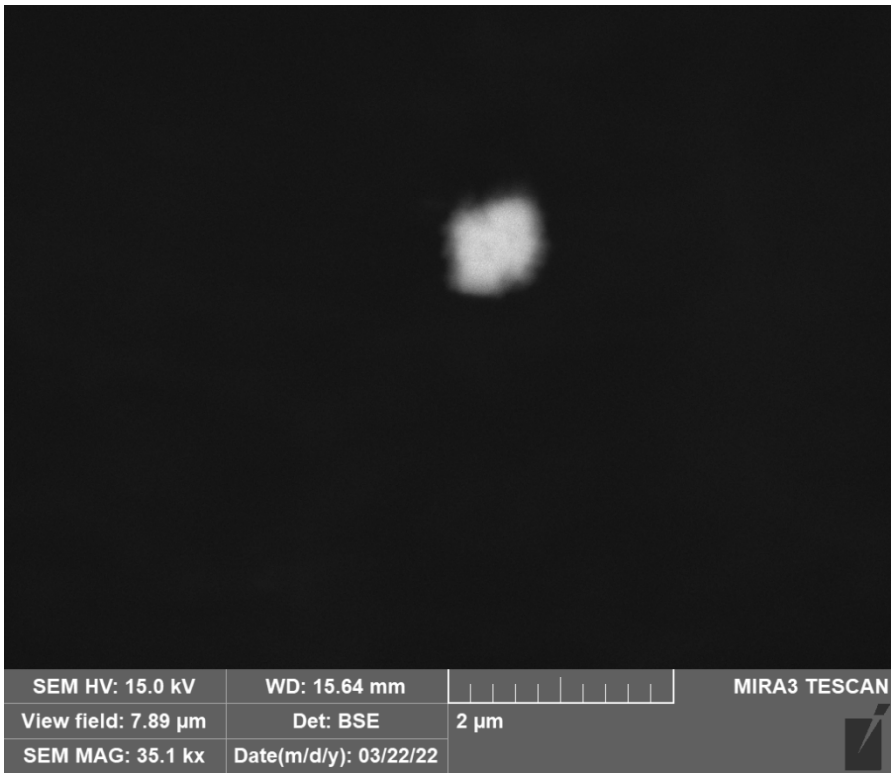

Figure 95: STD14Run7 Image 1 BSE

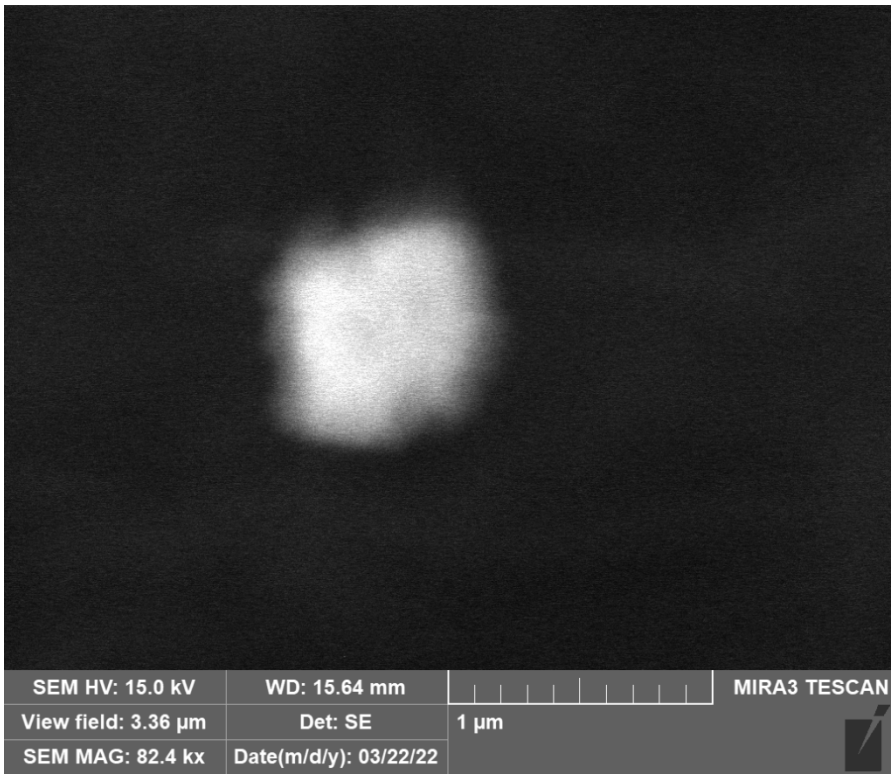

Figure 96: STD14Run7 Image 1 SE

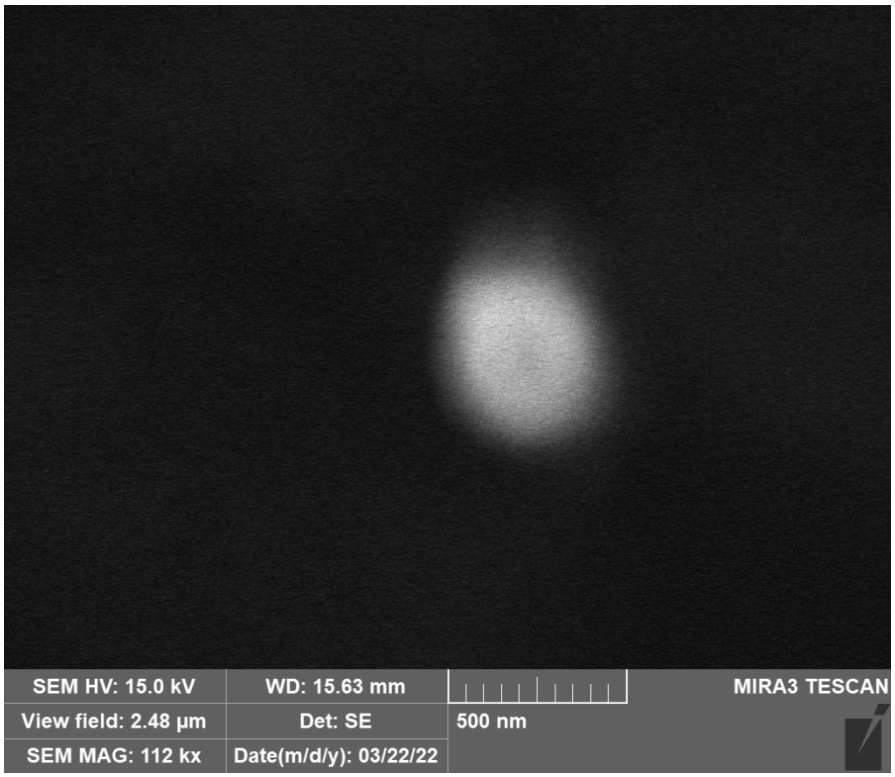

Figure 97: STD14Run7 Image 2 SE

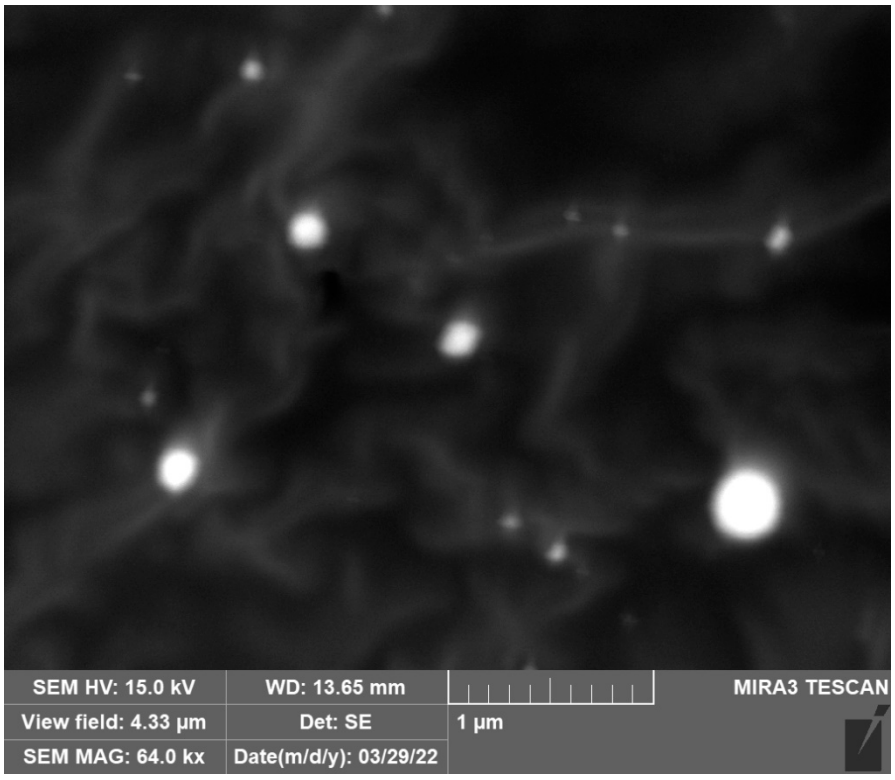

Figure 98: STD15Run15 Image 1 SE

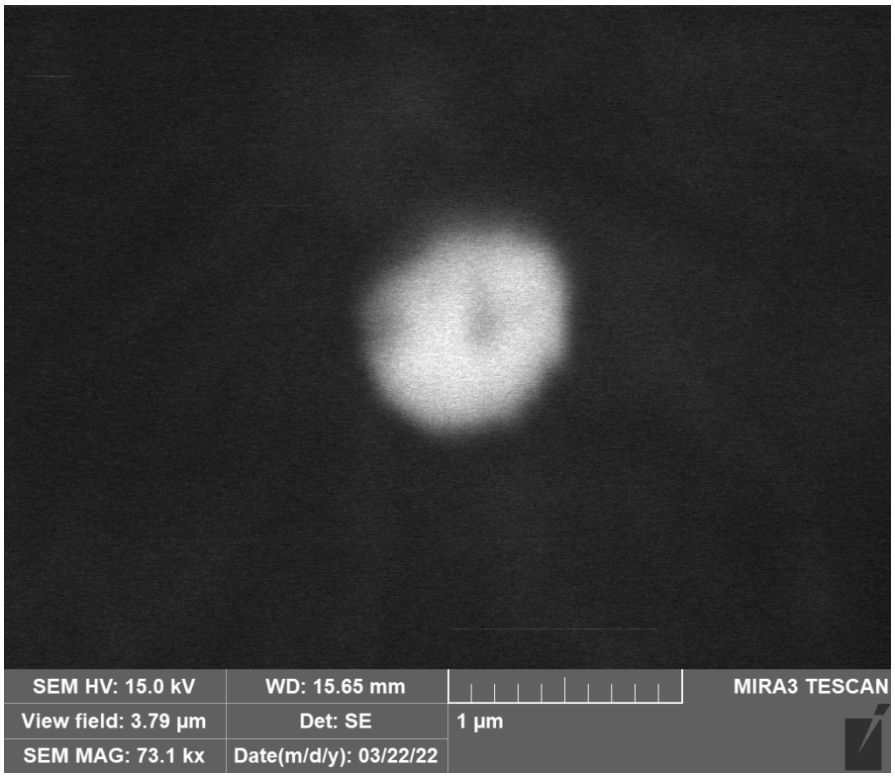

Figure 99: STD16Run4 Image 1 SE

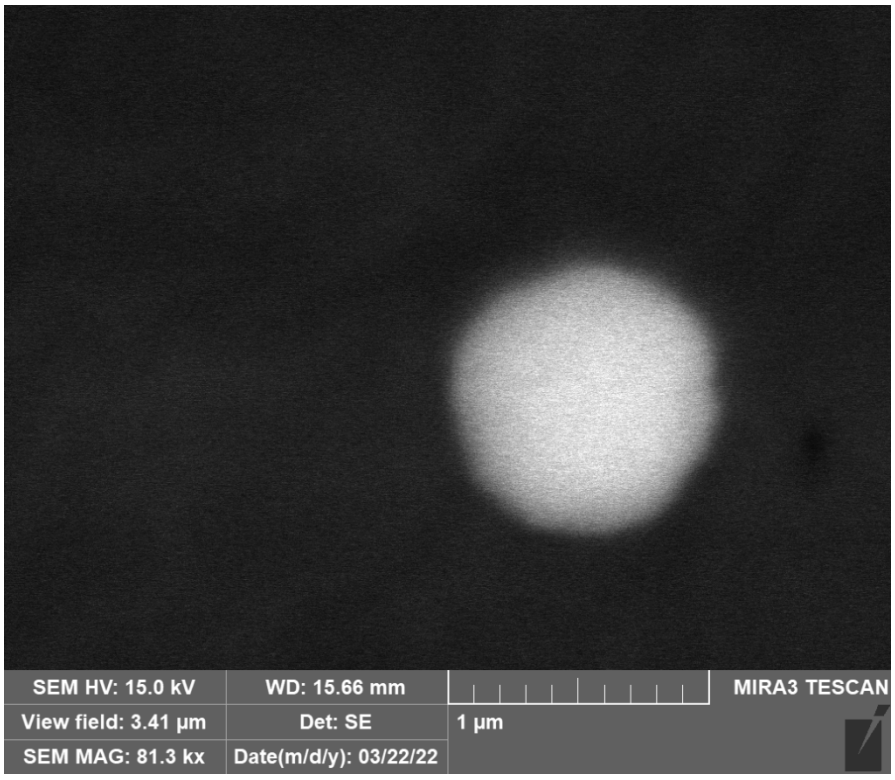

Figure 100: STD17Run8RR Image 1 SE

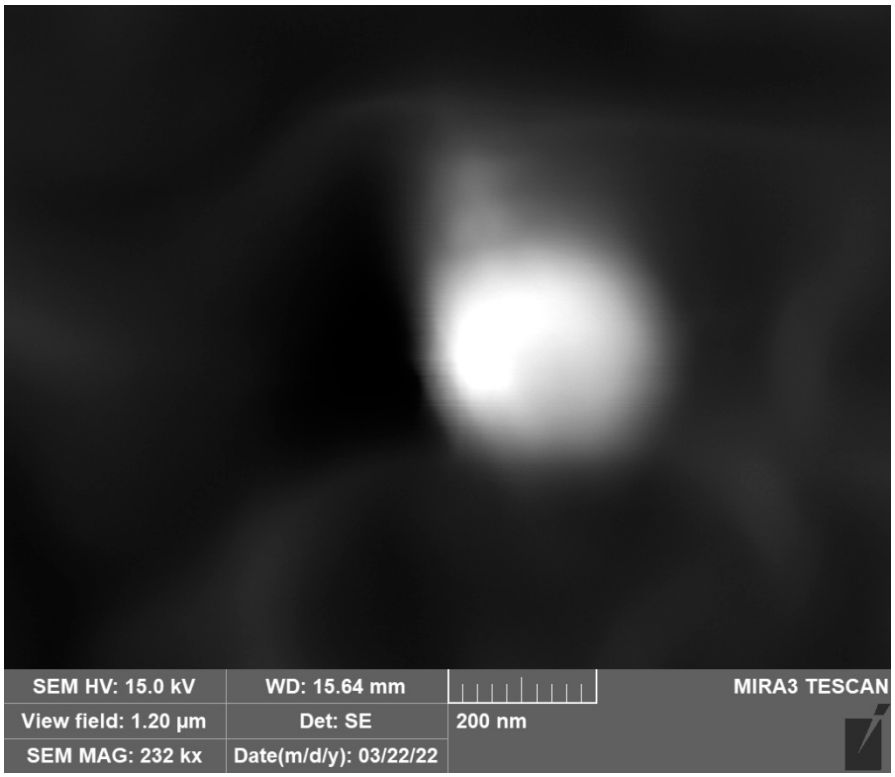

Figure 101: STD17Run8RR Image 2 SE

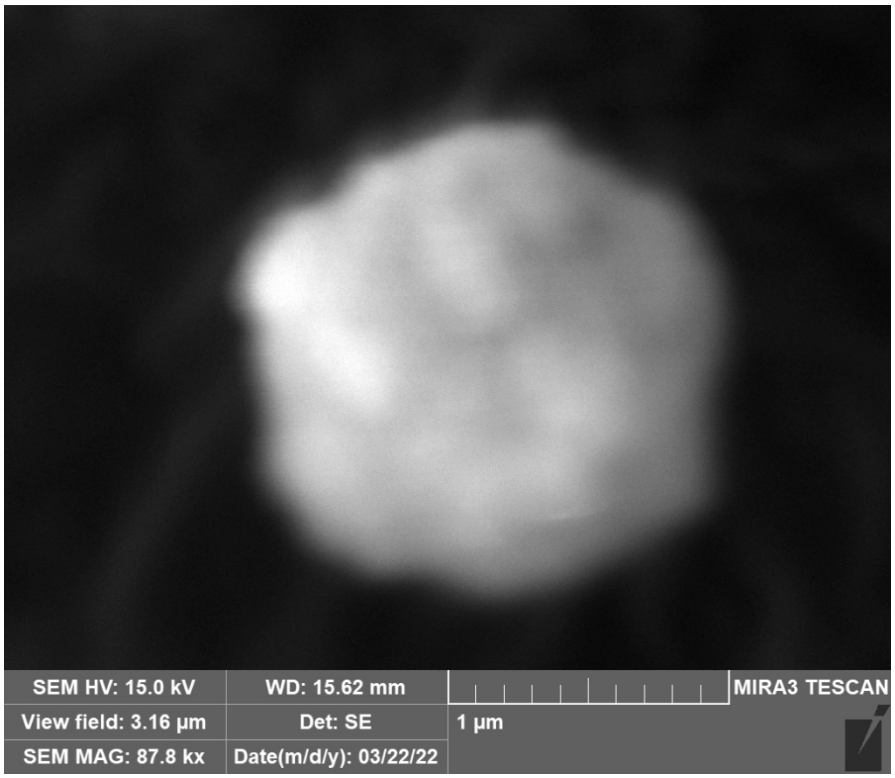

Figure 102: STD18Run6 Image 1 SE

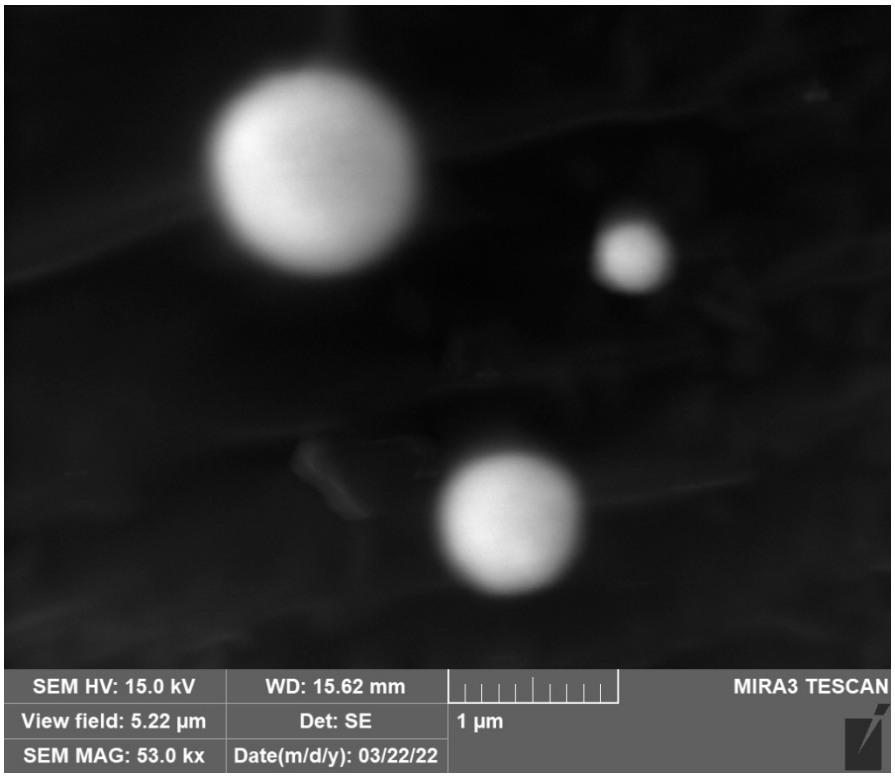

Figure 103: STD18Run6 Image 2 SE

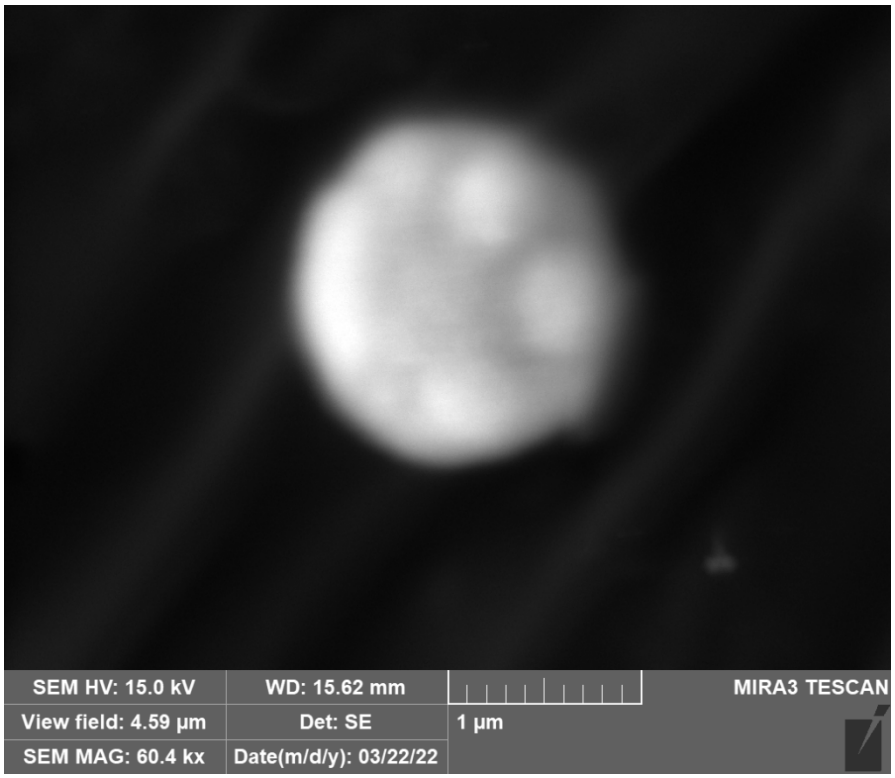

Figure 104: STD18Run6 Image 3 SE

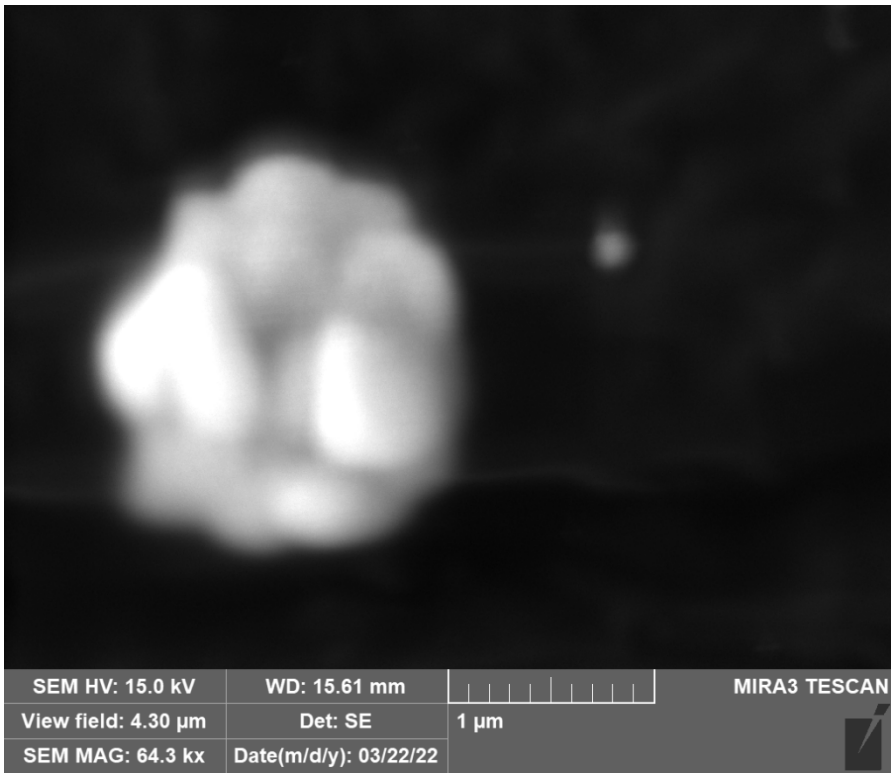

Figure 105: STD18Run6 Image 4 SE

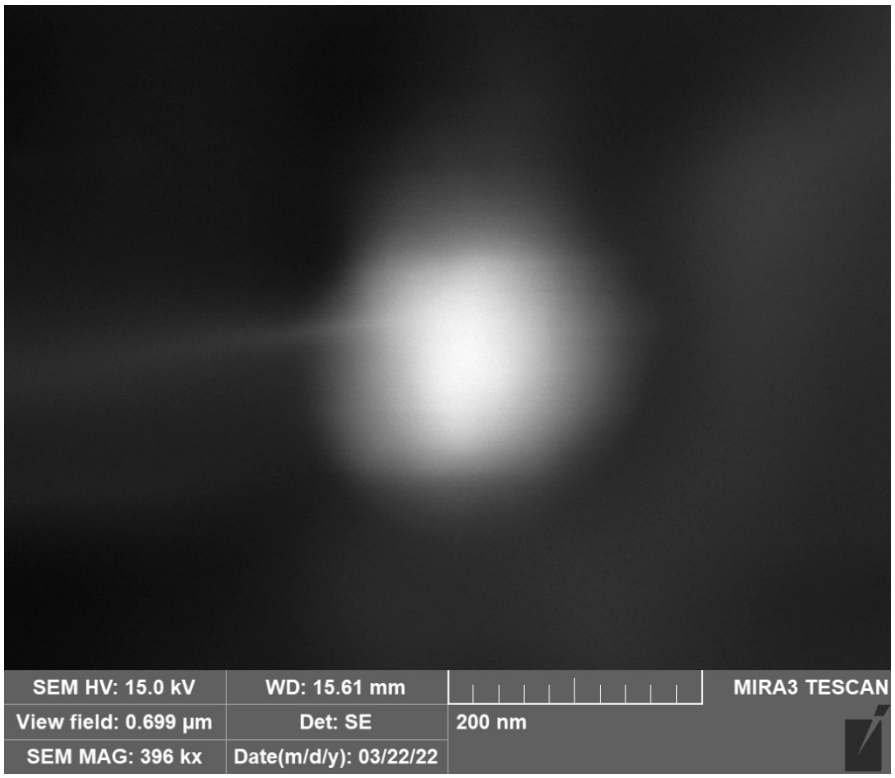

Figure 106: STD18Run6 Image 5 SE

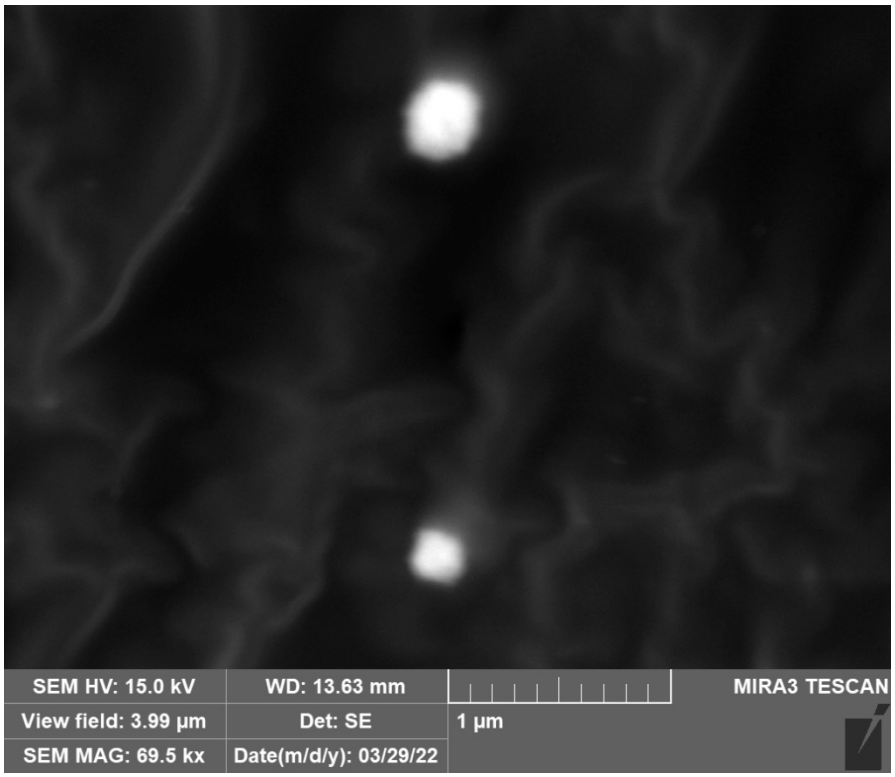

Figure 107: STD19Run19 Image 1 SE

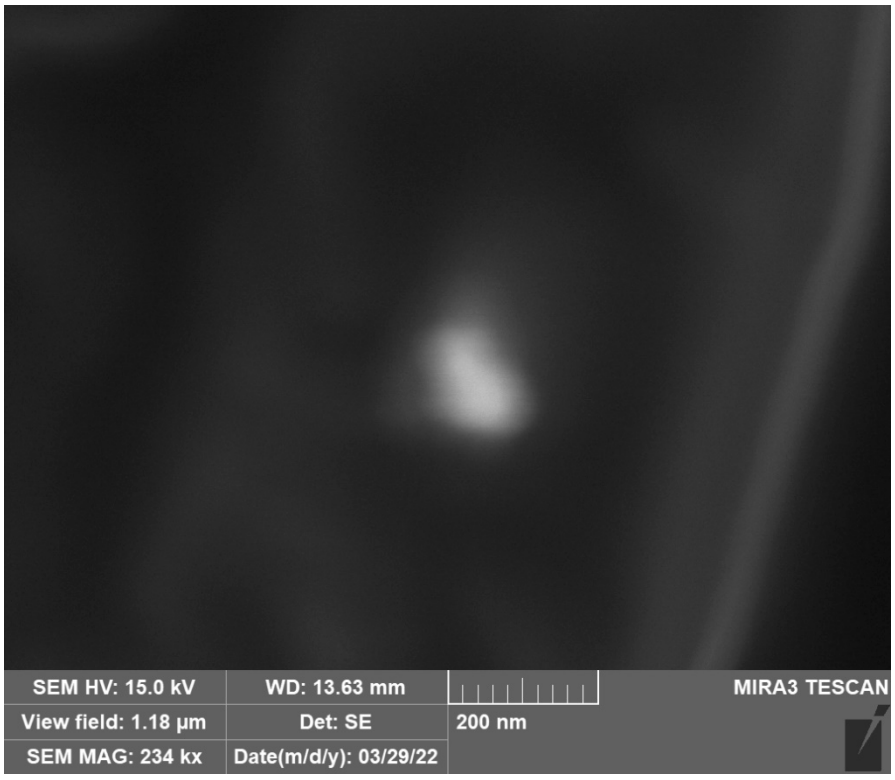

Figure 108: STD19Run19 Image 2 SE

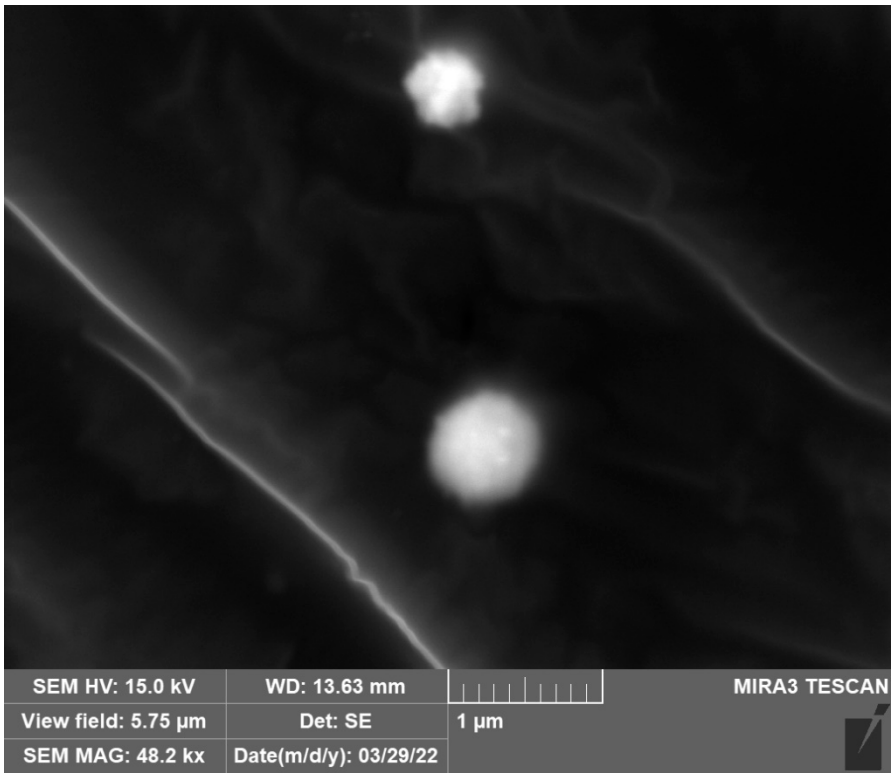

Figure 109: STD19Run19 Image 3 SE

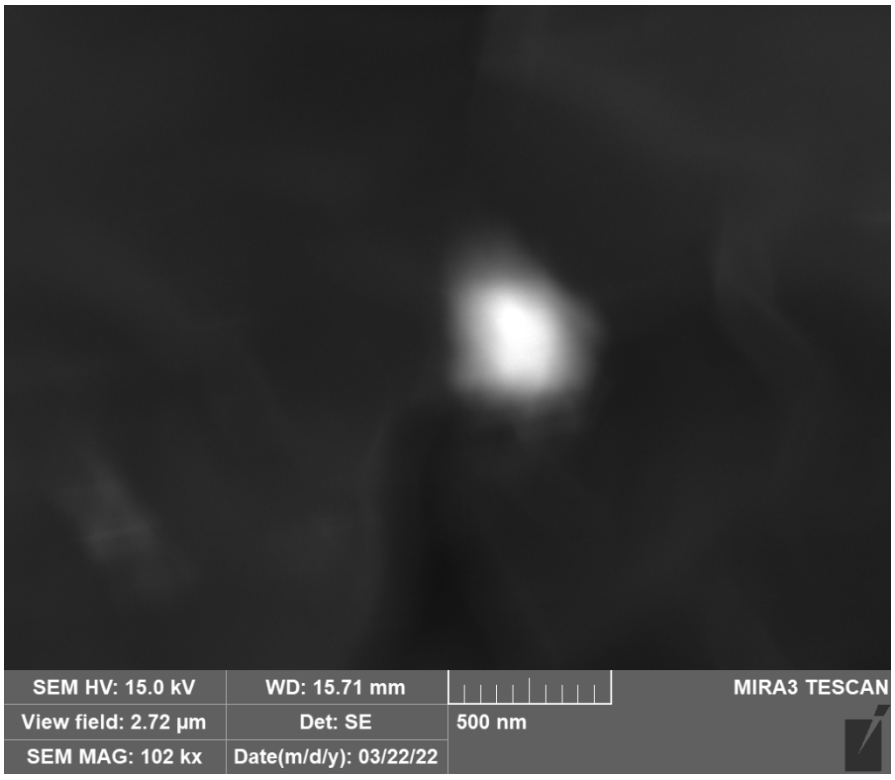

Figure 110: STD20Run1 Image 1 SE

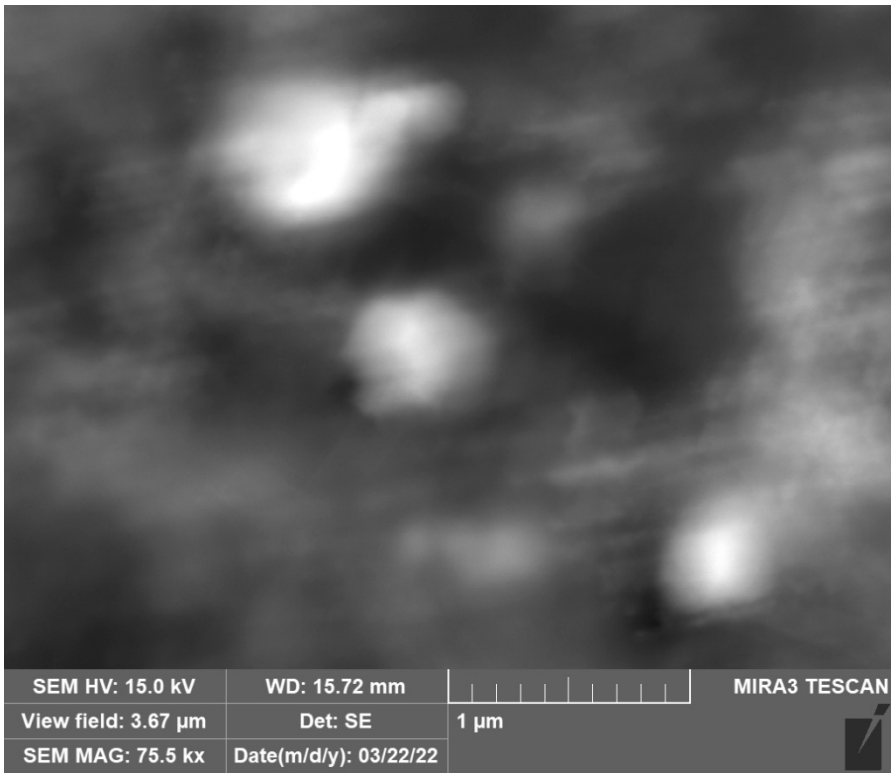

Figure 111: STD20Run1 Image 2 SE

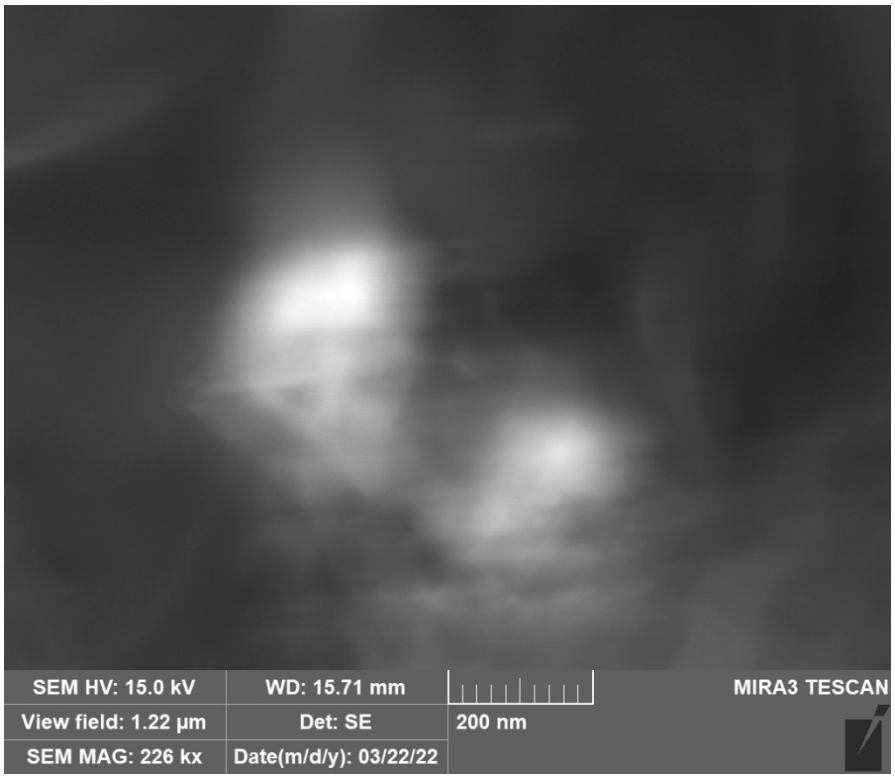

Figure 112: STD20Run1 Image 3 SE

9. Appendix D: FESEM Images of Gold Cyanide System

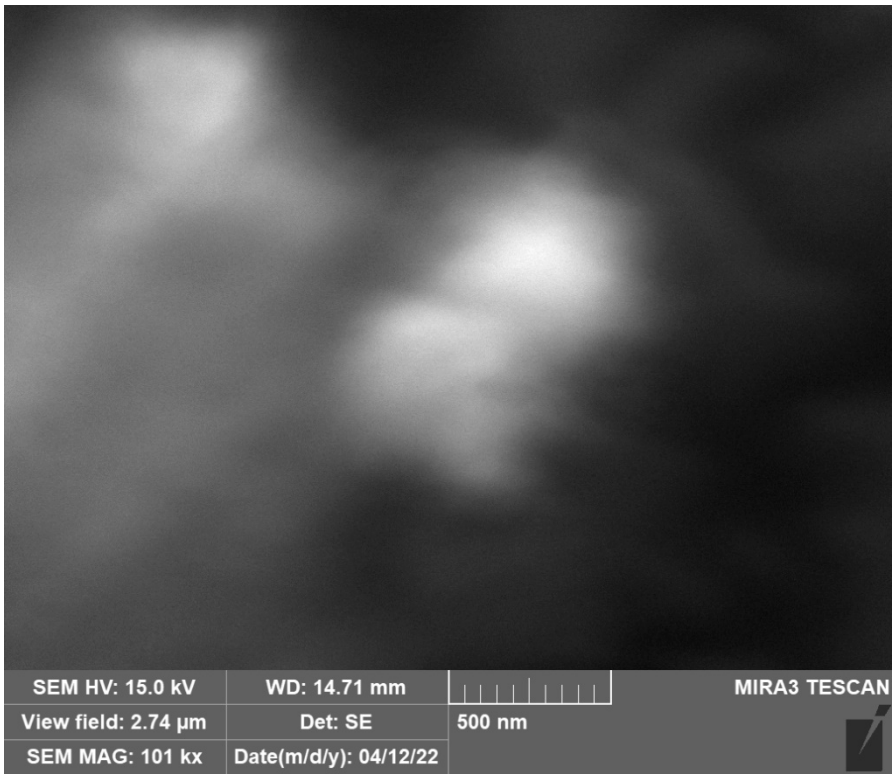

Figure 113: STD3 Image 1

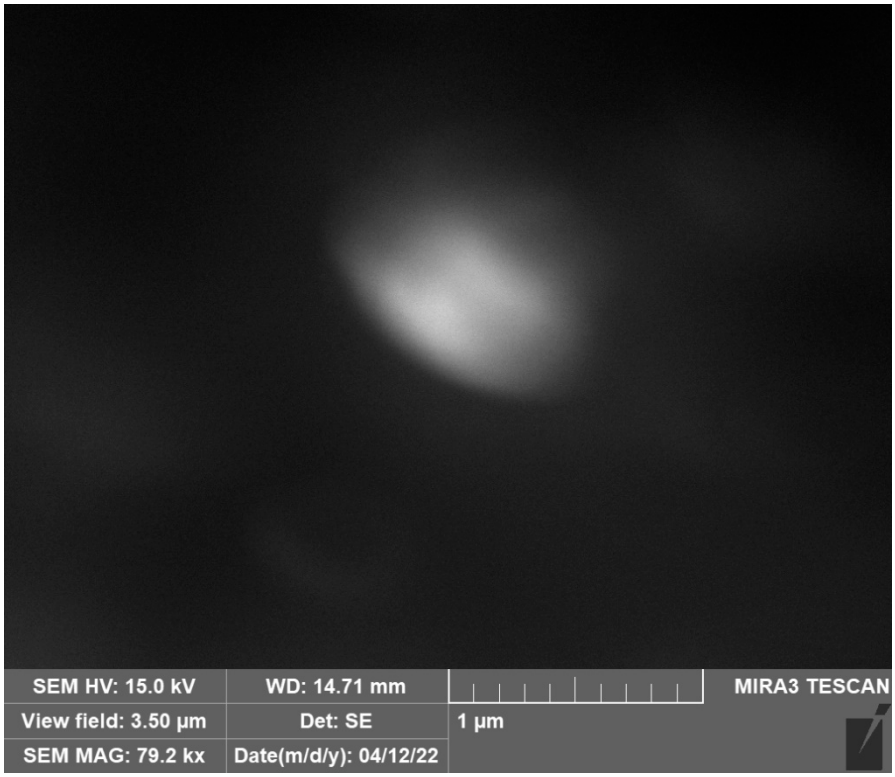

Figure 114: STD3 Image 2

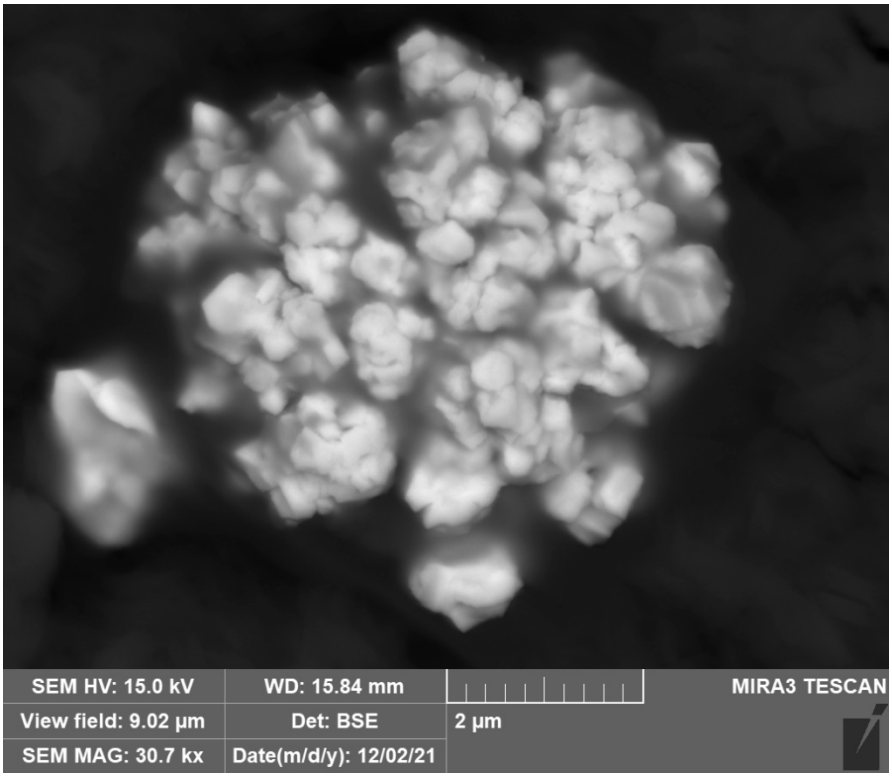

Figure 115: STD 6 Image 1

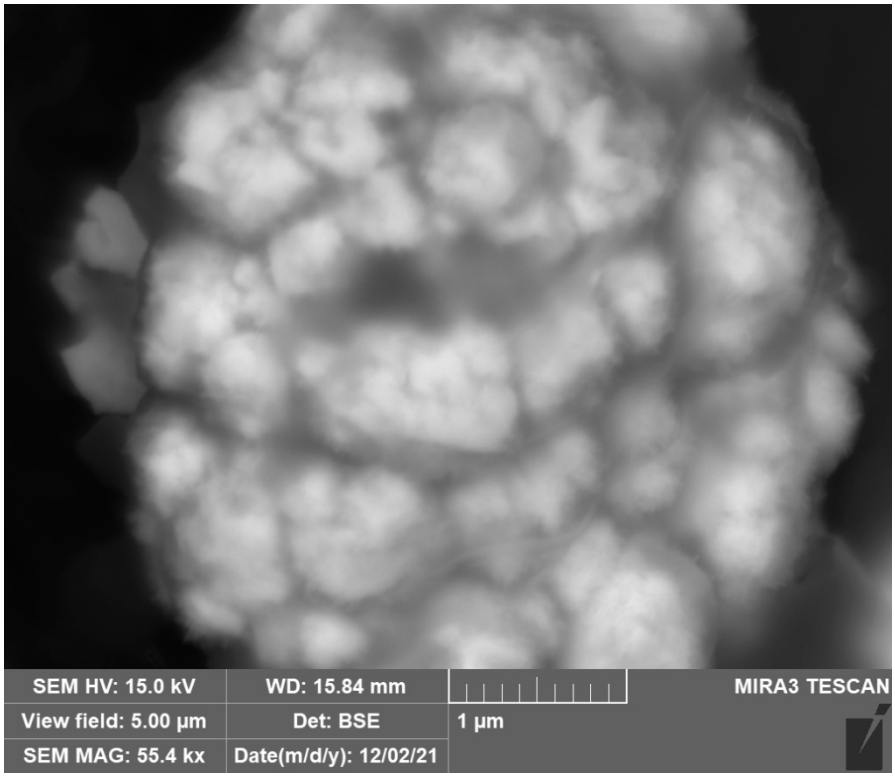

Figure 116: STD6 Image 2

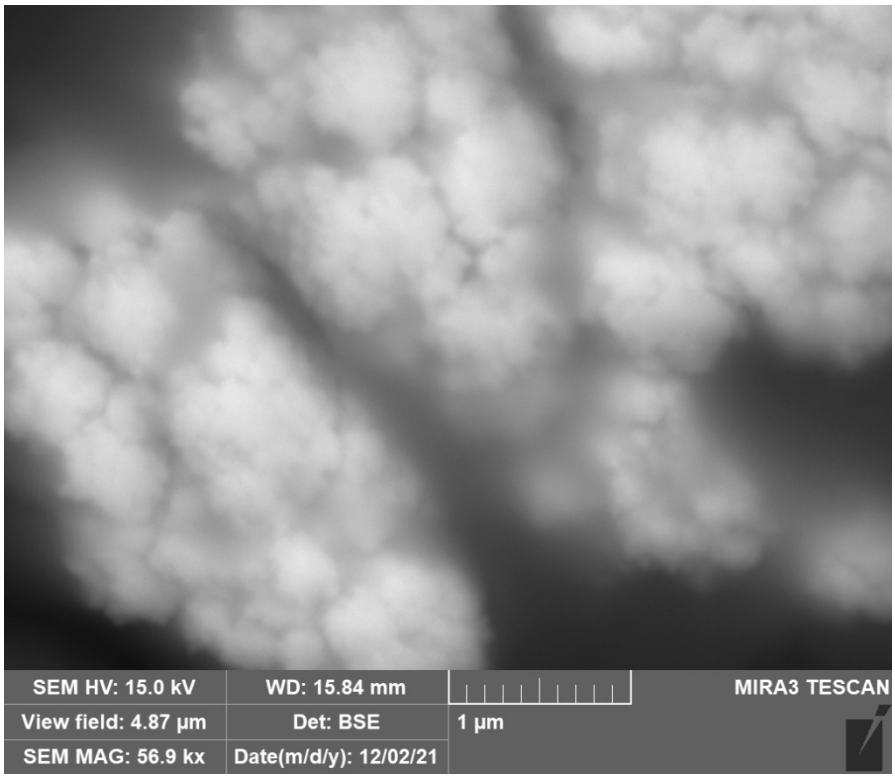

Figure 117: STD6 Image 3

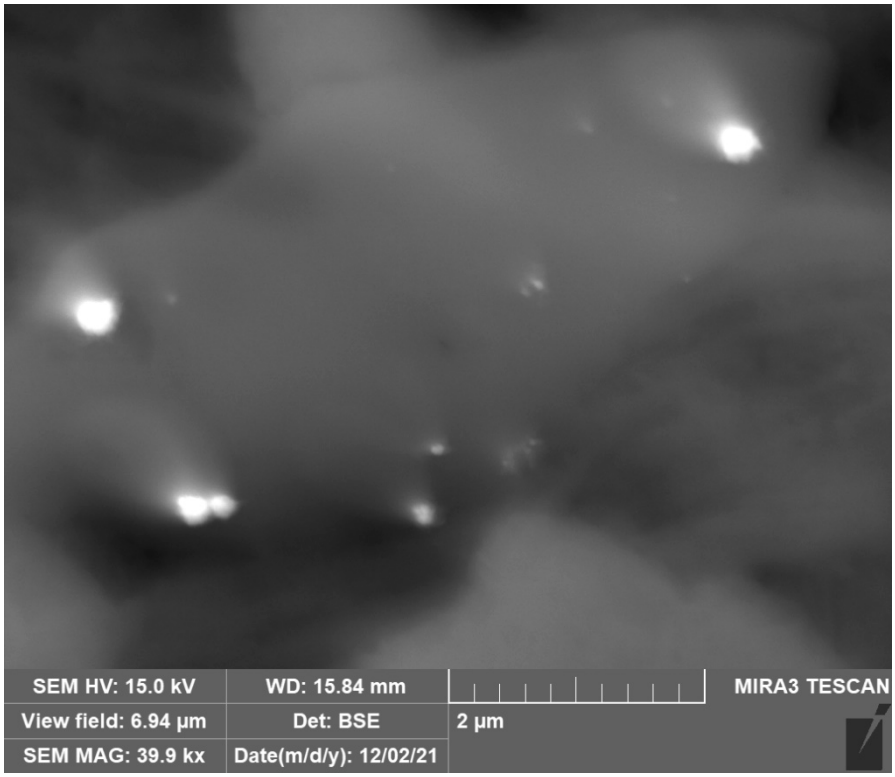

Figure 118: STD6 Image 4

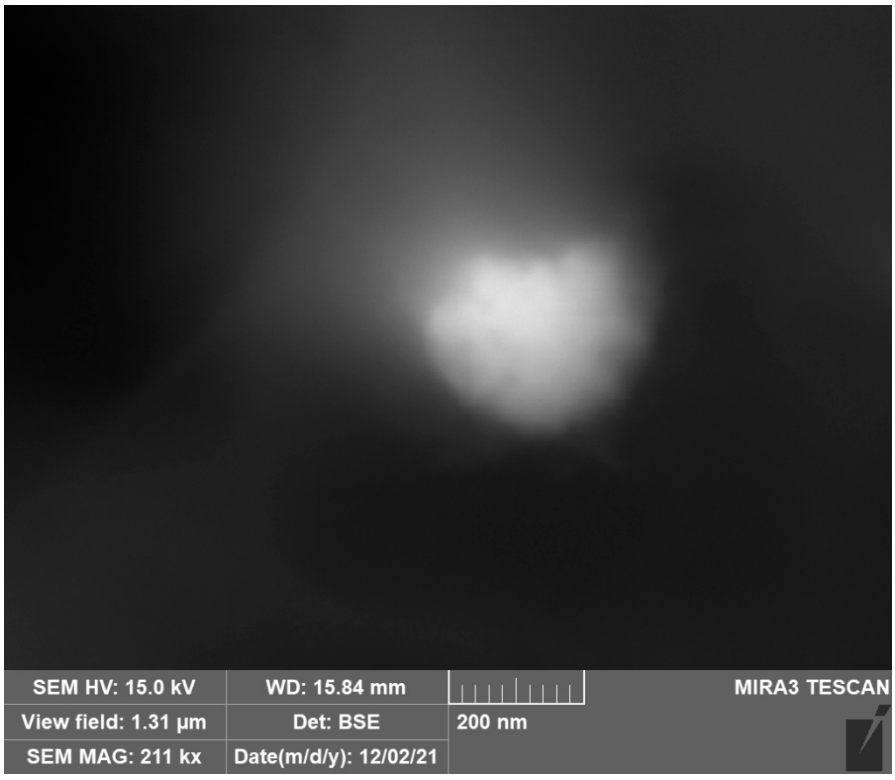

Figure 119: STD6 Image 4 zoomed in on one particle.

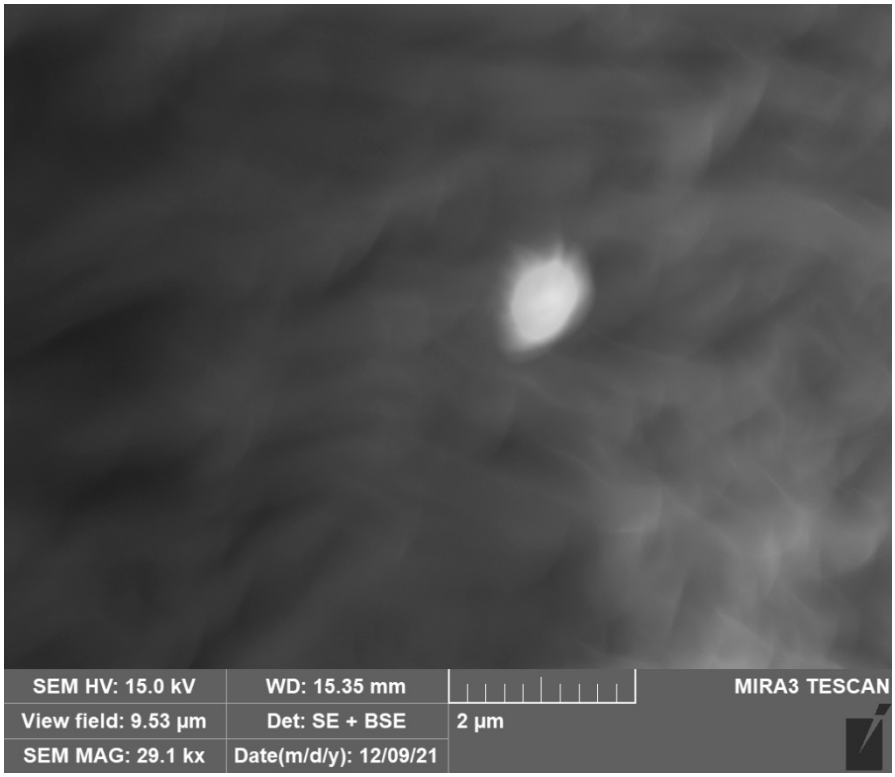

Figure 120: STD6 Image 5 using SE and BSE detectors.

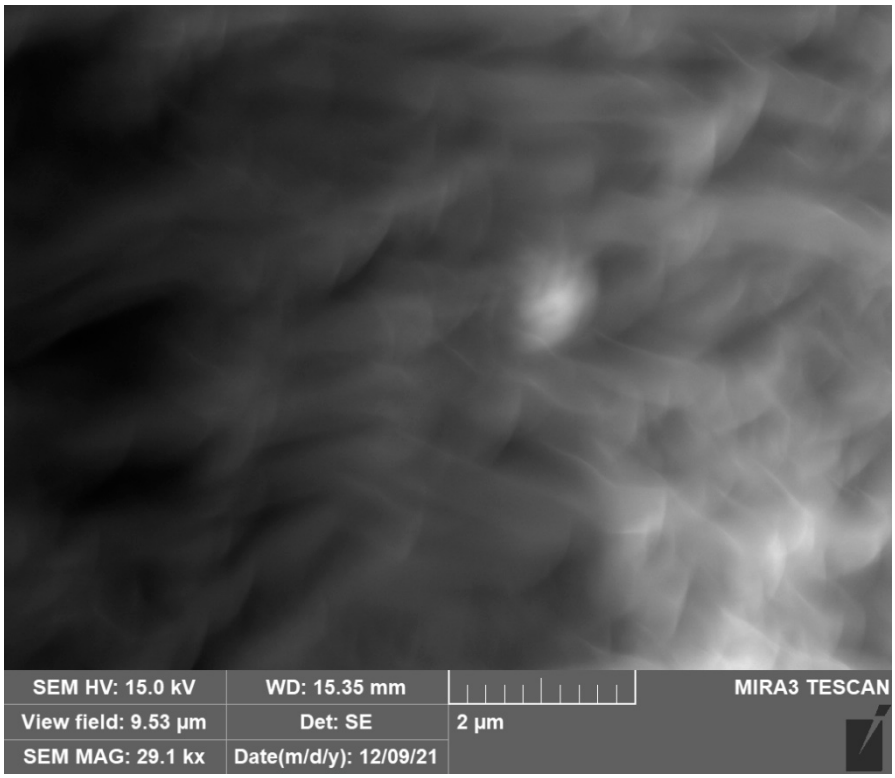

Figure 121: STD6 Image 5 using SE detector.

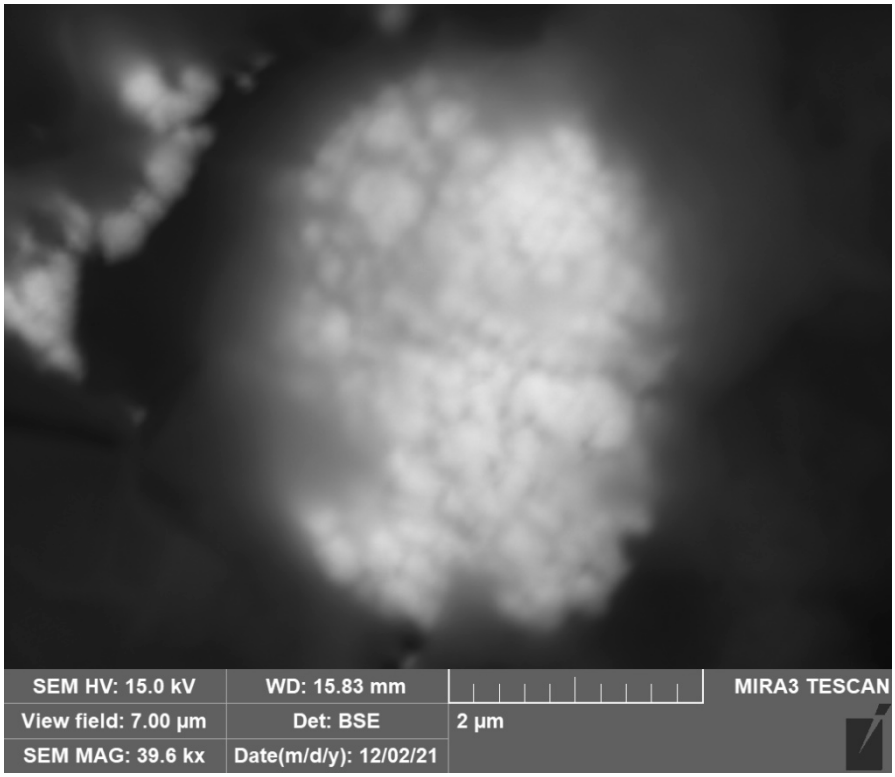

Figure 122: STD8 Image 1

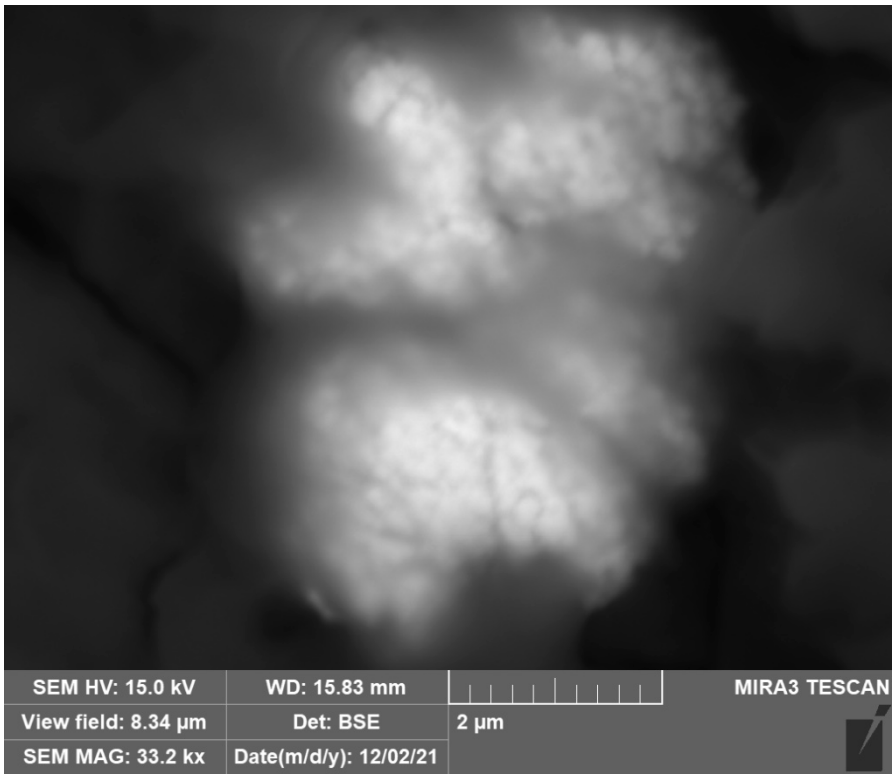

Figure 123: STD8 Image 2

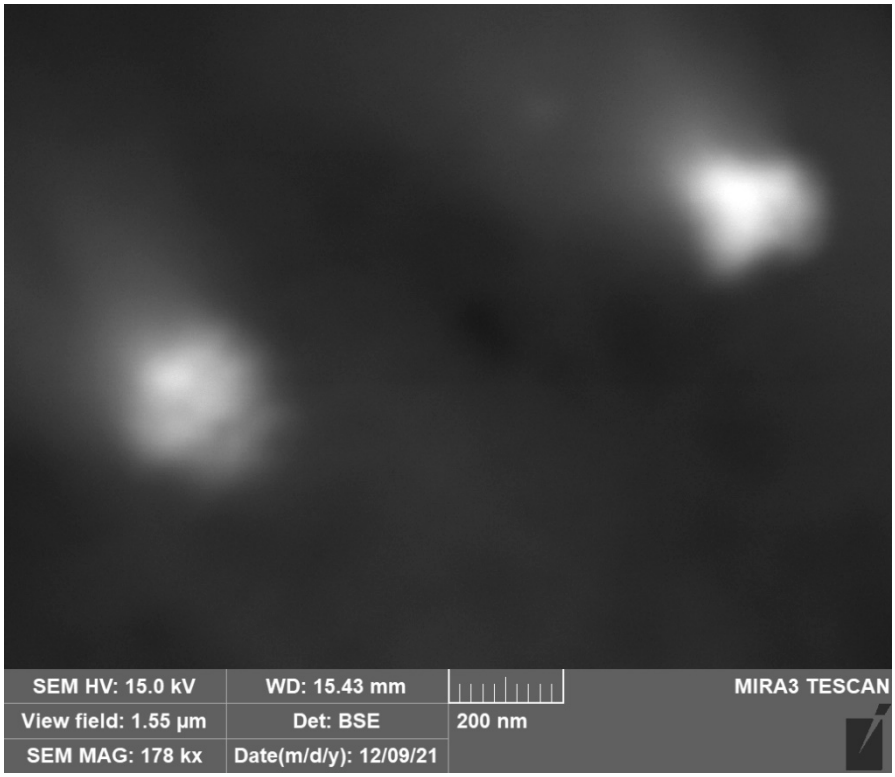

Figure 124: STD8 Image 3

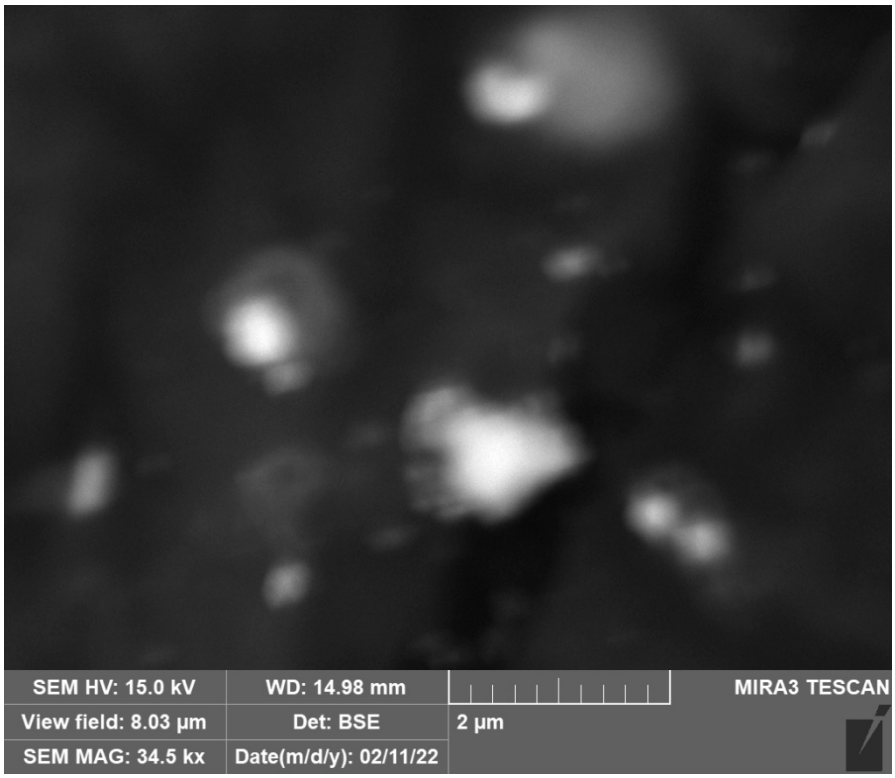

Figure 125: STD10 Image 1

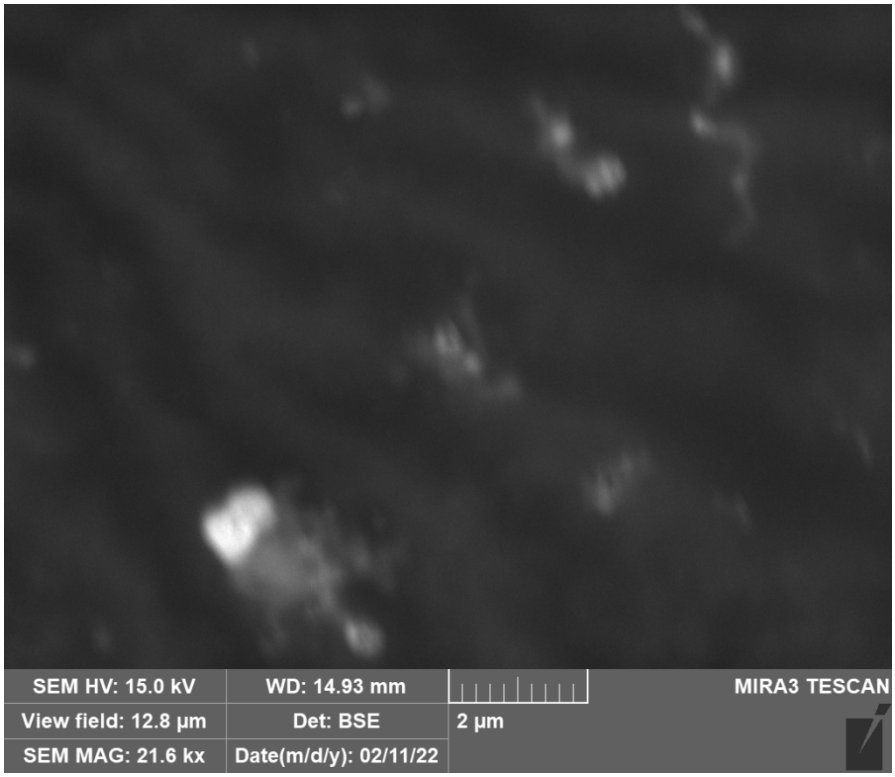

Figure 126: STD12 Image 1

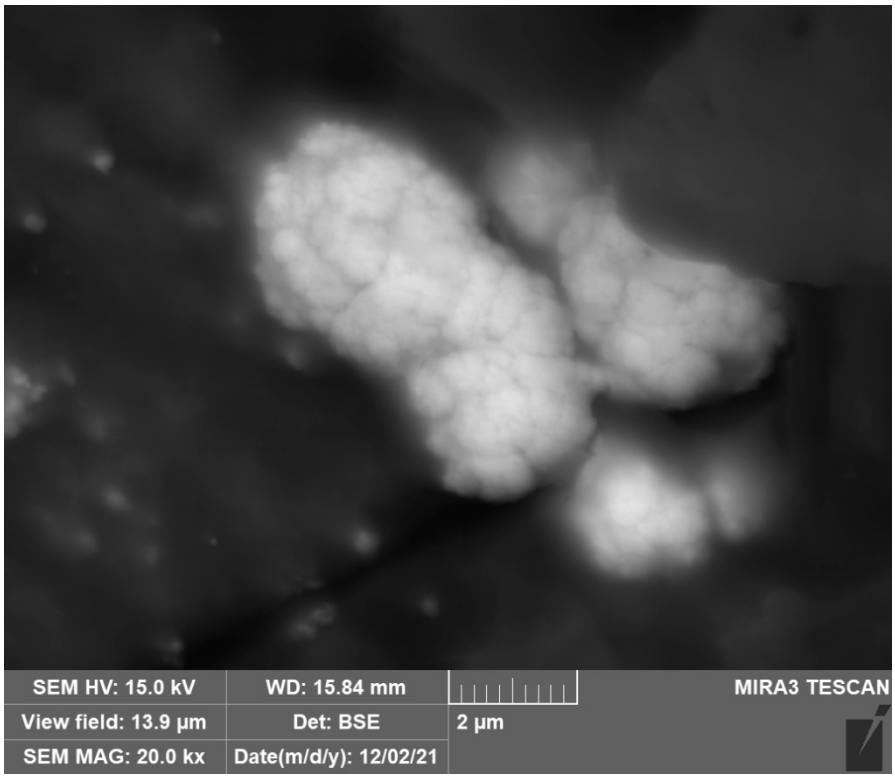

Figure 127: STD14 Image 1

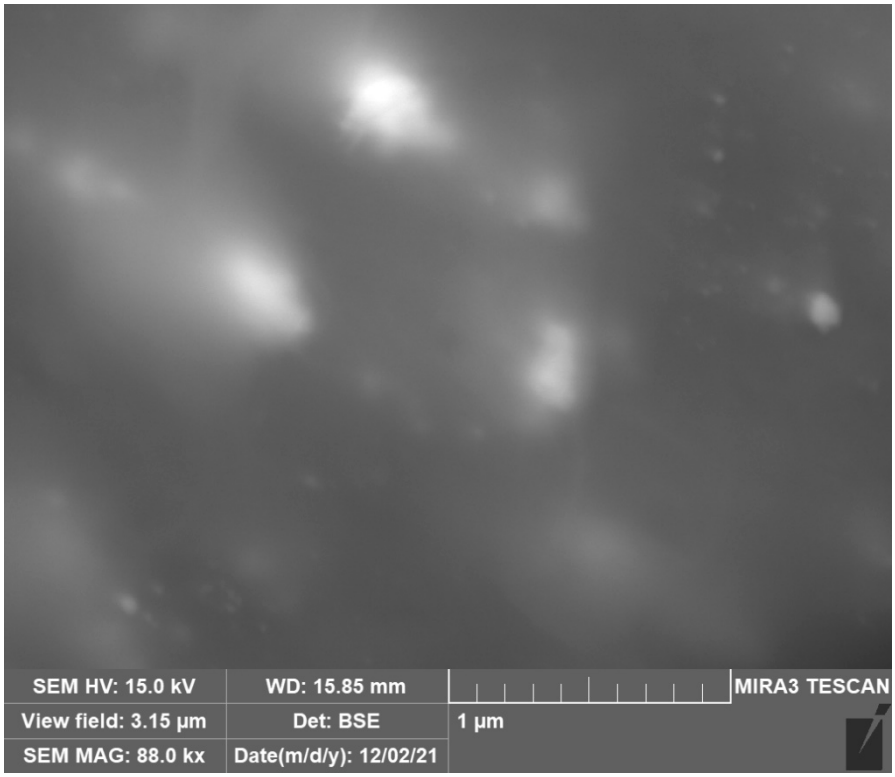

Figure 128: STD14 Image 2

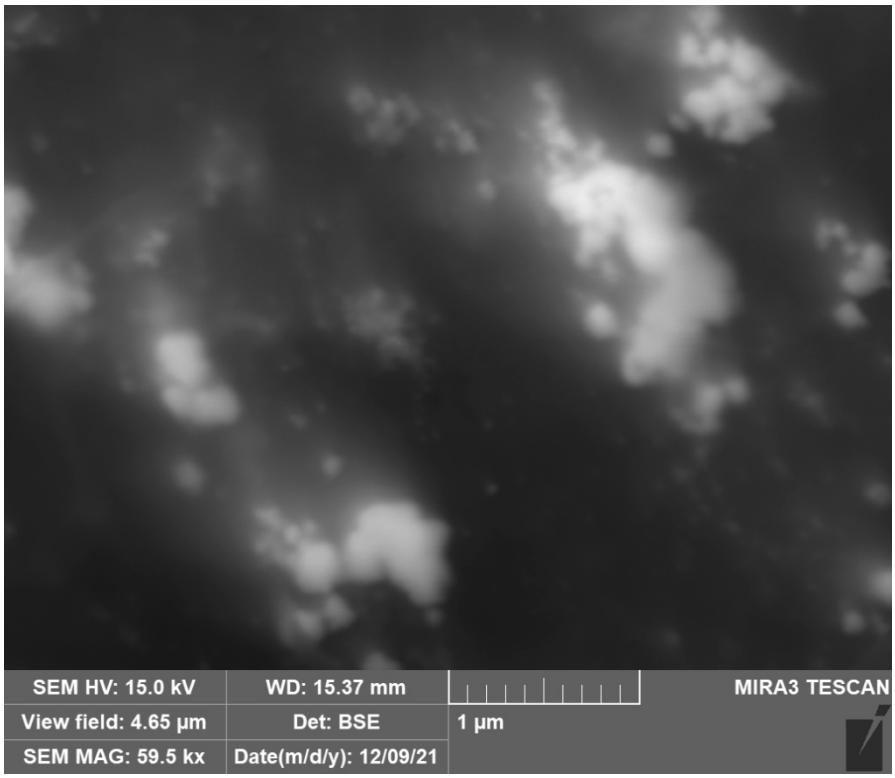

Figure 129: STD14 Image 3

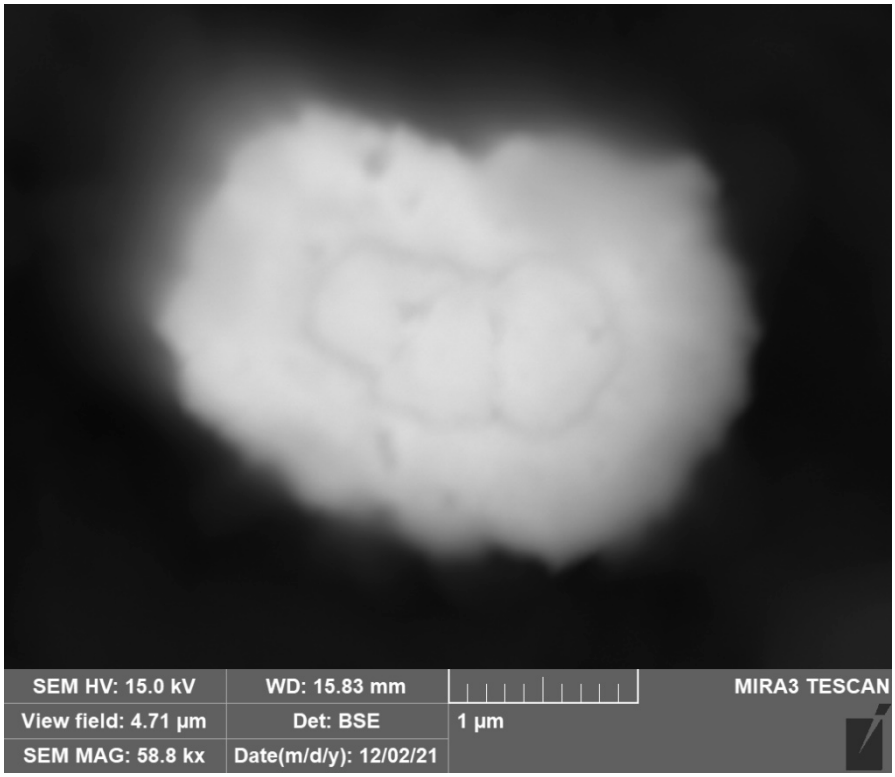

Figure 130: STD16 Image 1

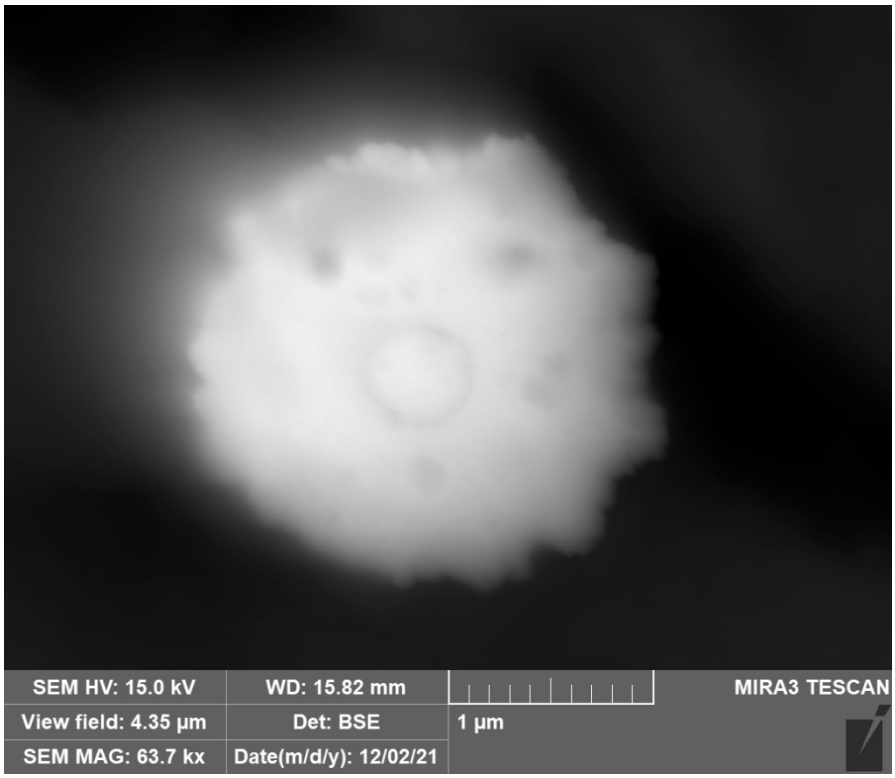

Figure 131: STD16 Image 2

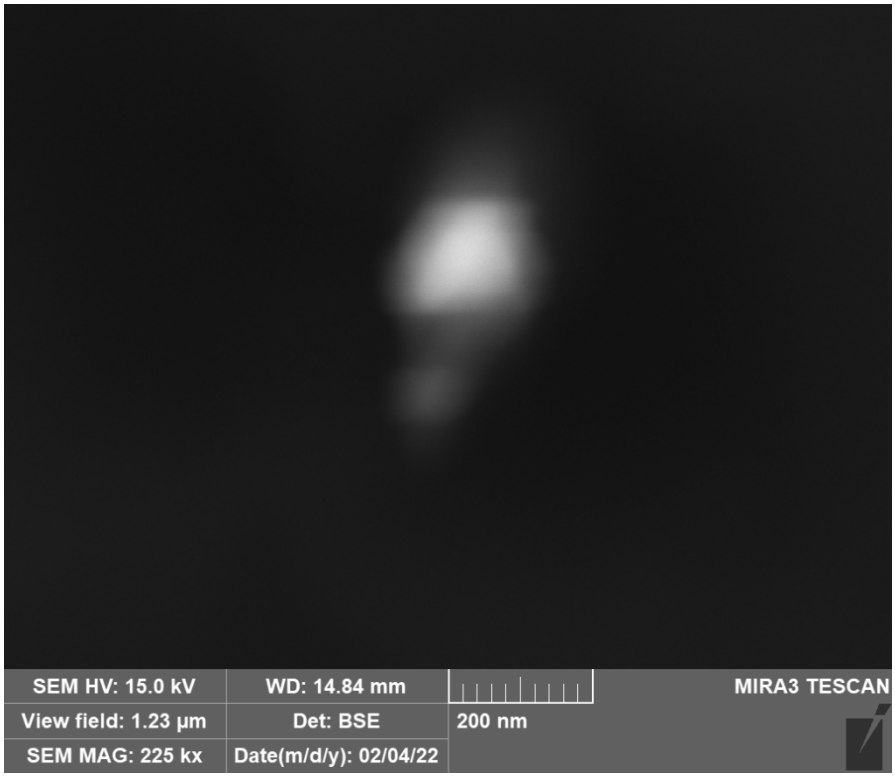

Figure 132: STD17 Image 1

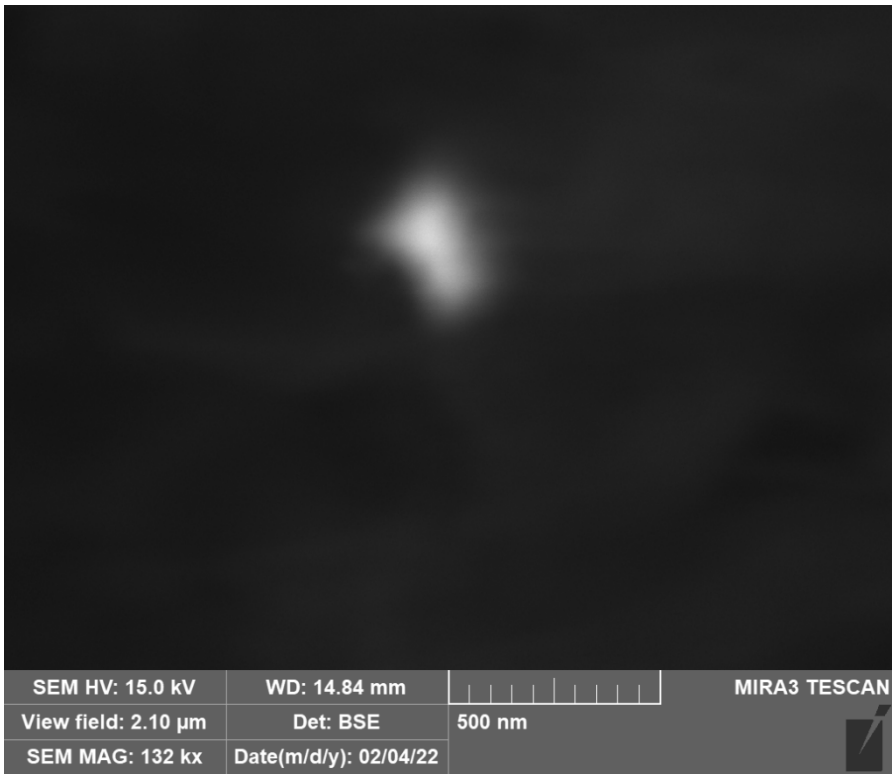

Figure 133: STD17 Image 2

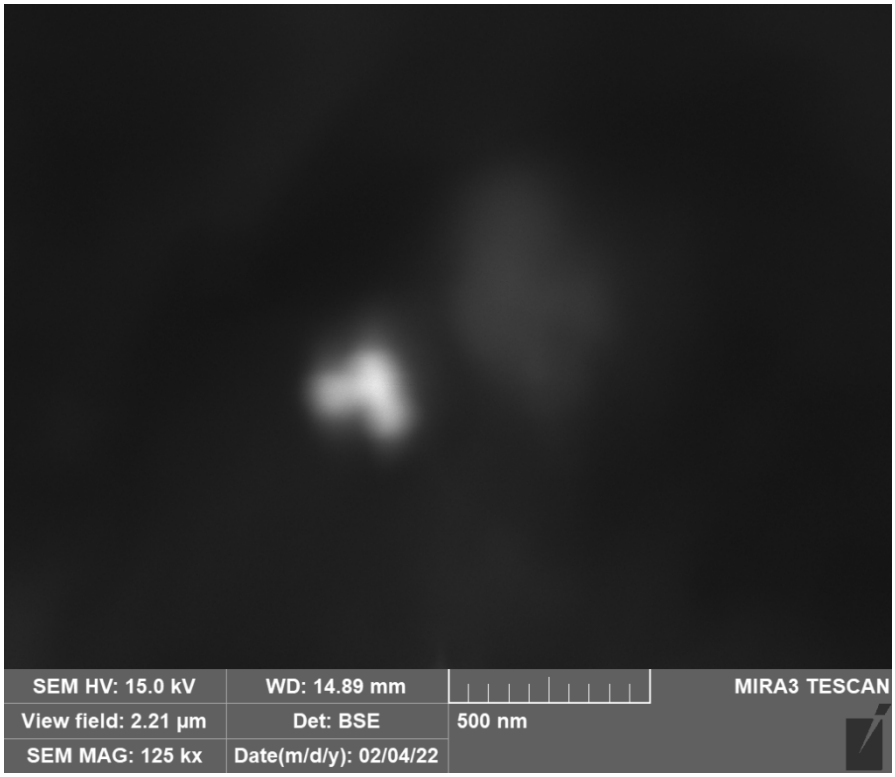

Figure 134: STD17 Image 3

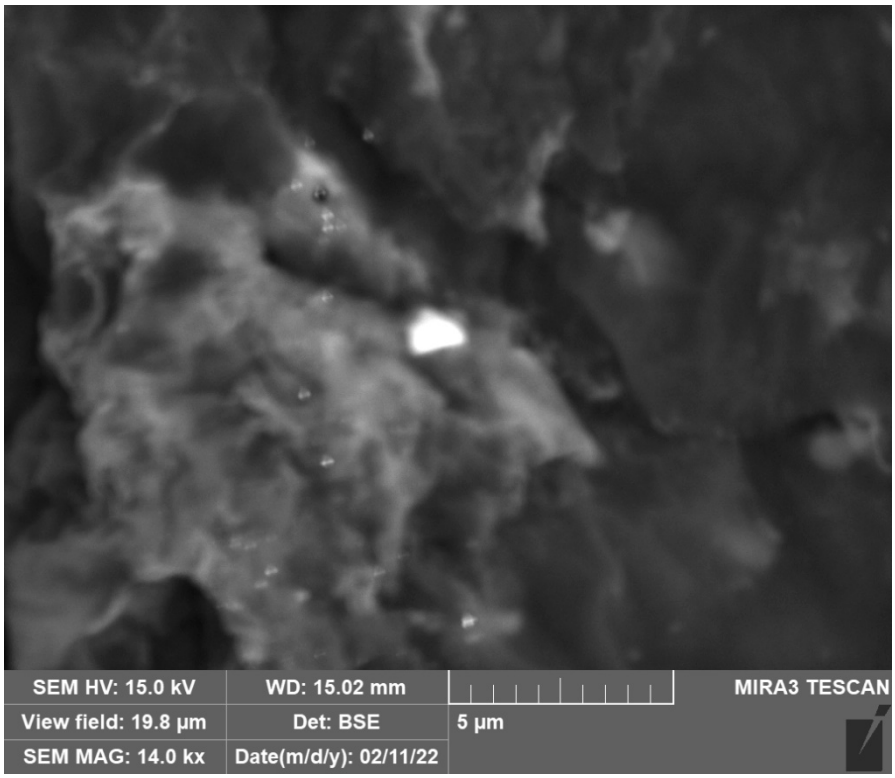

Figure 135: STD18 Image 1

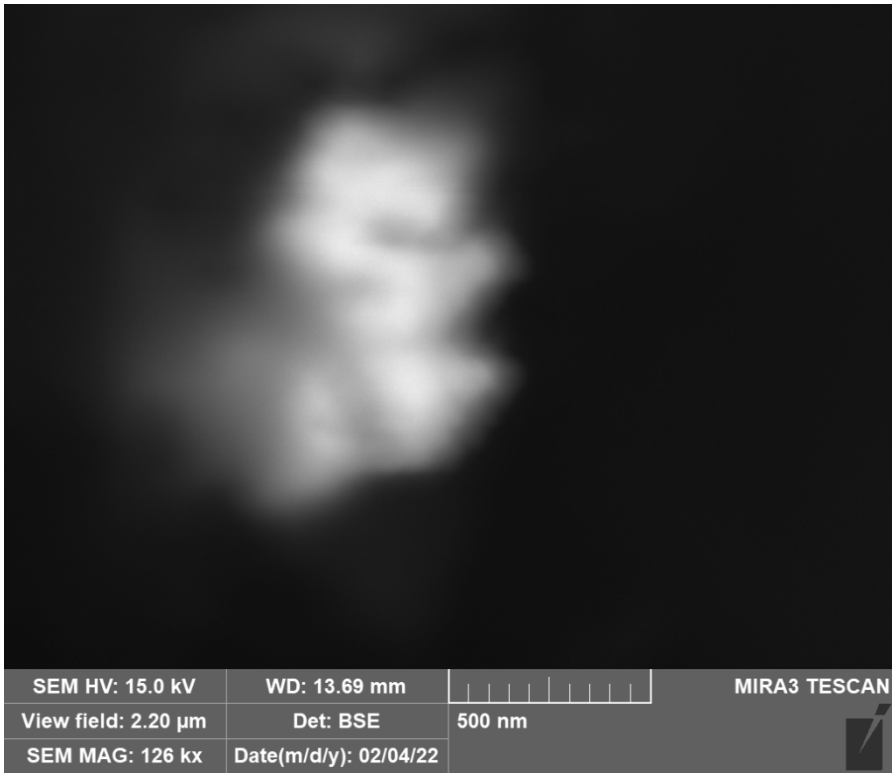

Figure 136: STD19 Image 1

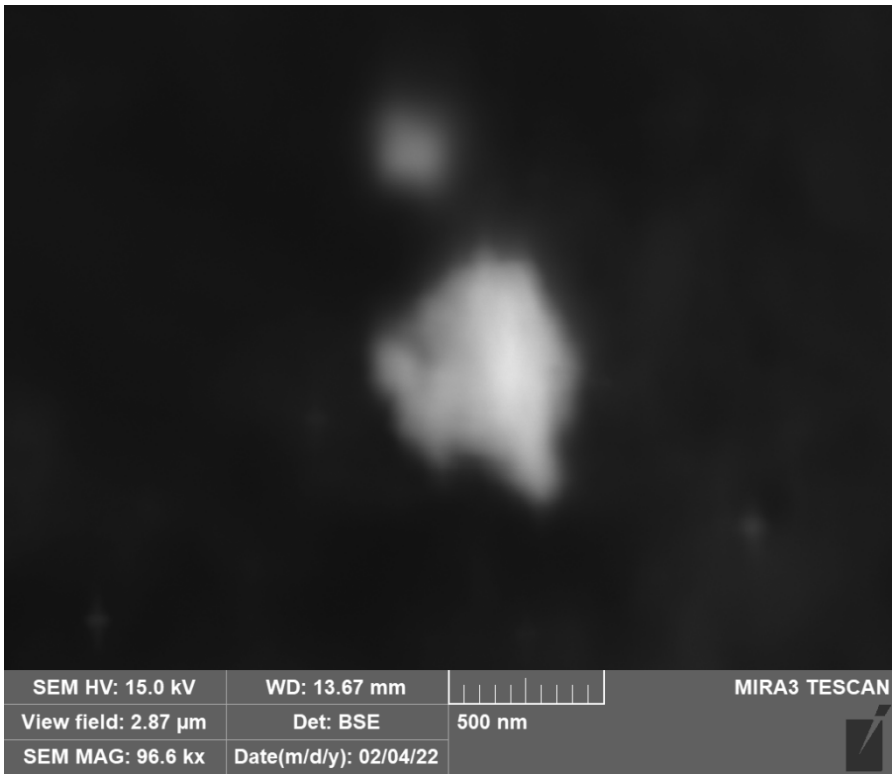

Figure 137: STD19 Image 2

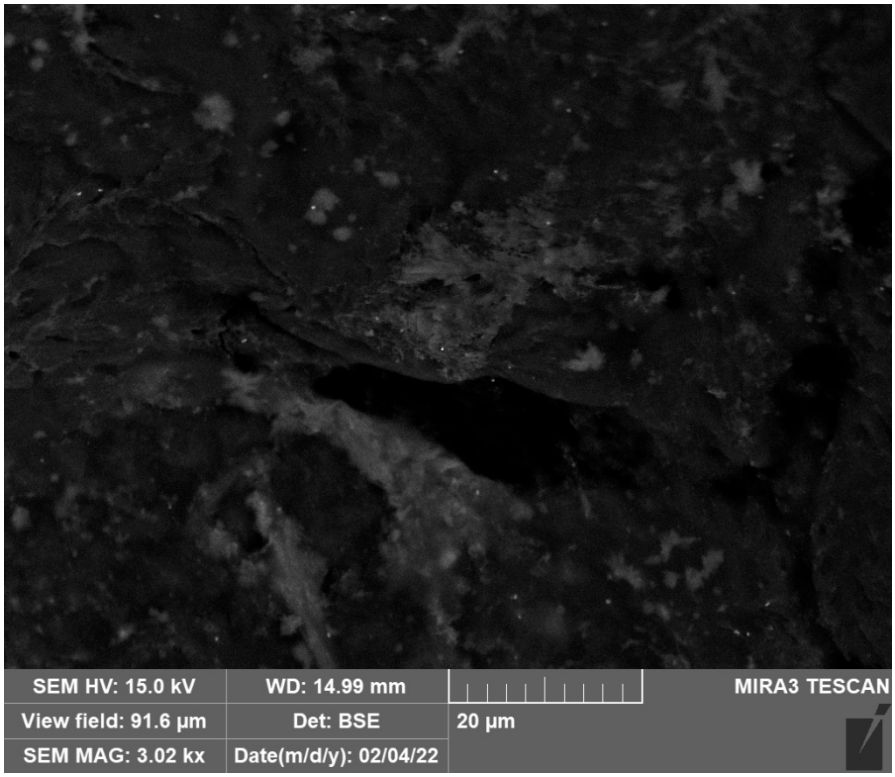

Figure 138: STD20 Image 1

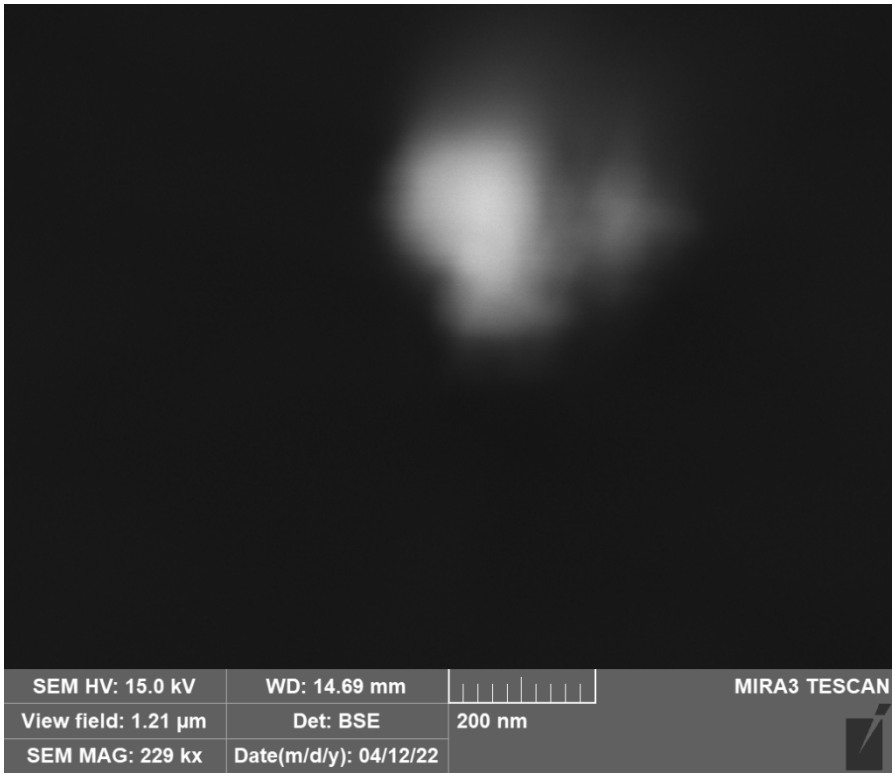

Figure 139: STD21 Image 1

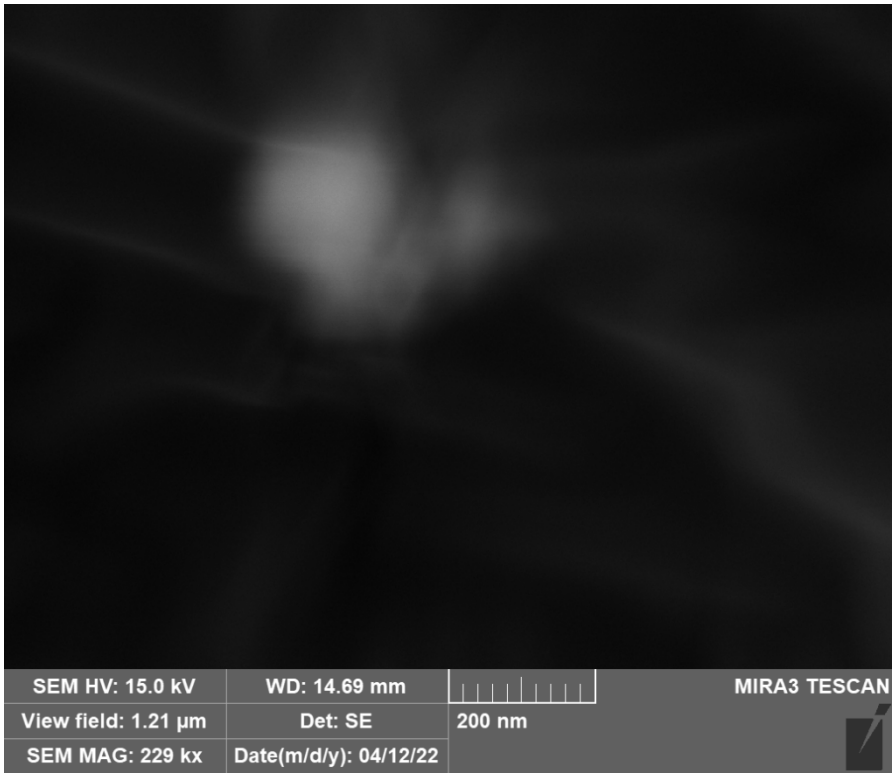

Figure 140: STD 21 Image 2

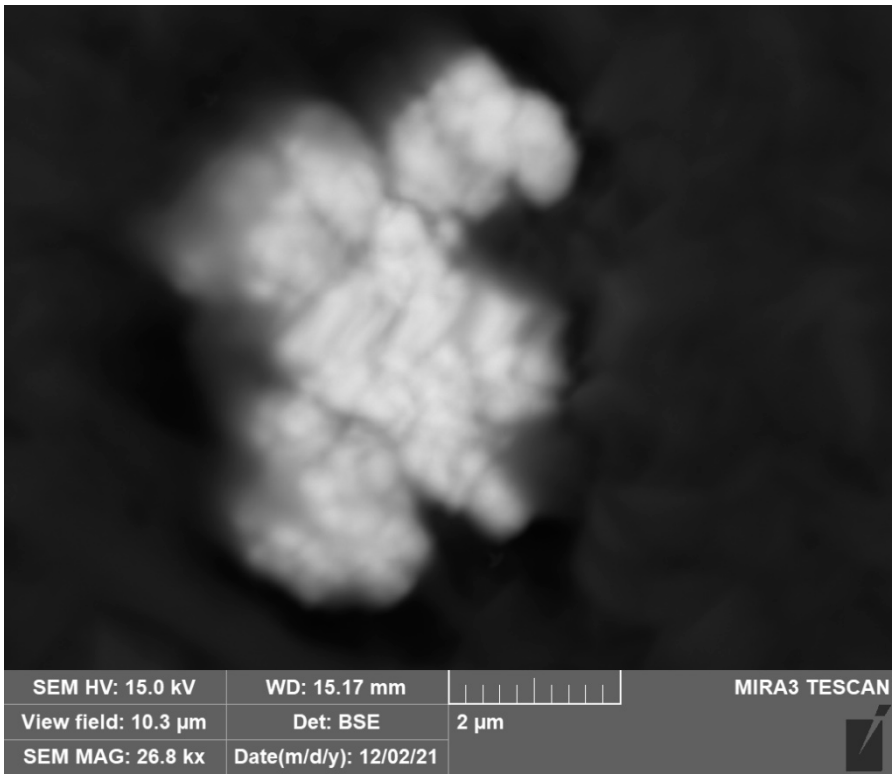

Figure 141: STD22 Image 1

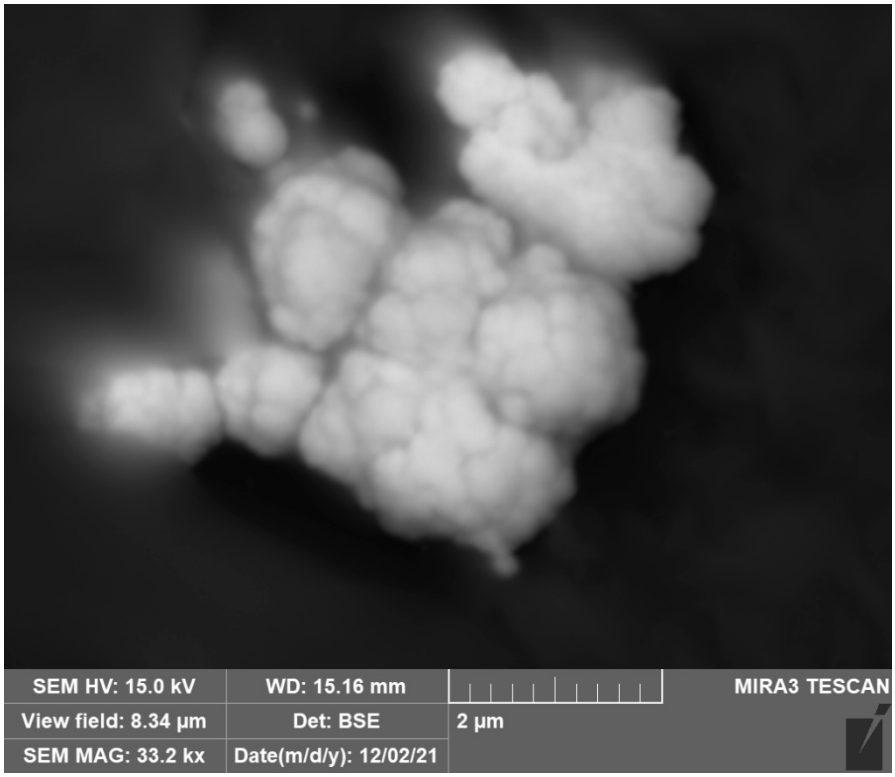

Figure 142: STD22 Image 2

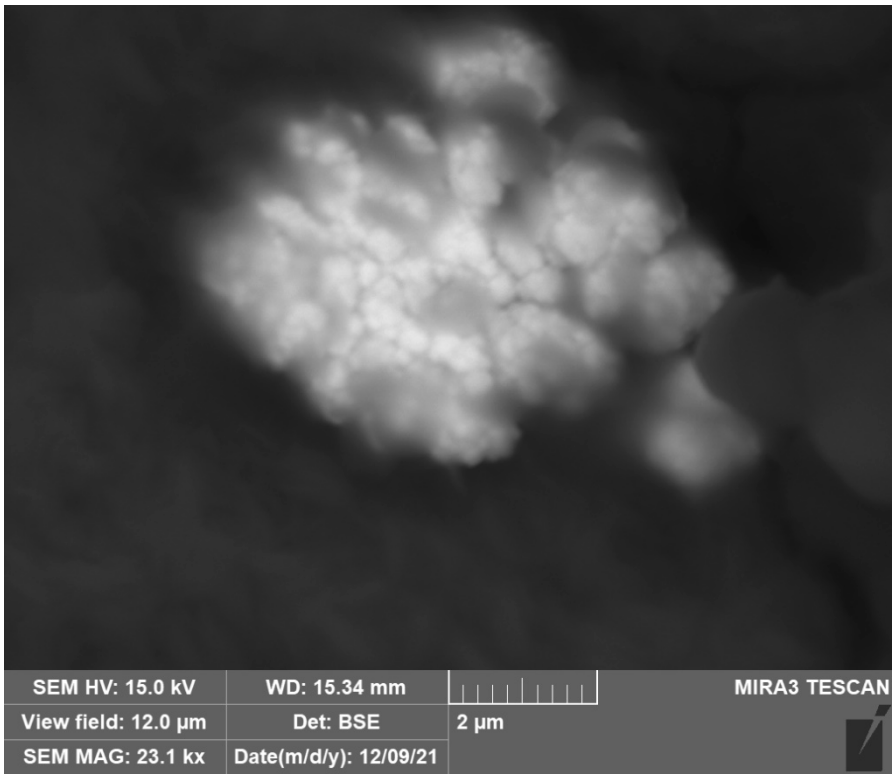

Figure 143: STD22 Image 3

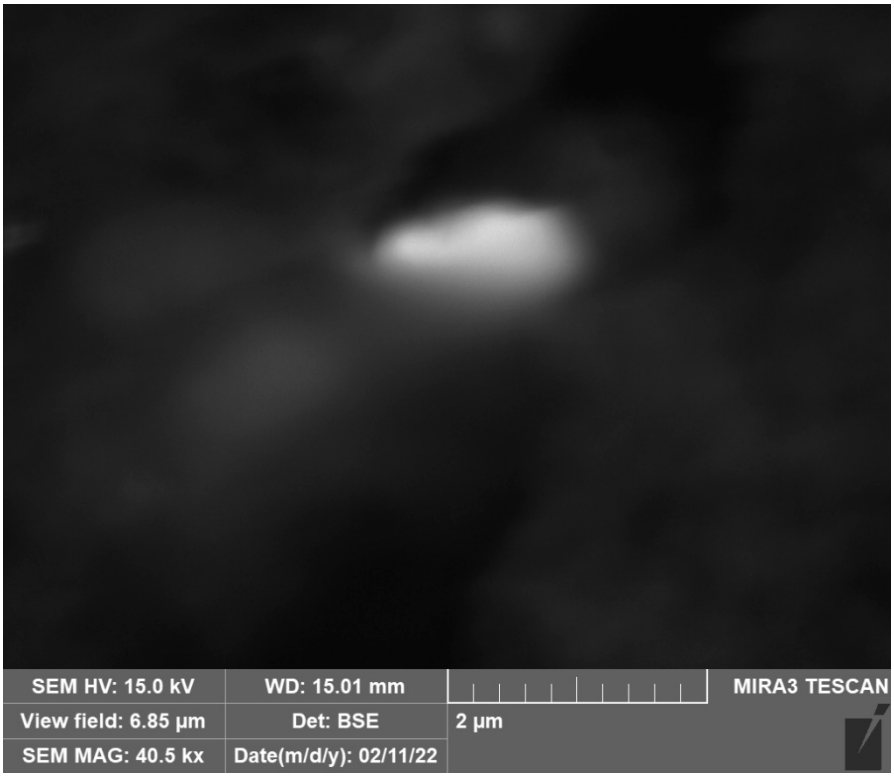

Figure 144: STD23 Image 1

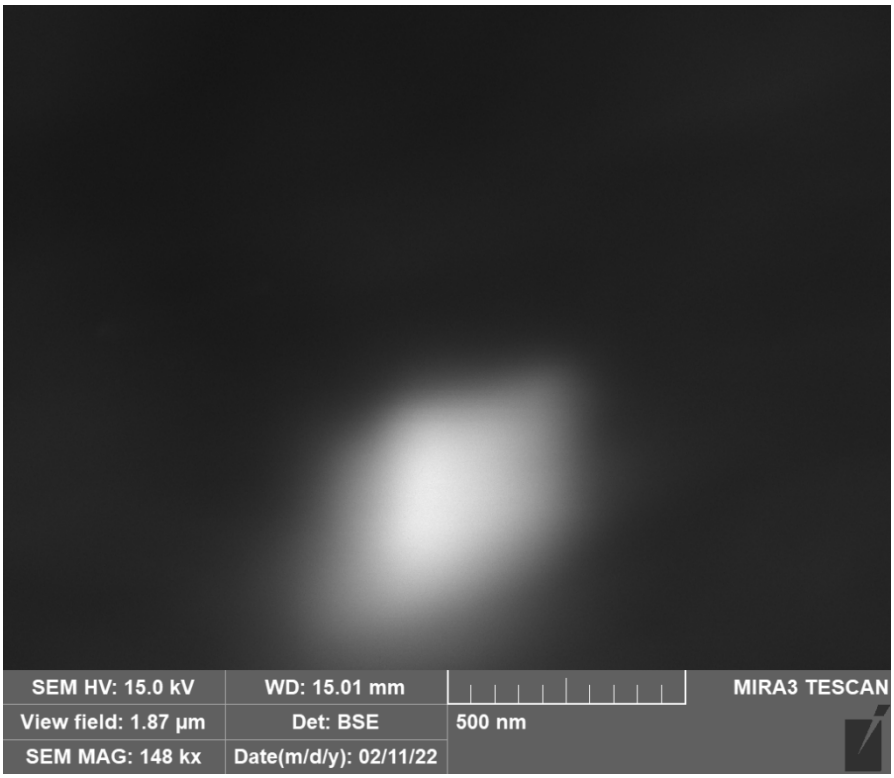

Figure 145: STD23 Image 2

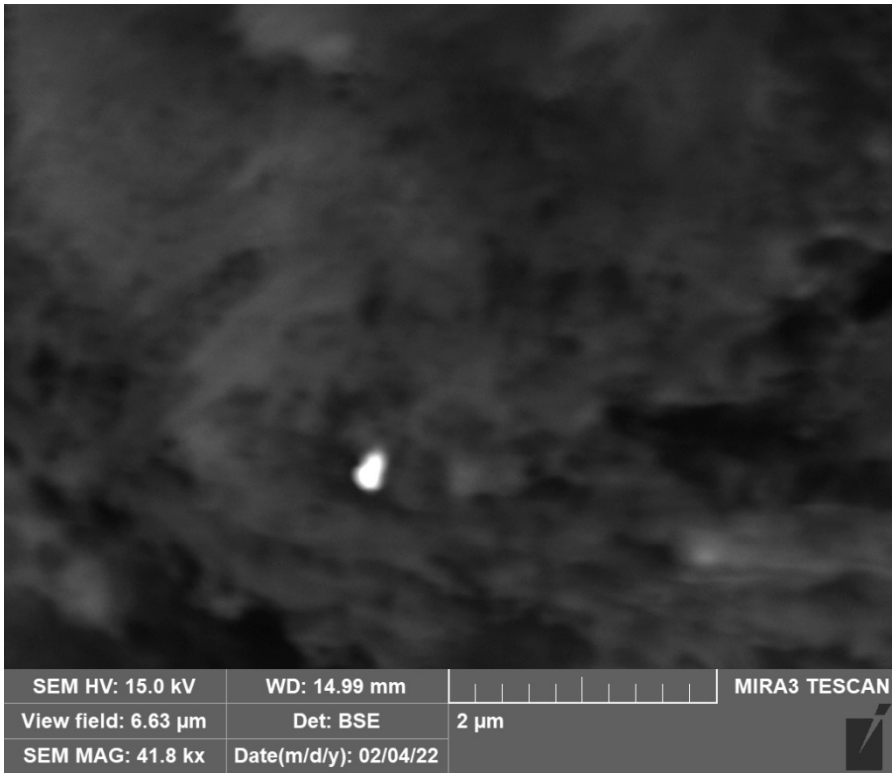

Figure 146: STD24 Image 1

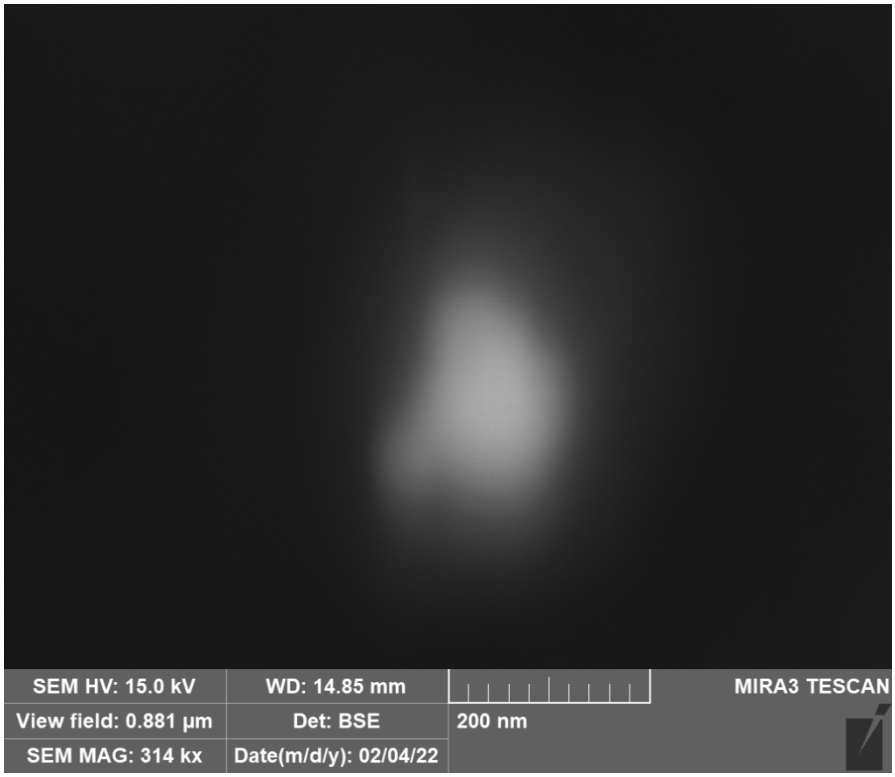

Figure 147: STD 25 Image 1

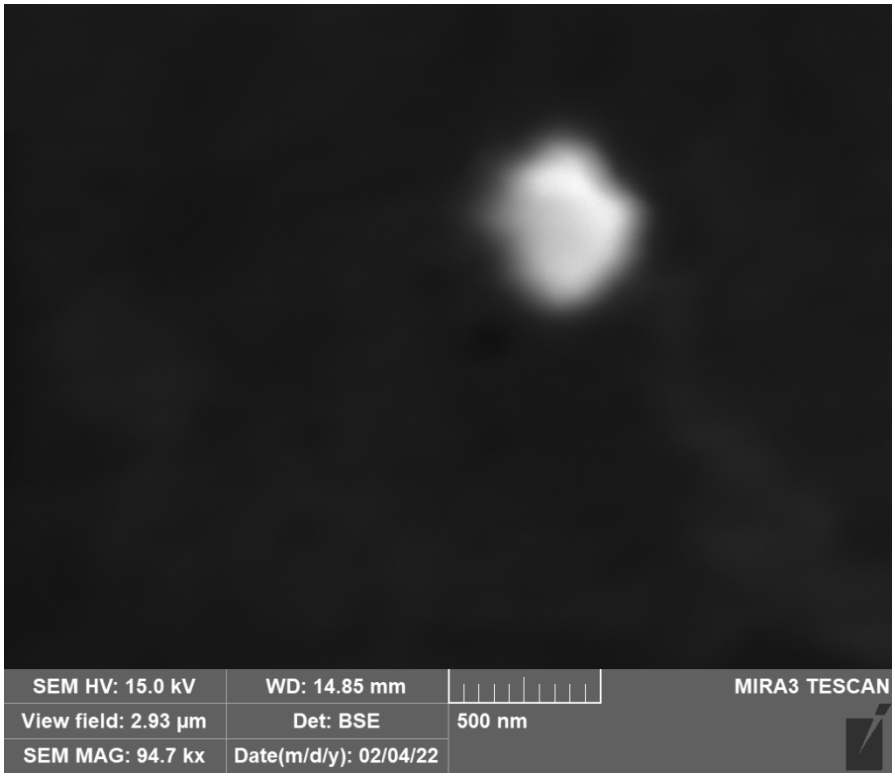

Figure 148: STD25 Image 2

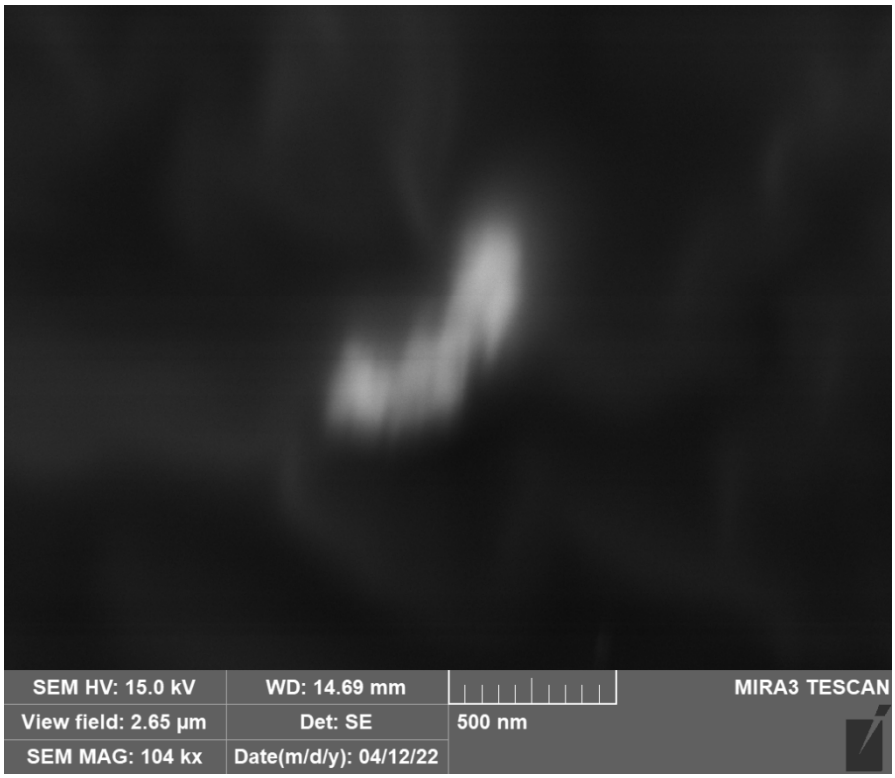

Figure 149: STD27 Image 1

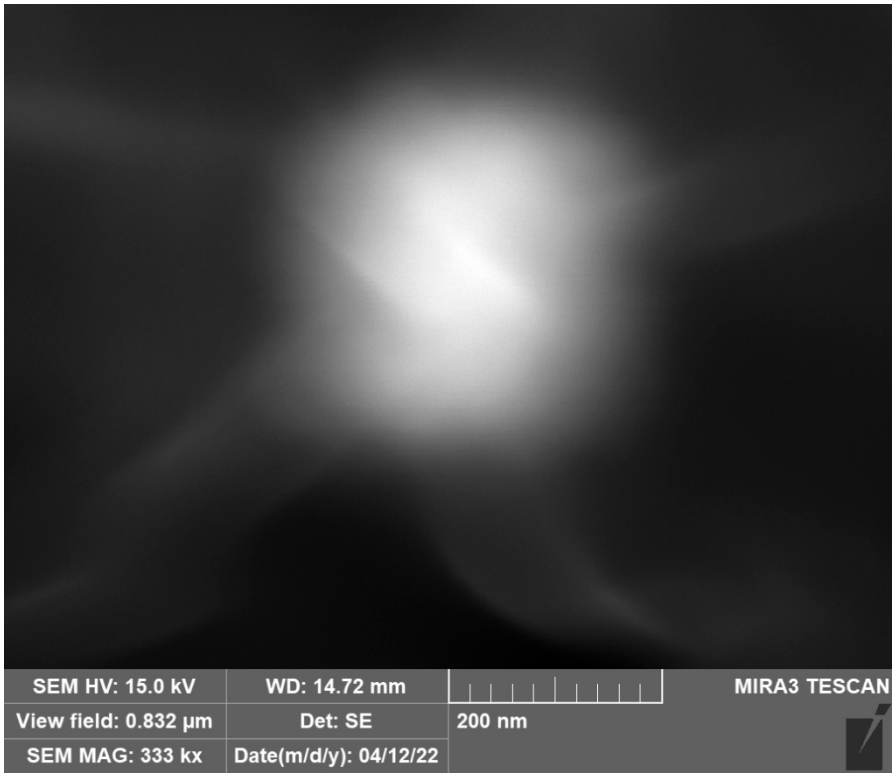

Figure 150: STD28 Image 1

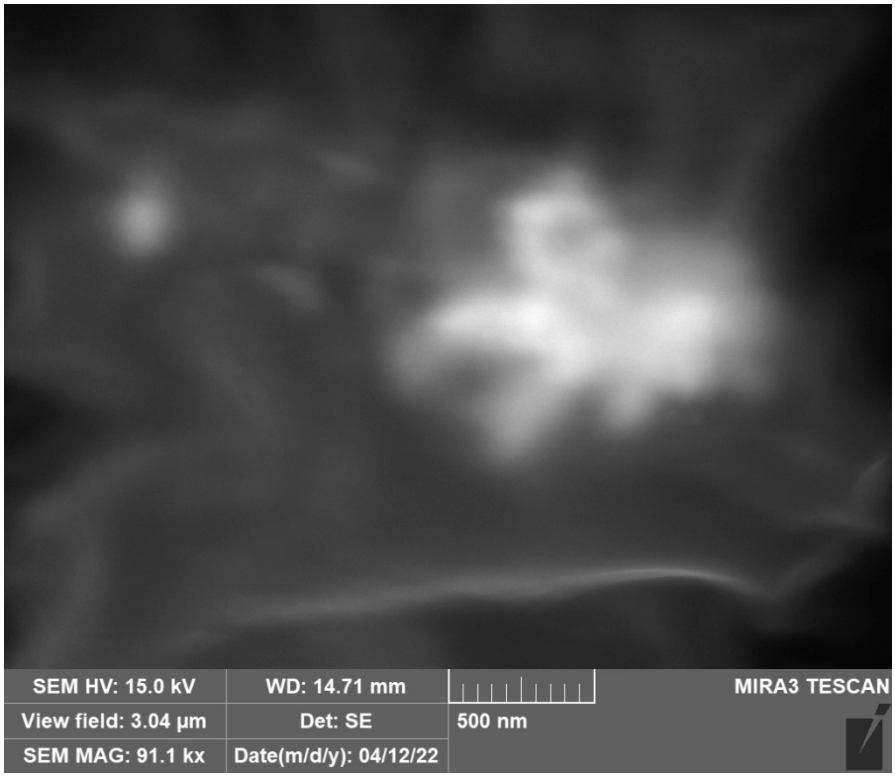

Figure 151: STD28 Image 2

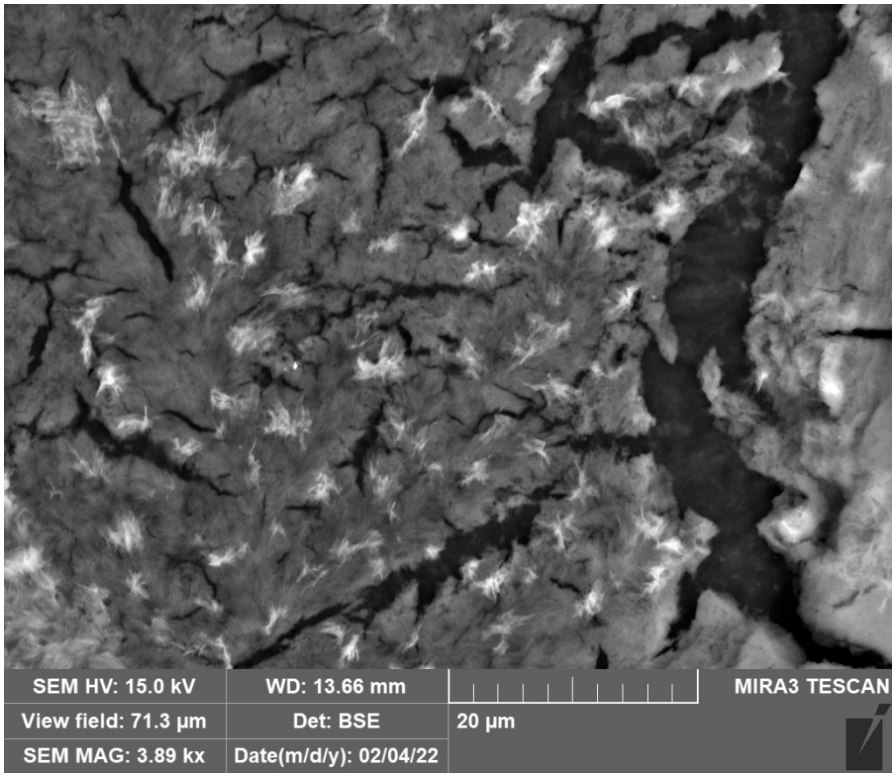

Figure 152: STD29 Image 1

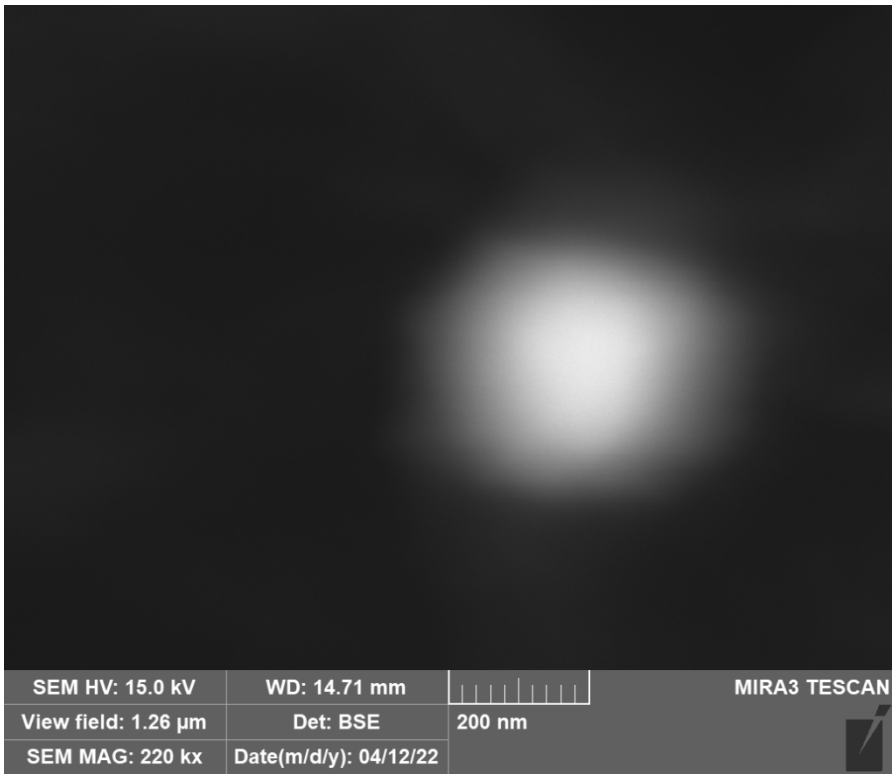

Figure 153: STD30 Image 1

10. Appendix E: Size and Zeta Potential Full Results

Table XIX: Initial gold chloride system Malvern Zetasizer results.

Run	Temp	pH	Au Conc. (ppm)	Hydrazine Added?	Size (nm)	Standard Deviation
1	60	0	500	No	603.4	107.3
2	20	2	252.5	No	309.7	66.26
2	20	2	252.5	Yes	741.6	118.4
3	40	2	500	No	-	-
3	40	2	500	Yes	-	-
4	40	2	252.5	No	546	93.62
4	40	2	252.5	Yes	570.7	100.6
5	60	2	252.5	No	400.1	67.73
5	60	2	252.5	Yes	440.4	75.64
6	40	2	252.5	No	382.6	87.47
6	40	2	252.5	Yes	357.7	60.74
7	20	0	500	No	529.5	84
8	20	0	5	No	791	170.3
9	40	0	252.5	No	600	97.52
10	60	0	5	Yes	563	108.8
11	40	2	252.5	No	410.9	66.41
11	40	2	252.5	Yes	451.2	82.82
12	60	4	500	No	-	-
12	60	4	500	yes	523.1	96.36
13	40	4	252.5	no	536.2	102.5
13	40	4	252.5	yes	402.9	104.2
14	60	4	5	No	488	72.22
14	60	4	5	Yes	410.9	103.8
15	40	2	252.5	No	496.3	91.15
15	40	2	252.5	Yes	450	79.42
16	20	4	500	No	DOS	-
16	20	4	500	Yes	595.9	101
17	40	2	5	No	594.2	110.4
17	40	2	5	Yes	-	-
18	40	2	252.5	No	490.6	88.06
18	40	2	252.5	Yes	526.9	91.55
19	40	2	252.5	No	510.8	122.1
19	40	2	252.5	Yes	607.1	97.01
20	20	4	5	No	669.5	102.6
20	20	4	5	Yes	637.1	130.5

Table XX: Secondary gold chloride system Malvern Zetasizer size and zeta potential results.

					Size Run 1		Size Run 2		Size Run 3			Zeta Potential		
Std	Run	Au Conc [ppm]	Temp [C]	Thiol Conc	Peak 1	Peak 2	Peak 1	Peak 2	Peak 1	Peak 2	Average Size	Run 1	Run 2	Run 3	Average
20	1	10.5	42.5	5	217.2		281.1		211.7		236.7	6.65	-3.5	-5.32	-0.7
11	2	10.5	25	5	325.6		364.4		318.8		336.3	-5.1	-23.9	-35.7	-21.6
7	3	1	60	10	372.3		427.0		766.5	182.7	437.1	-1.77	-15.8	-28.2	-15.3
16	4	10.5	42.5	5	579.8		414.8		602.2		532.3	6.14	-5.88	-8.41	-2.7
5	5	1	25	10	593.1	104.6	458.7		312.6	69.2	307.6	-12.7	-10.9	-26.8	-16.8
18	6	10.5	42.5	5	679.2	156.4	682.9	170.2	685.9	131.3	417.7	-1.87	-12	-13.4	-9.1
14	7	10.5	42.5	10	309.9	500.9	329.5		423.7		391.0	-20.7	-30.6	-27.3	-26.2
17	8	10.5	42.5	5	417.3		389.7		463.1		423.4	9.82	6.61	6.45	7.6
4	9	20	60	0	430.6		406.5		392.2		409.8	2.82	3.3	3.2	3.1
2	10	20	25	0	480.5		492.0		427.5		466.7	5.95	0.349	2.32	2.9
3	11	1	60	0	168.5	570.5	207.5	584.9	275.5	120.2	321.2	-1.93	-3.08	-3.96	-3.0
6	12	20	25	10	376.3	81.3	530.5		584.5		393.1	0.933	-9.75	-3.29	-4.0
12	13	10.5	60	5	219.0		221.0		251.1		230.4	5.92	-0.777	1.23	2.1
1	14	1	25	0	357.0		328.8		347.1		344.3	3.74	-0.101	4.8	2.8
15	15	10.5	42.5	5	468.9	111.8	424.1	90.8		353.2	289.8	-2.68	-6.09	1.54	-2.4
8	16	20	60	10	312.7		272.9		358.1		314.6	1.55	-3.18	-10.1	-3.9
10	17	20	42.5	5	463.0		663.6		265.0		463.9	-7.16	-0.9	-5.72	-4.6
13	18	10.5	42.5	0	376.4		371.8		364.0		370.7	-11	-12	-11.6	-11.5
19	19	10.5	42.5	5	300.6		257.4		267.4		275.1	-6.44	1.14	-3.06	-2.8
9	20	1	42.5	5	356.4		289.0		396.8	110.1	288.1	5.63	13.3	-3.08	5.3

Table XXI: Gold cyanide system Malvern Zetasizer size and zeta potential results.

						Size Run 1		Size Run 2		Size Run 3		Average Size		Zeta Potential			
Std	Run	Au Conc [ppm]	Temp [C]	pH	Thiol conc	Peak 1	Peak 2	Peak 1	Peak 2	Peak 1	Peak 2	100-999 nm	<100 nm	Run 1	Run 2	Run 3	Average
1	12	1	25	11	0	221.6		221.4		153.4		198.8		-19.2	-15.5	-21.4	-18.7
2	30	20	25	11	0	307.1	66.6	327.0	55.6	233.1		289.1	61.1	-37.6	-20.1	-19.1	-25.6
3	7	1	60	11	0	307.5		277.1		512.1		365.6		-10.3	-17.7	-13.2	-13.7
4	21	20	60	11	0	127.2		217.3		319.3		221.3		-41.5	-31.8	-40.8	-38.0
5	19	1	25	13	0	278.6		371.0	51.0	459.1	79.6	369.6	65.3	-21.7	-19.9	-20.0	-20.5
6	26	20	25	13	0	449.8		453.8		141.8		348.5		-20.3	-14.8	-22.0	-19.0
7	13	1	60	13	0	469.0	96.1	463.6	77.6	384.0	84.0	438.9	85.9	-29.7	-21.2	-27.5	-26.1
8	3	20	60	13	0	186.1	717.8	337.7	48.9	764.2	143.7	429.9	48.9	-20.1	-22.2	-21.0	-21.1
9	24	1	25	11	10	235.1		522.0	77.7	248.7	42.7	335.3	60.2	-17.4	-14.1	-11.9	-14.5
10	25	20	25	11	10	196.9		233.9		312.7	26.5	247.8	26.5	-22.6	-39.5	-39.5	-33.9
11	4	1	60	11	10	293.6	54.6	460.0	65.9	980.5	131.6	466.4	60.2	-32.3	-34.3	-33.8	-33.5
12	27	20	60	11	10	197.9	610.1	166.8		143.9		279.7		-20.7	-30.9	-35.9	-29.2
13	9	1	25	13	10	484.3	53.8	239.5		375.9		366.6	53.8	-24.0	-15.0	-22.7	-20.6
14	28	20	25	13	10	325.3	61.4	269.6	42.9	253.3	43.6	282.7	49.3	-21.6	-14.6	-17.2	-17.8
15	11	1	60	13	10	327.0	76.0	290.9	76.3	332.8	73.6	316.9	75.3	-17.6	-18.6	-20.9	-19.0
16	23	20	60	13	10	463.6	58.6	618.5		324.9	56.2	469.0	57.4	-20.7	-18.4	-27.8	-22.3
17	2	1	42.5	12	5	499.3	114.8	608.6	20.5	204.5		356.8	20.5	-35.8	-34.6	-42.9	-37.8
18	16	20	42.5	12	5	102.4	362.5	127.7	20.9	167.6		190.1	20.9	-33.4	-35.7	-42.3	-37.1
19	20	10.5	25	12	5	300.9		303.5		306.2		303.5		-8.0	-6.4	-24.5	-13.0
20	8	10.5	60	12	5	227.2		224.9		352.3	41.8	268.1	41.8	-23.8	-21.9	-22.5	-22.7
21	17	10.5	42.5	11	5	225.7		247.1		275.8		249.5		-31.4	-20.9	-19.4	-23.9
22	29	10.5	42.5	13	5	333.7	51.2	205.2	2.3	163.6	16.3	234.2	23.2	-18.1	-16.8	-21.6	-18.8
23	15	10.5	42.5	12	0	427.3		361.4		417.3		402.0		-45.7	-56.7	-68.2	-56.9
24	10	10.5	42.5	12	10	302.1		346.0		327.7		325.3		-34.7	-40.7	-40.6	-38.7
25	6	10.5	42.5	12	5	237.8		228.7		291.4		252.6		-18.3	-35.9	-28.3	-27.5
26	5	10.5	42.5	12	5	363.1	88.4	475.6	140.9	258.8		309.6	88.4	-39.6	-35.3	-31.3	-35.4
27	14	10.5	42.5	12	5	175.9		175.2		184.3		178.5		-35.3	-36.1	-35.4	-35.6
28	22	10.5	42.5	12	5	139.9	23.4	150.3		161.7	29.2	150.6		-43.1	-46.8	-44.4	-44.8
29	18	10.5	42.5	12	5	196.0		259.9		242.6		232.8		-38.7	-39.7	-43.9	-40.8
30	1	10.5	42.5	12	5	225.7		571.0	104.9	857.4	126.5	377.1		-35.1	-29.8	-29.6	-31.5
3	7	1	60	11	0	236.2	61.1	212.8		212.9		220.6	61.1	-31.1	-29.9	-38.5	-33.2
21	17	10.5	42.5	11	5	127.5	455.6	260.4		326.9	92.4	292.6	92.4	-25.1	-29.7	-25.5	-26.8
27	14	10.5	42.5	12	5	190.5		144.2		199.5		178.1		-2.4	-5.2	-8.2	-5.3
28	22	10.5	42.5	12	5	150.2		213.9				182.1		-5.7	-5.5	-9.9	-7.0
30	1	10.5	42.5	12	5	82.3		245.8		208.9		227.4	82.3	-6.0	-5.8	-12.1	-8.0
11	4	1	60	11	10	221.3		289.3		249.9		253.5		-18.7	-33.9	-27.8	-26.8
17	2	1	42.5	12	5	188.8		184.0		179.1		184.0		-28.3	-24.3	-33.5	-28.7
23	15	10.5	42.5	12	0	153.6		135.3		174.2		154.4		-12.9	-15.7	-27.8	-18.8